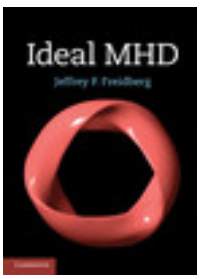

Ideal MHD

Jeffrey P. Freidberg

Book DOI: http://dx.doi.org/10.1017/CBO9780511795046

Online ISBN: 9780511795046

Hardback ISBN: 9781107006256

Chapter

12 - Stability: multi-dimensional configurations pp. 570-677

Chapter DOI: http://dx.doi.org/10.1017/CBO9780511795046.013

Cambridge University Press

12

Stability: multi-dimensional configurations

12.1 Introduction

Chapter 12 is concerned with the MHD stability of toroidal systems, specifically tokamaks and stellarators. As might be expected the complexities associated with multidimensional systems make analysis quite difficult. Consequently, in practice stability results are often obtained numerically. There are, however, a variety of simple models which do provide physical insight into qualitative geometric features that lead to favorable and unfavorable stability behavior. This chapter describes several of these simple models plus summarizes several of the major numerical studies.

The discussion begins with a general analysis of ballooning modes. These are radially localized modes with short perpendicular wavelengths and long parallel wavelengths. They arise because most toroidal configurations have magnetic geometries with alternating regions of favorable and unfavorable curvature. The most unstable perturbations are those whose amplitude "balloons" out in the region of unfavorable curvature. The modes are important because they set one limit on the maximum stable β in toroidal configurations.

Mathematically, it is possible to exploit the localization of the mode. The result is a general reduction of the Energy Principle to a one-dimensional differential equation that allows testing of stability one magnetic line at a time. This represents an enormous saving in computing time compared to the general fully coupled two- or three-dimensional stability problems. The simplified analysis is another reason why ballooning modes have received so much attention.

Once the general ballooning mode equation is derived, attention is focused on the stability of tokamaks. The analysis shows that toroidicity produces qualitative changes in the stability of pressure-driven modes as compared to the straight tokamak. This is demonstrated explicitly by means of the ballooning mode equation. Two results are derived. First, the condition for the ballooning mode equation to be

valid leads to the Mercier criterion, a 2-D generalization of Suydam's criterion. In practice, satisfying the condition requires a minimum q on axis. When the Mercier criterion is satisfied, the ballooning mode equation is valid. When it is not, the plasma is unstable to localized interchange modes.

Assuming the Mercier criterion is satisfied, one then solves the ballooning mode equation for a simple model leading to a prediction for the maximum stable beta which is compared to more extensive numerical results. Elongated, outward pointing triangular shapes are favorable for stability.

Next, a second general reduction of the Energy Principle is derived by utilizing the large aspect ratio, high beta tokamak expansion. The end formulation remains two dimensional but is simplified because the potential energy can be written in terms of a single potential function rather than the two components of $\boldsymbol{\xi}_\perp$. The simplified Energy Principle is applied to the problem of $n = 0$ axisymmetric instability. It is shown that elongated cross sections tend to be unstable. A conducting wall is necessary for stability. This converts the instability into a resistive wall mode which requires feedback stabilization.

The toroidal tokamak is then examined for stability against non-localized internal and external modes. Like for the straight tokamak, internal modes lead to a condition on the minimum allowable q on axis. The external modes are the most dangerous instabilities. Physically the low n unstable current-driven kink modes in a straight tokamak develop a strong ballooning component, transforming them into ballooning-kink modes. These modes set the strictest limits on beta. Furthermore, the highest achievable beta occurs at an optimum value of q_*. The external kink stability results are demonstrated by means of the relatively simple surface current model and compared to extensive numerical results. Again, a combination of elongation and outward pointing triangularity are favorable for stability. Overall, the theoretical maximum stable β_t is probably sufficient for energy applications although there is not a large safety margin.

Still, there remains an important problem facing the tokamak – the need for steady state operation. This requires external non-inductive current drive, which is technologically feasible but inefficient from an energy point of view. The end result is that to overcome current drive inefficiency the toroidal current must be driven primarily by the bootstrap effect. This in turn requires high β_t values, typically exceeding the limits predicted by numerical studies. Again, a conducting wall is required implying conversion of the instability to a resistive wall mode which requires feedback for stabilization. The achievement of steady state operation is encompassed in the advanced tokamak (AT) discussion.

The stability of tokamaks concludes with a discussion of $n = 0$ axisymmetric modes. These modes limit the allowable elongation of the tokamak cross section, a feature that is desirable for both equilibrium and stability. In general, a conducting

wall is required to stabilize a finite elongation. As for other instabilities, the presence of a finite conductivity wall transforms the wall stabilized mode into a resistive wall mode. Stabilization is provided by feedback which for practical engineering reasons limits the elongation to about $\kappa_{\max} \simeq 1.8$. Violation of the elongation criterion leads to a major disruption.

The final topic discussed is the stability of stellarators. Since stellarators in general have small or zero toroidal current, kink modes are not very important. Instead, stability is determined primarily by pressure-driven modes, both local and global. Although no simple but rigorous stability criteria exist a useful guideline is introduced, known as the average curvature. This quantity is shown to be related to an alternate figure of merit known as the magnetic well. By using this guideline it is possible to develop some intuition as to how to design a stellarator with favorable MHD stability properties.

Several simple models are analyzed. It is shown that a straight stellarator always has unfavorable average curvature. Shear can provide stability against unfavorable average curvature but only at very low values of beta. Toroidal effects are shown to help stability. Specifically, a vertical field can create a favorable shift of the flux surfaces to provide stability at higher values of β_t. Full 3-D stability results have been obtained numerically. These studies predict complete stability at values of β_t sufficiently high for energy applications without the need for a conducting wall.

12.2 Ballooning and interchange instabilities

12.2.1 Introduction

Recall that interchange stability in a cylinder is determined by Suydam's criterion. The modes of interest correspond to a special subclass of trial functions which are radially localized about a resonant surface $r = r_s : [\mathbf{k}\cdot\mathbf{B}]_{r_s} = 0$. Application of Suydam's criterion is simple – one simply substitutes the equilibrium profiles into the analytic formula for Suydam's criterion and examines whether the resulting expression is positive or negative for all r. Also, since the analysis focuses on a special subclass of trial functions the resulting criterion is a necessary but not sufficient condition for stability.

An analogous situation exists for toroidal plasmas. However, the analysis is substantially more complicated because of the multi-dimensional geometric effects arising from toroidicity. The aim of this section is to investigate the toroidal analogs of Suydam's criterion. This leads to a modified form of Suydam's criterion known as the Mercier criterion. The analysis also leads to a generalized form of the interchange instability known as the ballooning mode.

The difference between interchange and ballooning modes is as follows. Both modes are driven by the interaction of the pressure gradient and the curvature.

Interchange modes are approximately constant along the field lines (i.e., $\mathbf{k} \cdot \mathbf{B} \approx 0$) to minimize the stabilizing effects of field line bending. This form of trial function implies that stability is essentially determined by the "average" field line curvature resulting from the $(\boldsymbol{\xi}_\perp \cdot \nabla p)(\boldsymbol{\xi}_\perp^* \cdot \boldsymbol{\kappa})$ term in δW. In contrast, a ballooning perturbation recognizes that the field line curvature can oscillate between being favorable and unfavorable along a field line. Therefore, by allowing a small amount of line bending the perturbation has the potential to localize in regions of unfavorable curvature, thereby having a net effect which is more unstable than the nearly constant interchange perturbation. In effect, the trial function "balloons out" in the region of unfavorable curvature.

In terms of application the Mercier criterion is qualitatively similar to Suydam's criterion. One substitutes equilibrium profiles into an analytic expression and examines whether or not the resulting value is positive or negative over all flux surfaces in the plasma. The actual substitution procedure is more complicated since flux surface averages must be performed, but this is a technical rather than conceptual distinction. For tokamaks, the Mercier criterion usually results in a limit on the minimum allowable $q(\psi)$ at the magnetic axis.

Application of the ballooning mode stability criterion requires the solution of a one-dimensional differential equation where the independent variable is basically distance along a field line. Newcomb's analysis then implies that stability or instability is determined by whether or not the minimizing solution has a zero crossing at some point along the field line. The procedure must be applied to all flux surfaces in the plasma. Although many solutions to the 1-D differential equation are thus required to test overall ballooning stability this is still a far, far simpler procedure than solving the fully coupled two- or three-dimensional stability problems for tokamaks or stellarators. Ballooning modes are important because they set upper limits on the allowable β values. Excitation of ballooning modes does not in general lead to major disruptions but instead to enhanced MHD turbulent transport.

As stated, the analysis of interchange and ballooning modes carried out in this section is somewhat complicated. Several steps are required as follows:

1 A discussion is presented that focuses on the basic incompatibility that arises when one attempts to create a trial function that maintains poloidal and toroidal periodicity in a multidimensional configuration with magnetic shear. The situation is further complicated by the need for the trial function to be localized around a flux surface. The end result is the introduction of a very clever transformation, known as the "ballooning mode formalism."
2 This transformation is then applied to δW, leading to the general 1-D ballooning mode differential equation. The derivation is somewhat elegant in that the details are coordinate independent.

3 Specific coordinate systems are next introduced resulting in more practical forms of the ballooning mode differential equation for tokamaks and stellarators.
4 Attention is next focused on tokamaks. It is shown that the validity of the ballooning mode differential equation is closely connected to the Mercier criterion. The actual Mercier criterion is derived and in simple limits, applied to tokamaks.
5 Assuming the plasma is Mercier stable one must then test for ballooning mode stability by means of the 1-D differential equation. A simple semi-analytic model for the tokamak is introduced and it is shown how ballooning modes lead to β limits. These results are compared to extensive numerical results for more realistic configurations which provide a good guide to the practical β limit in tokamaks due to ballooning modes.

12.2.2 Shear, periodicity, and localization

The stability analysis of interchange and ballooning modes requires the construction of a trial function which is localized around a flux surface and satisfies the periodicity requirements in θ and ϕ. The trial function that meets these requirements results from the ballooning mode formalism and is not at all obvious. The analysis begins with a discussion of the difficulty of constructing such a trial function. Once the difficulties are understood it is then possible to motivate the choice of the ballooning mode trial function.

Straightforward Fourier analysis

Consider a two- or three-dimensional toroidal configuration whose outer flux surface is chosen for simplicity to be circular. The interior flux surfaces are non-circular. A straightforward approach is to write each component of the plasma displacement as a Fourier series. For example, if one focuses on the normal component of plasma displacement $\mathbf{n} \cdot \boldsymbol{\xi}_\perp = \xi(r,\theta,\phi)$, then

$$\xi(r,\theta,\phi) = \sum_{m,n} \xi_{mn}(r)\, e^{im\theta - in\phi} \tag{12.1}$$

While this is a mathematically correct form of the displacement it is not very useful. The reason is that it is not possible to easily exploit the localization requirement since the interior flux surfaces are not circular. In other words, since $r =$ constant is not a flux surface, a local trial function would require many terms in the Fourier series. The resulting analysis is thus a multidimensional coupled harmonic problem with no mathematical advantage due to localization.

A simple attempt at localization

A cleverer approach to exploit localization is to introduce the flux ψ as the radial variable: $r,\theta,\phi \rightarrow \psi,\theta,\phi$. For simplicity focus on axisymmetric configurations (i.e., tokamaks) so that $\psi(r,\theta,\phi) \rightarrow \psi(r,\theta)$. A trial function that is easily localized around a flux surface can then be written as $\xi = \xi_0 \exp[-in\phi + iS_p(\psi,\theta)]$. To localize, one simply expands $S_p(\psi,\theta)$ about the flux surface of interest, $\psi = \psi_0 + \delta\psi$. A valid local trial function vanishes rapidly as $\delta\psi$ increases.

Now, the function $S_p(\psi, \theta)$ must be chosen to correspond to an interchange-like perturbation in order to minimize line bending. This requires setting $\mathbf{B} \cdot \nabla\xi = \xi_0 \mathbf{B} \cdot \nabla(-in\phi + iS_p) = 0$. A short calculation shows that $S_p(\psi,\theta)$ satisfies

$$\frac{\partial S_p}{\partial \theta} = n\frac{rB_\phi}{RB_\theta} \tag{12.2}$$

which has as its solution

$$S_p(\psi,\theta) = n\int_{\theta_0}^{\theta} \frac{rB_\phi}{RB_\theta}\, d\theta \tag{12.3}$$

where θ_0 is a free integration constant and it is understood that the integrand is evaluated on the flux surface. Note that the radial wave number, which is a measure of localization, is approximately given by $k_\psi \approx (\partial S_p/\partial\psi)|\nabla\psi|$. The implication is that a local trial function requires $k_\psi a \gg 1$ which is equivalent to $n \gg 1$.

The last requirement to be satisfied by $S_p(\psi,\theta)$ is periodicity and corresponds to $S_p(\psi,\theta + 2m\pi) = S_p(\psi,\theta) + 2m\pi$. On $\psi = \psi_0$, the flux surface of interest, Eq. (12.3) implies that periodicity requires

$$n\int_0^{2\pi} \left(\frac{rB_\phi}{RB_\theta}\right)_{\psi_0} d\theta = 2\pi m \tag{12.4}$$

Recalling the definition of the safety factor allows one to rewrite Eq. (12.4) as

$$\frac{1}{2\pi}\int_0^{2\pi} \left(\frac{rB_\phi}{RB_\theta}\right)_{\psi_0} d\theta \equiv q(\psi_0) = \frac{m}{n} \tag{12.5}$$

The localization must take place around a rational surface.

It is at this point that the fundamental incompatibility between shear and periodicity arises. While periodicity is satisfied on a rational surface, a short distance away (in flux) the function $S_p(\psi,\theta)$ has the value

$$S_p(\psi_0 + \delta\psi,\theta) \approx n\left[\int_{\theta_0}^{\theta} \left(\frac{rB_\phi}{RB_\theta}\right)_{\psi_0} d\theta + \delta\psi\int_{\theta_0}^{\theta} \frac{\partial}{\partial\psi_0}\left(\frac{rB_\phi}{RB_\theta}\right) d\theta\right] \tag{12.6}$$

The periodicity constraint reduces to

$$S_p(\psi_0 + \delta\psi, \theta + 2m\pi) - S_p(\psi_0 + \delta\psi, \theta) \approx 2\pi m\left(1 + \frac{1}{q}\frac{\partial q}{\partial \psi_0}\delta\psi\right) \tag{12.7}$$

In a system with shear (i.e., $\partial q/\partial\psi_0 \neq 0$), a trial function with $m \sim n \gg 1$ is no longer periodic away from the rational surface even if $\delta\psi$ is small!

The ballooning mode formalism

The incompatibility between shear and periodicity was resolved by Connor, Hastie, and Taylor (1979) by the introduction of the ballooning mode formalism. The basic idea is as follows. Since the equilibrium and all perturbed quantities must be periodic in θ, ϕ in a physical system, no information is lost or gained if one extends the angular domain of validity from $0 \leq \theta \leq 2\pi$, $0 \leq \phi \leq 2\pi$ to $-\infty < \theta < \infty$, $-\infty < \phi < \infty$. Actually, as is shown below, only a single combination of angles must be extended, the other combination maintaining a finite range of integration. For present purposes, however, it is convenient to assume both angles are extended as this helps determine the proper combination to be extended.

The motivation for extension is that it allows one, perhaps unexpectedly, to construct a perturbation that is periodic in θ,ϕ by means of an infinite sum of terms, none of which is periodic. This is the ballooning mode formalism. Specifically, the displacement vector is written as

$$\boldsymbol{\xi}(r,\theta,\phi) = \sum_{m,n} \overline{\boldsymbol{\xi}}(r,\theta + 2m\pi, \phi + 2n\pi) \tag{12.8}$$

The function $\overline{\boldsymbol{\xi}}(r,\theta,\phi)$, often called a "quasi-mode," extends over the doubly infinite domain and is not periodic. Typically it has small amplitude periodic oscillations superimposed on a non-periodic envelope. Note that each term in the summation corresponds to the same quasi-mode, just shifted in angle. The actual eigenfunction $\boldsymbol{\xi}(r,\theta,\phi)$ is periodic since shifting θ and/or ϕ by $2l\pi$ just corresponds to a relabeling of the summation indices: for example, $m = m' - l$. The only possible problem is the accumulation or loss of contributions from the ends of the summation. This problem is resolved by requiring that the quasi-mode decay sufficiently rapidly for large $|\theta|$ and $|\phi|$ so that terms from the ends of the summation are small and thus make no contribution.

As is shown shortly, there is a sharp criterion that distinguishes "sufficiently rapidly" and "not sufficiently rapidly." The transition corresponds to the Mercier criterion. The proper procedure to test stability therefore requires first testing the Mercier criterion. If the Mercier criterion is violated, the ballooning mode formulation is not valid. However, violation of the criterion implies that the plasma is

already unstable so one need not proceed any further. If the Mercier criterion is satisfied, then the ballooning mode formulation is valid and one can proceed to test stability by analyzing the ballooning mode differential equation.

An important simplifying property of the quasi-mode expansion is that $\overline{\boldsymbol{\xi}}(r,\theta,\phi)$ satisfies the same equation as $\boldsymbol{\xi}(r,\theta,\phi)$. To see this recall that at marginal stability $\boldsymbol{\xi}(r,\theta,\phi)$ satisfies

$$\mathbf{F}(\boldsymbol{\xi}) = 0 \tag{12.9}$$

where $\mathbf{F}$ is the MHD force operator. Since the equilibria of interest are periodic this implies that $\mathbf{F}(r,\theta + 2m\pi,\phi + 2n\pi) = \mathbf{F}(r,\theta,\phi)$. As a consequence, application of the force operator to Eq. (12.8) shows that

$$\begin{aligned}\mathbf{F}(\boldsymbol{\xi}) &= \sum_{m,n} \mathbf{F}(r,\theta,\phi)[\overline{\boldsymbol{\xi}}(r,\theta + 2m\pi,\phi + 2n\pi)] \\ &= \sum_{m,n} \mathbf{F}(r,\theta + 2m\pi,\phi + 2n\pi)[\overline{\boldsymbol{\xi}}(r,\theta + 2m\pi,\phi + 2n\pi)]\end{aligned} \tag{12.10}$$

In other words, each term in the summation satisfies the same equation

$$\mathbf{F}(\overline{\boldsymbol{\xi}}) = 0 \tag{12.11}$$

There is an important conclusion that can be drawn from Eq. (12.11). If a marginally stable solution can be found for a single quasi-mode, for instance leading to a critical β, then this critical β will be identical for all quasi-modes in the summation. The implication is that marginal stability can be investigated by analyzing a single quasi-mode, thereby eliminating the need to consider the entire summation.

To summarize, the ballooning mode formalism allows one to investigate marginal stability by (1) analyzing a single quasi-mode, (2) focusing on a mode structure localized around a flux surface, (3) choosing the mode structure to be interchange-like (i.e., $\mathbf{B}\cdot\nabla\overline{\boldsymbol{\xi}} \approx 0$), but (4) *not* requiring the quasi-mode to be periodic in θ, ϕ. The ballooning mode formalism resolves the incompatibility between shear and periodicity.

Localizing the quasi-mode

One last step is required to finalize the form of the quasi-mode in order to account for the localization around a flux surface. To exploit localization mathematically one needs to introduce a small parameter that measures the width in radius of the quasi-mode compared to the characteristic minor radius of the plasma. This can be conveniently accomplished by introducing a local perpendicular wavelength $\mathbf{k}_\perp(\mathbf{r})$ and assuming that $|\mathbf{k}_\perp a| \gg 1$. Mathematically, the stability problem now has two scale lengths, the slowly varying equilibrium length a and the rapidly varying

perturbation wavelength $\mathbf{k}_\perp^{-1}$. This is the ideal situation to represent the quasi-mode by means of a WKB expansion.

For the ballooning mode analysis under consideration the appropriate form for the quasi-mode can thus be written as

$$\overline{\boldsymbol{\xi}}(\mathbf{r}) = \overline{\boldsymbol{\eta}}(\mathbf{r})\, e^{iS(\mathbf{r})} \tag{12.12}$$

Here, the envelope $\overline{\boldsymbol{\eta}}(\mathbf{r})$ is assumed to vary slowly on the equilibrium scale. The local wave number of the mode is defined as $\mathbf{k} = \nabla S$ and must correspond to rapid variation. This implies that $S(\mathbf{r})$, known as the eikonal, must have the following properties:

$$\begin{aligned} \mathbf{B}\cdot\nabla S &= 0 \qquad && \text{interchange-like perturbation} \\ \nabla S &= \mathbf{k}_\perp \gg 1/a \qquad && \text{localized mode structure} \end{aligned} \tag{12.13}$$

For practical applications to tokamaks or stellarators it will be convenient, particularly for the localization requirement, to introduce some form of flux coordinates. However, this is not necessary for the next task which consists of a general, coordinate free reduction of δW obtained by exploiting the properties of the quasi-mode trial function.

12.2.3 General reduction of δW for ballooning modes

Because ballooning modes are localized in radial extent they naturally correspond to internal MHD modes. Thus, one need only consider δW_F . Furthermore, since marginal stability can be determined by analyzing only a single quasi-mode, the actual quantity of interest is defined as

$$\delta\overline{W}_F = -\frac{1}{2}\int \overline{\boldsymbol{\xi}}^{*}\cdot\mathbf{F}(\overline{\boldsymbol{\xi}})d\mathbf{r} \tag{12.14}$$

Here it is understood that the integration is carried out over the extended angular domain.

The reduction of $\delta\overline{W}_F$ makes use of the fact that all of the analysis presented in Chapter 8 involving the actual displacement $\boldsymbol{\xi}$ also applies to the quasi-mode displacement $\overline{\boldsymbol{\xi}}$ since $\boldsymbol{\xi}$ and $\overline{\boldsymbol{\xi}}$ satisfy the same equation, $\mathbf{F}(\boldsymbol{\xi}) = \mathbf{F}(\overline{\boldsymbol{\xi}}) = 0$, and the same boundary condition, $\mathbf{n}\cdot\boldsymbol{\xi} = \mathbf{n}\cdot\overline{\boldsymbol{\xi}} = 0$, on the plasma surface. The starting point of the analysis is chosen as the intuitive form of the potential energy given by Eq. (8.32), which is repeated here for convenience:

$$\begin{aligned} \delta\overline{W}_F = \frac{1}{2\mu_0}\int \Big[& |\overline{\mathbf{Q}}_\perp|^2 + B^2|\nabla\cdot\overline{\boldsymbol{\xi}}_\perp + 2\overline{\boldsymbol{\xi}}_\perp\cdot\boldsymbol{\kappa}|^2 + \mu_0\gamma p|\nabla\cdot\overline{\boldsymbol{\xi}}|^2 \\ & -2\mu_0(\overline{\boldsymbol{\xi}}_\perp\cdot\nabla p)(\overline{\boldsymbol{\xi}}_\perp^{*}\cdot\boldsymbol{\kappa}) - \mu_0 J_\parallel \overline{\boldsymbol{\xi}}_\perp^{*}\times\mathbf{b}\cdot\overline{\mathbf{Q}}_\perp \Big] d\mathbf{r} \end{aligned} \tag{12.15}$$

The first step is to substitute the quasi-mode trial function given by Eq. (12.12) into the expression for $\delta\overline{W}_F$. A key feature of the substitution is that $\overline{\mathbf{Q}}_\perp$ does not contain any explicit gradients in S:

$$\begin{aligned}\overline{\mathbf{Q}}_\perp &= e^{iS}[\nabla\times(\overline{\boldsymbol{\eta}}_\perp\times\mathbf{B})+i\nabla S\times(\overline{\boldsymbol{\eta}}_\perp\times\mathbf{B})]_\perp \\ &= e^{iS}[\nabla\times(\overline{\boldsymbol{\eta}}_\perp\times\mathbf{B})+i(\mathbf{k}_\perp\cdot\mathbf{B})\overline{\boldsymbol{\eta}}_\perp - i(\mathbf{k}_\perp\cdot\overline{\boldsymbol{\eta}}_\perp)\mathbf{B}]_\perp \\ &= e^{iS}\nabla\times(\overline{\boldsymbol{\eta}}_\perp\times\mathbf{B})_\perp\end{aligned} \tag{12.16}$$

Substituting $\overline{\boldsymbol{\xi}}$ and $\overline{\mathbf{Q}}_\perp$ into the expression for $\delta\overline{W}_F$ leads to

$$\delta\overline{W}_F=\frac{1}{2\mu_0}\int\Big[|\nabla\times(\overline{\boldsymbol{\eta}}_\perp\times\mathbf{B})_\perp|^2+B^2|i\mathbf{k}_\perp\cdot\overline{\boldsymbol{\eta}}_\perp+\nabla\cdot\overline{\boldsymbol{\eta}}_\perp+2\overline{\boldsymbol{\eta}}_\perp\cdot\boldsymbol{\kappa}|^2$$
$$-2\mu_0(\overline{\boldsymbol{\eta}}_\perp\cdot\nabla p)(\overline{\boldsymbol{\eta}}_\perp^*\cdot\boldsymbol{\kappa})-\mu_0 J_\parallel(\overline{\boldsymbol{\eta}}_\perp^*\times\mathbf{b})\cdot\nabla\times(\overline{\boldsymbol{\eta}}_\perp\times\mathbf{B})_\perp\Big]d\mathbf{r} \tag{12.17}$$

Note that the plasma compressibility term is not included in Eq. (12.17) since in systems with shear the most unstable modes are incompressible; that is, $\overline{\boldsymbol{\xi}}_\parallel$ is chosen to make $\nabla\cdot\overline{\boldsymbol{\xi}}=0$. Now, observe that the only explicit appearance of S occurs as $\mathbf{k}_\perp$ in the magnetic compressibility term which for $k_\perp a\gg 1$ tends to dominate the integrand. One is thus motivated to systematically minimize $\delta\overline{W}_F$ by expanding

$$\overline{\boldsymbol{\eta}}_\perp=\overline{\boldsymbol{\eta}}_{\perp 0}+\overline{\boldsymbol{\eta}}_{\perp 1}+\cdots \tag{12.18}$$

where $|\overline{\boldsymbol{\eta}}_{\perp 1}|/|\overline{\boldsymbol{\eta}}_{\perp 0}|\sim 1/k_\perp a$.

The zeroth-order contribution to $\delta\overline{W}_F$ reduces to

$$\delta\overline{W}_0=\frac{1}{2\mu_0}\int B^2|\mathbf{k}_\perp\cdot\overline{\boldsymbol{\eta}}_{\perp 0}|^2 d\mathbf{r} \tag{12.19}$$

Clearly the minimizing perturbation satisfies $\mathbf{k}_\perp\cdot\overline{\boldsymbol{\eta}}_{\perp 0}=0$, which implies that $\overline{\boldsymbol{\eta}}_{\perp 0}$ can be written as

$$\overline{\boldsymbol{\eta}}_{\perp 0}=Y\,\mathbf{b}\times\mathbf{k}_\perp \tag{12.20}$$

Here, $Y(\mathbf{r})$ is a scalar quantity varying on the slow equilibrium length scale.

The first non-vanishing contribution to $\delta\overline{W}_F$ occurs in second order. In this expression the only appearance of the quantity $\overline{\boldsymbol{\eta}}_{\perp 1}$ is in the magnetic compressibility term,

$$\delta\overline{W}_2(\text{comp})=\frac{1}{2\mu_0}\int B^2|i\mathbf{k}_\perp\cdot\overline{\boldsymbol{\eta}}_{\perp 1}+\nabla\cdot\overline{\boldsymbol{\eta}}_{\perp 0}+2\overline{\boldsymbol{\eta}}_{\perp 0}\cdot\boldsymbol{\kappa}|^2 d\mathbf{r} \tag{12.21}$$

Clearly $\delta\overline{W}_2$ is minimized by choosing $i\mathbf{k}_\perp\cdot\overline{\boldsymbol{\eta}}_{\perp 1}=-\nabla\cdot\overline{\boldsymbol{\eta}}_{\perp 0}-2\overline{\boldsymbol{\eta}}_{\perp 0}\cdot\boldsymbol{\kappa}$. The most unstable perturbations for localized modes characterized by $k_\perp a\gg 1$ do not produce any compression of the magnetic field.

The next step in the evaluation of $\delta\overline{W}_2$ is to simplify the quantity $\nabla \times (\overline{\boldsymbol{\eta}}_\perp \times \mathbf{B})_\perp$ as follows:

$$\begin{aligned} \nabla \times (\overline{\boldsymbol{\eta}}_\perp \times \mathbf{B})_\perp &= \nabla \times [YB(\mathbf{b} \times \mathbf{k}_\perp) \times \mathbf{b}]_\perp \\ &= \nabla \times (YB\nabla S)_\perp \\ &= (\nabla X \times \mathbf{k}_\perp)_\perp \end{aligned} \tag{12.22}$$

where $X(\mathbf{r}) = YB$. One now writes $\nabla X = \nabla_\perp X + (\mathbf{b} \cdot \nabla X)\mathbf{b}$. The quantity $\nabla_\perp X \times \mathbf{k}_\perp$ only has a non-vanishing contribution along $\mathbf{b}$ and thus does not make a contribution. The remaining term in $\nabla \times (\overline{\boldsymbol{\eta}}_\perp \times \mathbf{B})_\perp$ can then be expressed as

$$\nabla \times (\overline{\boldsymbol{\eta}}_\perp \times \mathbf{B})_\perp = (\mathbf{b} \cdot \nabla X)\, \mathbf{b} \times \mathbf{k}_\perp \tag{12.23}$$

This relation is substituted into the kink contribution to $\delta\overline{W}_2$ leading to

$$\begin{aligned} \delta\overline{W}_2(\text{kink}) &= -\frac{1}{2}\int J_\parallel (\overline{\boldsymbol{\eta}}^*_\perp \times \mathbf{b}) \cdot \nabla \times (\overline{\boldsymbol{\eta}}_\perp \times \mathbf{B})_\perp d\mathbf{r} \\ &= -\frac{1}{2}\int \frac{J_\parallel}{B}[X^*(\mathbf{b} \cdot \nabla X)][\mathbf{k}_\perp \cdot (\mathbf{b} \times \mathbf{k}_\perp)] d\mathbf{r} \\ &= 0 \end{aligned} \tag{12.24}$$

In the limit $k_\perp a \gg 1$ the kink term makes no contribution to ballooning mode instability.

The remaining terms in $\delta\overline{W}_2$ describe a competition between the stabilizing effects of line bending and the destabilizing effects of unfavorable curvature:

$$\delta\overline{W}_2 = \frac{1}{2\mu_0}\int \left[k_\perp^2 |\mathbf{b} \cdot \nabla X|^2 - \frac{2\mu_0}{B^2}(\mathbf{b} \times \mathbf{k}_\perp \cdot \nabla p)(\mathbf{b} \times \mathbf{k}_\perp \cdot \boldsymbol{\kappa})|X|^2\right] d\mathbf{r} \tag{12.25}$$

This is the desired general form of the potential energy for ballooning modes. The basic unknown is the single scalar variable $X(\mathbf{r})$ which varies on the equilibrium length scale. It is assumed that a function S and correspondingly $\mathbf{k}_\perp = \nabla_\perp S$ can be found since these quantities depend only on the equilibrium fields. Observe that the variation of the integrand leads to a differential equation in only one variable. The reason is that the only derivatives that appear are along a single direction, parallel to $\mathbf{B}$. The one-dimensional nature becomes explicit when specific coordinate systems are introduced for the tokamak and stellarator.

However, before proceeding with the analysis it is of interest to write down the corresponding ballooning mode equation for the double adiabatic model. The derivation closely follows the one given above and is left as an assignment in the Problems at the end of the chapter. The double adiabatic form for $\delta\overline{W}_2$ is derived from Eq. (10.27) and can be expressed as

$$\delta\overline{W}_2 = \frac{1}{2\mu_0}\int \left[k_\perp^2|\mathbf{b}\cdot\nabla X|^2 + \Omega|X|^2\right]d\mathbf{r}$$
$$\Omega = \frac{2\mu_0}{B^2}\left[-(\mathbf{b}\times\mathbf{k}_\perp\cdot\nabla p)(\mathbf{b}\times\mathbf{k}_\perp\cdot\boldsymbol{\kappa}) + p(\mathbf{b}\times\mathbf{k}_\perp\cdot\boldsymbol{\kappa})^2\left(\frac{7B^2+5\mu_0 p}{2B^2+4\mu_0 p}\right)\right] \tag{12.26}$$

There is again a stabilizing line bending term plus a modified driving term. As expected the additional driving term in Ω is always stabilizing, regardless of the sign of the curvature vector. In the low β, large aspect ratio limit the additional stabilizing term is nominally smaller by ε than the pressure gradient-curvature term, although the numerical factor of 7/2 may in practice make both terms comparable.

12.3 The ballooning mode equations for tokamaks

Equation (12.25) describes ballooning mode stability for an arbitrary 3-D geometry. To actually apply the equation one needs to specify a specific geometry and introduce a corresponding set of flux coordinates. Once this is done it is then possible to explicitly determine the eikonal function S plus $\mathbf{k}_\perp = \nabla S$. The ultimate result is a 1-D differential equation where the dependent variable is a measure of arc length along the magnetic field. In this subsection the ballooning mode differential equation is derived for tokamaks.

The analysis for the tokamak is somewhat simplified because the equilibrium is toroidally axisymmetric: $\partial/\partial\phi = 0$. Convenient flux coordinates for the calculation are $\psi(R,Z)$, $l(R,Z)$, ϕ, where ψ and ϕ have their usual meaning and l is poloidal arc length. Other forms of poloidal angle rather than l could be used and are equally valid, although the Jacobian J resulting from arc length is particularly simple, leading to a more transparent form of the ballooning mode equation.

The relevant equilibrium relations for the tokamak, derived in Chapter 6, are given by

$$\mathbf{B} = B_\phi\mathbf{e}_\phi + \mathbf{B}_p$$
$$B_\phi = \frac{F(\psi)}{R}$$
$$\mathbf{B}_p = \frac{1}{R}\nabla\psi\times\mathbf{e}_\phi \tag{12.27}$$
$$\boldsymbol{\kappa} = \mathbf{b}\cdot\nabla\mathbf{b}$$

The magnitude and direction of the poloidal arc length gradient are defined as

$$\nabla l\cdot\nabla\psi = 0$$
$$\mathbf{B}_p\cdot\nabla l = B_p \tag{12.28}$$

A practical method for calculating the flux coordinates is given in the Problems at the end of the chapter.

Two further equilibrium relations are needed to carry out the analysis. First, the transformation of the toroidal volume element to flux coordinates is given by

$$d\mathbf{r} = RdR\, dZd\phi = Jd\psi\, dl\, d\phi \tag{12.29}$$

where the Jacobian satisfies

$$\frac{R}{J} = \begin{vmatrix} \partial\psi/\partial R & \partial\psi/\partial Z & 0 \\ \partial l/\partial R & \partial l/\partial Z & 0 \\ 0 & 0 & 1 \end{vmatrix} = \nabla l \cdot \nabla\psi \times \mathbf{e}_\phi \tag{12.30}$$

From the equilibrium relations one sees that

$$J = \frac{1}{B_p} \tag{12.31}$$

The second relation of interest defines a set of mutually orthogonal unit vectors,

$$\begin{aligned} \mathbf{n} &= \frac{\nabla\psi}{|\nabla\psi|} = \frac{\nabla\psi}{RB_p} \\ \mathbf{b} &= \frac{B_p}{B}\mathbf{b}_p + \frac{B_\phi}{B}\mathbf{e}_\phi \\ \mathbf{t} &= \mathbf{n} \times \mathbf{b} = \frac{B_\phi}{B}\mathbf{b}_p - \frac{B_p}{B}\mathbf{e}_\phi \end{aligned} \tag{12.32}$$

Here, $\mathbf{b}_p = \mathbf{B}_p/B_p$. Note that $\mathbf{n}$ is a normal vector while $\mathbf{b}$ and $\mathbf{t}$ are tangential vectors lying in the flux surface, parallel and perpendicular to the equilibrium magnetic field respectively. All vectors appearing in the analysis are decomposed into these three components.

With this as background one can now start to simplify the ballooning mode equation. The first step is to evaluate the eikonal function S. Recall that $S(\psi,l,\phi)$ must satisfy two requirements: (1) it must produce rapid oscillations perpendicular to the field and (2) it must be constant along a field line, $\mathbf{B} \cdot \nabla S = 0$. For a general tokamak this last condition can be written as

$$\frac{B_\phi}{R}\frac{\partial S}{\partial \phi} + B_p \frac{\partial S}{\partial l} = 0 \tag{12.33}$$

Now, axisymmetry implies that Fourier analysis can be carried out with respect to ϕ. In other words the solution to Eq. (12.33) has the form $S = -n\phi + S_p(\psi, l)$. Rapid oscillation requires that the toroidal mode number n satisfy $n \gg 1$. With this form of S, Eq. (12.33) can be formally integrated, yielding

$$S = n\left(-\phi + \int_{l_0}^{l} \frac{B_\phi}{RB_p}\, dl\right) \tag{12.34}$$

where l_0 is a free integration constant whose determination is discussed shortly. Observe that on a rational surface (i.e. $m'q(\psi_0) = n'$), the function S is periodic in l over an appropriate number of complete poloidal transits, each of length $L(\psi)$:

$$\begin{aligned} S(\psi_0, l + m'L, \phi + 2\pi n') - S(\psi_0, l) &= n\left[-2\pi n' + m' \int_0^L \left(\frac{B_\phi}{RB_p}\right)_{\psi_0} dl\right] \\ &= 2\pi n[-n' + m'q(\psi_0)] \\ &= 0 \end{aligned} \tag{12.35}$$

and use has been made of Eq. (6.35), the general definition of $q(\psi)$. Off the rational surface, S is no longer periodic.

Knowing S one can next evaluate the perpendicular wave number appearing in the ballooning mode equation,

$$\begin{aligned} \mathbf{k}_\perp &= k_n \mathbf{n} + k_t \mathbf{t} = \nabla S \\ k_n &= \mathbf{n} \cdot \nabla S = (\mathbf{n} \cdot \nabla \psi) \frac{\partial S}{\partial \psi} = nRB_p \frac{\partial}{\partial \psi}\left(F \int_{l_0}^{l} \frac{dl}{R^2 B_p}\right) \\ k_t &= \mathbf{t} \cdot \nabla S = (\mathbf{t} \cdot \nabla \phi) \frac{\partial S}{\partial \phi} + (\mathbf{t} \cdot \nabla l) \frac{\partial S}{\partial l} = n \frac{B}{RB_p} \end{aligned} \tag{12.36}$$

Observe that the free constant l_0 is associated with the normal component of the wave number vector, k_n.

These expressions are substituted into the general ballooning mode equation (i.e., Eq. (12.25)). Two further simplifications should be noted. First, since the ϕ dependence has been Fourier analyzed and included in $S(\psi,l,\phi)$, this implies that $X(\psi,l,\phi) \rightarrow X(\psi,l)$. No further ϕ dependence is required. Second, because the ϕ dependence is automatically periodic by the form chosen for S, there is no need to extend the ϕ domain from $-\infty$ to $+\infty$. One can simply integrate over the single period $0 \leq \phi \leq 2\pi$. Therefore it follows that

$$\int d\phi = 2\pi \tag{12.37}$$

However, the integral over θ or equivalently l must be carried out over the extended domain.

The desired form of the ballooning mode potential energy can now be written as

$$\delta\overline{W}_2 = \frac{\pi}{\mu_0}\int_0^{\psi_a} \overline{W}(\psi,l_0)\,d\psi$$
$$\overline{W}(\psi,l_0) = \int_{-\infty}^{\infty}\left[(k_n^2+k_t^2)\left(\frac{B_p}{B}\frac{\partial X}{\partial l}\right)^2 - \frac{2\mu_0 RB_p}{B^2}\frac{dp}{d\psi}(k_t^2\kappa_n - k_t k_n\kappa_t)X^2\right]\frac{dl}{B_p} \tag{12.38}$$

Here, $\kappa_n = \mathbf{n}\cdot\boldsymbol{\kappa}$ is the normal curvature and $\kappa_t = \mathbf{t}\cdot\boldsymbol{\kappa}$ is the geodesic curvature (which is perpendicular to $\mathbf{B}$ but lies in the flux surface). After a short calculation these quantities can be rewritten in terms of the equilibrium fields and flux coordinates as

$$\kappa_n = \frac{\mu_0 RB_p}{B^2}\frac{\partial}{\partial\psi}\left(p+\frac{B^2}{2\mu_0}\right)$$
$$\kappa_t = \frac{\mu_0 F}{RB^3}\frac{\partial}{\partial l}\left(\frac{B^2}{2\mu_0}\right) \tag{12.39}$$

The final reasoning used to determine stability is based on the observation that the integrand in $W(\psi,l_0)$ has no ψ derivatives on X, only l derivatives. In other words, ψ, as well as l_0, are parameters in the integrand. Then, for fixed ψ and l_0, if one can find an l dependence of $X(\psi,l_0,l)$ that makes $\overline{W}(\psi,l_0) < 0$ it follows that a sufficiently localized trial function about the given ψ will in turn lead to $\delta\overline{W}_2 < 0$. The plasma is unstable. The major benefit of the ballooning mode analysis is that stability can be tested one flux surface at a time, which is a far simpler procedure than solving the coupled 2-D partial differential equations that arise in a general stability analysis.

The standard procedure to construct the $X(\psi,l_0,l)$ with the most unstable l dependence is to simply set the variation of $\overline{W}(\psi,l_0)$ with respect to l equal to zero. The result is the 1-D ballooning mode differential equation given by

$$\frac{\partial}{\partial l}\left[\frac{(k_n^2+k_t^2)B_p}{B^2}\frac{\partial X}{\partial l}\right] + \frac{2\mu_0 R}{B^2}\frac{dp}{d\psi}(k_t^2\kappa_n - k_t k_n\kappa_t)X = 0 \tag{12.40}$$

If the solutions decay sufficiently rapidly for $l = \pm\infty$, then Newcomb's procedure can be used to determine stability. Specifically, for a given ψ and l_0, Eq. (12.40) is integrated (usually numerically) from $l = -\infty$ to $l = +\infty$. If X has a zero crossing anywhere in the interval the plasma is unstable. On each flux surface this procedure must be carried out for a range of l_0 defined by $0 < l_0 < L(\psi)$ to find the most unstable l_0. Often, but not always, $l_0 = 0$ is the most unstable case. If there is no

zero crossing for all l_0 the plasma is stable to ballooning modes on the given flux surface. Complete stability against ballooning modes requires no zero crossings on any flux surface.

12.4 The ballooning mode equation for stellarators

The derivation of the ballooning mode equation for stellarators is similar to that of the tokamak. The analysis is conveniently carried out by introducing a set of generalized straight line field coordinates. The generalized coordinates become unique when a specific choice is made for the Jacobian. At the end of the derivation two specific examples are illustrated, corresponding to two choices for J: arc length and Boozer coordinates. Although the analysis applies to general 3-D configurations in some ways the details are simpler and more elegant than for the 2-D case. The complexity, however, is hidden in the difficulty of actually calculating and inverting the field line and laboratory coordinates.

The key equilibrium quantities derived in Chapter 7 that are required for the ballooning mode analysis are repeated here for convenience (see Eq. (7.251)). They include the representation of the magnetic field and an expression for the Jacobian in terms of the generalized flux coordinates, ψ, χ, ζ:

$$\begin{aligned} \mathbf{B} &= q\nabla\psi \times \nabla\chi - \nabla\psi \times \nabla\zeta \\ \frac{1}{J} &= \nabla\psi \times \nabla\chi \cdot \nabla\zeta \\ d\mathbf{r} &= J d\psi\, d\chi\, d\zeta \end{aligned} \tag{12.41}$$

Here, $q = q(\psi)$ is a flux function and the dependence on both χ and ζ is periodic with period 2π.

The derivation below is made simpler by a shift to straight field line coordinates defined by

$$\begin{aligned} \psi' &= \psi \\ \chi' &= \chi \\ \alpha' &= -\zeta + q(\psi)\chi \end{aligned} \tag{12.42}$$

In terms of the new coordinates the relevant equilibrium relations can be rewritten as

$$\begin{aligned} \mathbf{B} &= \nabla\psi \times \nabla\alpha \\ \frac{1}{J} &= \nabla\psi \times \nabla\alpha \cdot \nabla\chi \\ d\mathbf{r} &= J d\psi\, d\alpha\, d\chi \end{aligned} \tag{12.43}$$

where the primes have been dropped from ψ', α', χ'. Note that in accordance with the discussion in Section 7.7.6 the quantities ψ, α now serve as field line labels.

The quantity χ has the role of an extended variable analogous to poloidal arc length in the tokamak analysis.

The usefulness of this transformation is that the operator $\mathbf{B} \cdot \nabla$ reduces to the simple form

$$\mathbf{B} \cdot \nabla = \frac{1}{J} \frac{\partial}{\partial \chi} \tag{12.44}$$

Equation (12.44) implies that the eikonal function, which satisfies $\mathbf{B} \cdot \nabla S = 0$, must be of the form $S = S(\psi, \alpha)$. An appropriate choice that produces rapid oscillation while maintaining periodicity in ζ is given by

$$S(\psi, \alpha) = n[\alpha - \alpha_0(\psi)] \tag{12.45}$$

where n is an integer satisfying $n \gg 1$ and α_0 is a free function

Next, the unit vectors $\mathbf{n}$ and $\mathbf{t}$ are defined as

$$\begin{aligned} \mathbf{n} &= \frac{\nabla \psi}{|\nabla \psi|} \\ \mathbf{t} &= \frac{\nabla \alpha}{|\nabla \alpha|} \end{aligned} \tag{12.46}$$

Note that both $\mathbf{n}$ and $\mathbf{t}$ are perpendicular to $\mathbf{B}$ but in a 3-D geometry they are not in general orthogonal to each other: $\mathbf{n} \cdot \mathbf{t} \neq 0$. These definitions are used to decompose the perpendicular wave number $\mathbf{k}_\perp$ and curvature vector $\boldsymbol{\kappa}$ as follows:

$$\begin{aligned} \mathbf{k}_\perp &= \nabla S = \frac{\partial S}{\partial \psi} \nabla \psi + \frac{\partial S}{\partial \alpha} \nabla \alpha = k_\psi \nabla \psi + k_\alpha \nabla \alpha \\ \boldsymbol{\kappa} &= \kappa_\psi \nabla \psi + \kappa_\alpha \nabla \alpha \end{aligned} \tag{12.47}$$

with

$$\begin{aligned} k_\psi &= \frac{\partial S}{\partial \psi} = -n\alpha_0' \\ k_\alpha &= \frac{\partial S}{\partial \alpha} = n \\ \kappa_\psi &= \frac{1}{2B^2} \frac{\partial}{\partial \psi} \left(2\mu_0 p + B^2\right) \\ \kappa_\alpha &= \frac{1}{2B^2} \frac{\partial}{\partial \alpha} \left(B^2\right) \end{aligned} \tag{12.48}$$

Here, k_ψ, k_α are wave number-like quantities similar to k_n, k_t in the tokamak, but normalized differently. Similarly for κ_ψ, κ_α and κ_n, κ_t. The last quantity needed for

substitution into the ballooning mode potential energy is $\mathbf{b} \times \mathbf{k}_\perp$. A simple calculation leads to

$$\mathbf{b} \times \mathbf{k}_\perp = k_\psi \mathbf{b} \times \nabla\psi + k_\alpha \mathbf{b} \times \nabla\alpha \tag{12.49}$$

The above relations are now substituted into the 3-D expression for the ballooning mode potential energy given by Eq. (12.25). A straightforward calculation results in the desired form of the stellarator ballooning mode potential energy (see for instance Dewar and Glosset (1983) and Hegna and Nakajima (1998))

$$\begin{aligned} \delta\overline{W}_2 &= \frac{1}{2\mu_0}\int_0^{\psi_a}\int_0^{2\pi/q} \overline{W}(\psi,\alpha,\alpha_0)\, d\psi\, d\alpha \\ \overline{W}(\psi,\alpha,\alpha_0) &= \int_{-\infty}^{\infty}\left[\frac{k_\perp^2}{B^2J^2}\left|\frac{\partial X}{\partial\chi}\right|^2 - 2\mu_0\frac{dp}{d\psi}(k_\alpha^2\kappa_\psi - k_\alpha k_\psi \kappa_\alpha)|X|^2\right] J d\chi \end{aligned} \tag{12.50}$$

and the corresponding minimizing ballooning mode differential equation

$$\frac{\partial}{\partial\chi}\left(\frac{k_\perp^2}{B^2J}\frac{\partial X}{\partial\chi}\right) + 2\mu_0 J\frac{dp}{d\psi}(k_\alpha^2\kappa_\psi - k_\alpha k_\psi\kappa_\alpha)X = 0 \tag{12.51}$$

Observe that only the χ variable has to be extended over the infinite domain. The α variable has to vary only over one circuit (and not an infinite number of circuits) of the flux surface to ensure that stability is tested on every field line (with each field line identified by ψ, α). Equation (12.51) is quite similar conceptually to the tokamak equation given by Eq. (12.40), allowing stability to be tested one field line at a time.

The potential energy can be further reduced by choosing a specific J to make the field line coordinates unique. One simple choice is arc length corresponding to $J = 1/B$. For this case one relabels $\chi \to l$ and notes that $\mathbf{B}\cdot\nabla = B(\partial/\partial l)$. The potential energy now has the form

$$\overline{W}(\psi,\alpha,\alpha_0) = \int_{-\infty}^{\infty}\left[k_\perp^2\left|\frac{\partial X}{\partial l}\right|^2 - 2\mu_0\frac{dp}{d\psi}(k_\alpha^2\kappa_\psi - k_\alpha k_\psi\kappa_\alpha)|X|^2\right]\frac{dl}{B} \tag{12.52}$$

A second choice for J corresponds to Boozer coordinates: $J = (i_t - qi_p)/B^2$. In this case the potential energy can be written as

$$\overline{W}(\psi,\alpha,\alpha_0) = \frac{1}{(i_t - qi_p)}\int_{-\infty}^{\infty}\left[k_\perp^2\left|\frac{\partial X}{\partial\chi}\right|^2 - \frac{2\mu_0}{B^2}\frac{dp}{d\psi}(i_t - qi_p)^2(k_\alpha^2\kappa_\psi - k_\alpha k_\psi\kappa_\alpha)|X|^2\right] d\chi \tag{12.53}$$

Having derived several forms for the ballooning mode potential energy and ballooning mode differential equation, one can now proceed to investigate the criterion for sufficiently rapid convergence at $\chi = \pm\infty$ (or equivalently $l = \pm\infty$) and assuming the condition is satisfied, determine the critical β for stability. Most of the relevant analysis in the literature has focused on the tokamak geometry, and that is the strategy adopted here.

12.5 Stability of tokamaks – the Mercier criterion

12.5.1 Introduction

As has been discussed the ballooning mode formalism is valid only if the envelope function X decays sufficiently rapidly at $l = \pm\infty$. In this section the condition for sufficiently rapid decay is quantified leading to the Mercier criterion (Mercier, 1960), which turns out to be the toroidal analog of Suydam's criterion. Thus, the Mercier criterion examines interchange stability in a torus.

The analysis presented below follows the work of Connor *et al*. (1979) and proceeds in two steps. First, the condition for rapid decay is derived in the large aspect ratio cylindrical limit, thereby reproducing Suydam's criterion. The purpose of this calculation is to demonstrate how the ballooning mode formalism, in which the extended arc length l is the independent variable is related to the standard Suydam analysis where $x = r - r_0$ plays this role. It is easiest to understand this relationship in the familiar r, θ cylindrical geometry.

In the second step the analysis is repeated for the actual ballooning mode equation. For simplicity, the derivation focuses on the 2-D tokamak geometry where most of the practical applications have been carried out. Conceptually, the calculation is quite similar to the large aspect ratio cylinder, although the details are substantially more complicated because of the 2-D nature of the equilibrium. The end result is the Mercier criterion, which is valid for arbitrary β, ε and cross sectional shape. From a practical point of view, the Mercier criterion, when applied to tokamaks, leads to a minimum allowable $q(\psi)$ on axis. Several examples are discussed.

The basic strategy of both calculations is to examine the behavior of X for large l and to see whether the solutions are oscillatory or exponential. Oscillating solutions indicate that the ballooning mode formalism is not valid. However, such solutions violate the Mercier criterion, thus predicting instability. On the other hand, exponential solutions are Mercier stable implying that X decays sufficiently rapidly for large l for the ballooning mode equation to be valid. This equation must then be examined for ballooning mode stability which ultimately leads to a limit on β.

12.5.2 Cylindrical limit: the Suydam criterion

The starting point of the analysis is the axisymmetric ballooning mode potential energy given by Eq. (12.38). In the large aspect ratio cylindrical limit, which assumes that $R_0/a \to \infty$ and $\mu_0 p \sim B_\phi^2 \sim B_p^2$, the various quantities appearing in the integrand simplify to

$$\begin{aligned} R &\to R_0 \\ l &\to r\theta \\ \psi(r,\theta) &\to \psi(r) \\ J &\to 1/B_\theta(r) \end{aligned} \tag{12.54}$$

These limiting values in turn imply that

$$\begin{aligned} S &\to n[-\phi + q(r)(\theta - \theta_0)] \\ k_n &\to nq'(\theta - \theta_0) \\ k_t &\to nB/R_0 B_\theta \\ \kappa_n &\to -(B_\theta^2/B^2)(1/r) \\ \kappa_t &\to 0 \end{aligned} \tag{12.55}$$

where here and below prime denotes d/dr.

Equations (12.54) and (12.55) are substituted into Eq. (12.38) where, because of cylindrical symmetry, one can set $\theta_0 = 0$ without loss in generality. After a short calculation, the resulting expression for $\overline{W}$ reduces to

$$\frac{\overline{W}(r)}{W_0} = \int_{-\infty}^{\infty} \left[(\theta^2 + f)\left(\frac{\partial X}{\partial \theta}\right)^2 - D_S X^2 \right] d\theta \tag{12.56}$$

Here, $W_0 = n^2 q'^2 B_\theta / r B_z^2 > 0$, $f(r) = q^2/r^2 q'^2$, and $D_S = -2\mu_0 p' q^2 / r B_z^2 q'^2$. Note that D_S is Suydam's parameter as defined in Eq. (11.102). Also, with respect to θ, one sees that $f =$ constant.

The variational equation that determines the minimizing $X(\theta)$ for $\theta \to \pm\infty$ is easily obtained and is given by

$$\frac{d}{d\theta}\left(\theta^2 \frac{dX}{d\theta}\right) + D_S X = 0 \tag{12.57}$$

The solution can be written as

$$\begin{aligned} X &= c_1 |\theta|^{p_1} + c_2 |\theta|^{p_2} \\ p_{1,2} &= -\frac{1}{2} \pm \frac{1}{2}(1 - 4D_S)^{1/2} \end{aligned} \tag{12.58}$$

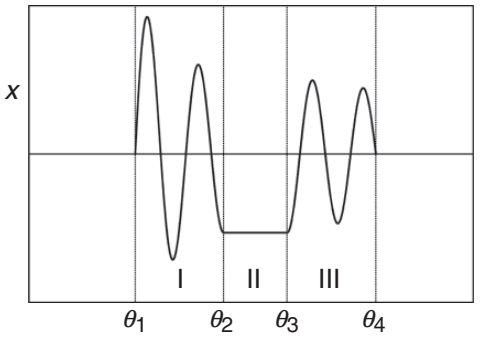

Figure 12.1 Trial function leading to the violation of Suydam's criterion.

Oscillatory solutions exist for $D_S > 1/4$. For this case $|X|^2 \propto 1/|\theta|$ leading to a logarithmic divergence of the potential energy integral. Such behavior is unphysical and implies that the convergence assumption used in the derivation of the ballooning mode equation is not valid. Even so, when $D_S > 1/4$ one can construct a truncated trial function as illustrated in Fig. 12.1, where X satisfies Eq. (12.58) in regions I and III and $X = X_0 =$ constant in region II. A simple calculation then shows that

$$\frac{\overline{W}(r)}{W_0} = -D_S X_0^2(\theta_3 - \theta_2) \tag{12.59}$$

Since $D_S > 1/4$ by assumption it follows that $\overline{W} < 0$ indicating instability. The condition $D_S > 1/4$ for instability is just Suydam's criterion.

It is interesting to observe that in the ballooning mode formalism Suydam's criterion arises from an analysis of X at large θ while in the standard analysis presented in Chapter 11 attention is focused on the localized behavior of ξ for small $x = r - r_0$. The two analyses are actually equivalent in that one is the Fourier transform of the other. To see this consider the standard analysis where the minimizing equation for ξ is given by (Eq. (11.103))

$$\frac{d}{dx}\left(x^2 \frac{d\xi}{dx}\right) + D_S \xi = 0 \tag{12.60}$$

Upon introducing the Fourier transform

$$X(k) = \int_{-\infty}^{\infty} \xi(x)\, e^{-ikx} dx \tag{12.61}$$

and assuming that ξ converges for large x (as it must for the truncated trial functions used in the derivation) one can easily show that X satisfies

$$\frac{d}{dk}\left(k^2 \frac{dX}{dk}\right) + D_S X = 0 \tag{12.62}$$

Now, when inverting the transform the integrand (including all dependences on angle) has the form

$$\xi(\mathbf{r}) = \frac{1}{2\pi}\int_{-\infty}^{\infty} X(k)\, e^{iS} dk \tag{12.63}$$

where the eikonal function S is given by

$$S = -n\phi + m\theta + kx \tag{12.64}$$

A comparison with Eq. (12.55) shows that in the vicinity of a rational surface defined by $r = r_0 + x$, the eikonal (with $\theta_0 = 0$) reduces to

$$S = -n\phi + nq(r_0)\theta + nq'(r_0)x\theta \tag{12.65}$$

Thus, one can identify $m = nq(r_0)$ and $k = q'(r_0)\theta$. Substituting into Eq. (12.62) then yields

$$\frac{d}{d\theta}\left(\theta^2 \frac{dX}{d\theta}\right) + D_S X = 0 \tag{12.66}$$

which is identical to Eq. (12.57).

The conclusion is that in the ballooning mode formalism the extended angle θ corresponds to the Fourier transform variable of the radius $x = r - r_0$ in real space. It is a well-known property of Fourier transforms that oscillatory behavior near $x \to 0$ in real space produces oscillatory behavior near $k \propto \theta \to \infty$ in transform space.

12.5.3 Toroidal geometry: the Mercier criterion

The derivation of the criterion for sufficiently rapid decay of X as $l \to \pm\infty$ in toroidal geometry is conceptually similar to the cylindrical case. Specifically, the general solution of the ballooning mode differential equation is examined for large l. Straightforward application of Newcomb's analysis (Section 11.5.3) shows that oscillatory behavior in l leads to instability. Non-oscillatory behavior is a necessary (but not sufficient) condition for stability. The transition point defines the Mercier criterion.

As has been stated, the Mercier criterion can be viewed as a quantification of the convergence requirement for the validity of the ballooning mode formalism. If the criterion is violated the ballooning mode potential energy has a logarithmic divergence at large l which is not allowed physically. Hence the ballooning mode formalism cannot be used. However, since the system is already unstable to Mercier interchange modes one need proceed no further. If the Mercier criterion is satisfied the system is stable to the interchange mode. In this case the

convergence requirements on X are satisfied and the ballooning mode equation can be used to test stability.

In carrying out the analysis for the toroidal geometry it will become apparent that the details are more complicated than for the cylindrical case because of the l dependence of the coefficients. Even so the critical feature of the analysis remains the same and involves the separation of the secular algebraic dependence of the coefficients from the periodic behavior. This allows a systematic asymptotic analysis of the solution for large l from which one can distinguish oscillatory from non-oscillatory behavior.

The derivation proceeds as follows. The starting point is the ballooning mode differential equation given by Eq. (12.40), which can be written as

$$\begin{aligned} &\frac{\partial}{\partial l}\left(f\frac{\partial X}{\partial l}\right) - gX = 0 \\ &f = \frac{(k_n^2 + k_t^2)B_p}{B^2} \\ &g = -\frac{2\mu_0 R}{B^2}\frac{dp}{d\psi}(k_t^2\kappa_n - k_t k_n \kappa_t) \end{aligned} \tag{12.67}$$

An examination of f and g indicates that the secular algebraic terms (i.e., those proportional to l^ν as $l \to \pm\infty$) appear only in the coefficient k_n. Specifically, from Eq. (12.36) one sees that secular terms appear in the integral

$$\begin{aligned} k_n &= nRB_p \int_{l_0}^{l} \frac{\partial Q}{\partial \psi} dl \\ Q(\psi, l) &= \frac{F(\psi)}{R^2 B_p} \end{aligned} \tag{12.68}$$

The secularity can be seen explicitly by recognizing that Q is periodic in l since it only depends on equilibrium quantities. Thus one can write $Q = \overline{Q}(\psi) + \tilde{Q}(\psi, l)$ where $\tilde{Q}$ has zero average value over $L(\psi)$, one poloidal circuit in l. Next, observe from the definition of $q(\psi)$ given by Eq. (6.35) that the relation between q and Q is given by

$$q(\psi) = \frac{1}{2\pi}\oint \overline{Q}\, dl = \frac{L(\psi)}{2\pi}\overline{Q}(\psi) \tag{12.69}$$

Using this relation in Eq. (12.68) leads to a simple expression for k_n in the limit $l \to \pm\infty$,

$$k_n = 2\pi n R B_p \left(\frac{1}{L}\frac{dq}{d\psi}\right) l \tag{12.70}$$

Equation (12.70) clearly exhibits a linear secular dependence on l.

After a straightforward calculation, the algebraic and periodic behavior in the coefficients f and g can be explicitly displayed by rewriting Eq. (12.67) as follows:

$$\begin{aligned}
&\frac{\partial}{\partial l}\left[\left(f_0\hat{l}^2+f_1\right)\frac{\partial X}{\partial l}\right]+\left(\frac{\partial g_0}{\partial l}\hat{l}+g_1\right)X=0\\
&\hat{l}(\psi,l)=\int_{l_0}^{l}\frac{\partial Q}{\partial \psi}\,dl\\
&f_0(\psi,l)=\frac{R^2B_p^3}{B^2}\\
&f_1(\psi,l)=\frac{1}{R^2B_p}\\
&g_0(\psi,l)=\frac{\mu_0 F}{B^2}\frac{dp}{d\psi}\\
&g_1(\psi,l)=\frac{\mu_0}{B^2B_p}\frac{dp}{d\psi}\frac{\partial}{\partial\psi}\left(2\mu_0 p+B^2\right)=\frac{2\mu_0}{RB_p^2}\frac{dp}{d\psi}\kappa_n
\end{aligned}\tag{12.71}$$

In this equation the coefficients f_0, f_1, g_0, g_1 are periodic functions of l. The quantity $\hat{l}(\psi,l)$ is valid for arbitrary l and exhibits secular behavior for large l: $\hat{l}\to(d\overline{Q}/d\psi)\,l$ as $l\to\infty$. In its present form Eq. (12.71) is still exact although obviously quite complicated.

The goal now is to calculate the asymptotic behavior of X as $l\to\infty$ in order to determine the threshold condition for oscillatory behavior. This goal is accomplished by exploiting the fact that $\hat{l}$ becomes large for large l, which suggests an asymptotic expansion for X of the form

$$X=l^{\nu}\left(X_0+\frac{X_1}{\hat{l}}+\frac{X_2}{\hat{l}^2}+\cdots\right)\tag{12.72}$$

Here, the $X_j(\psi,l)$ are assumed to be periodic functions of l with the equilibrium period $L(\psi)$. The parameter ν is the indicial coefficient determined in the course of solving Eq. (12.71). When ν is complex, then X oscillates for large l. If ν is real the solutions are non-oscillatory. The stability threshold which defines the Mercier criterion corresponds to the transition value of ν separating oscillatory and non-oscillatory behavior.

To determine ν Eq. (12.72) is substituted into Eq. (12.71). The result is a system of equations that can be written as a polynomial series in $\hat{l}$. By equating the coefficients of descending powers of $\hat{l}$ to zero and making use of appropriate periodicity constraints, one obtains the value of ν and the solutions for the X_j. To determine ν requires carrying out the analysis to second order (i.e., the X_2 level).

The leading-order equation corresponds to the highest power of $\hat{l}$, which is $\hat{l}^{\nu+2}$. This equation is given by

$$\frac{\partial}{\partial l}\left(f_0 \frac{\partial X_0}{\partial l}\right) = 0 \tag{12.73}$$

The solution that is bounded at $l = \pm\infty$ is simply

$$X_0 = 1 \tag{12.74}$$

The first-order equation corresponding to $\hat{l}^{\nu+1}$ can be written as

$$\frac{\partial}{\partial l}\left[f_0\left(\frac{\partial X_1}{\partial l} + \nu \frac{\partial Q}{\partial \psi}\right)\right] + \frac{\partial g_0}{\partial l} = 0 \tag{12.75}$$

This equation can be integrated yielding

$$\frac{\partial X_1}{\partial l} + \nu \frac{\partial Q}{\partial \psi} = \frac{G_0 - g_0}{f_0} \tag{12.76}$$

where $G_0(\psi)$ is a free integration function determined by requiring that X_1 be periodic. Thus, integrating Eq. (12.76) over one poloidal circuit yields

$$G_0 = \frac{\oint\left(\nu \frac{\partial Q}{\partial \psi} + \frac{g_0}{f_0}\right) dl}{\oint\left(\frac{1}{f_0}\right) dl} \tag{12.77}$$

The second-order equation is the last one necessary for the analysis and corresponds to $\hat{l}^{\nu}$. A short calculation leads to

$$\begin{aligned} &\frac{\partial}{\partial l}\left[f_0 \frac{\partial X_2}{\partial l} + (\nu - 1) f_0 X_1\right] \\ &\quad + (\nu + 1) f_0 \frac{\partial Q}{\partial \psi}\frac{\partial X_1}{\partial l} + \nu(\nu + 1) f_0 \left(\frac{\partial Q}{\partial \psi}\right)^2 + g_1 + \frac{\partial g_0}{\partial l} X_1 = 0 \end{aligned} \tag{12.78}$$

The solution for X_2 is not explicitly needed to determine the indicial coefficient ν. All that is required to determine ν is to integrate Eq. (12.78) over one poloidal circuit, assuming that X_2 is periodic. The result, after one simple integration by parts, is

$$\oint\left[(\nu + 1) f_0 \frac{\partial Q}{\partial \psi}\frac{\partial X_1}{\partial l} + \nu(\nu + 1) f_0 \left(\frac{\partial Q}{\partial \psi}\right)^2 + g_1 - g_0 \frac{\partial X_1}{\partial l}\right] dl = 0 \tag{12.79}$$

The expression for $\partial X_1/\partial l$ given by Eq. (12.76) is substituted into Eq. (12.79). After a slightly lengthy calculation one obtains the following equation for v:

$$v^2 + v + D_M = 0 \tag{12.80}$$

where D_M, the toroidal analog of the cylindrical Suydam parameter D_S, is a complicated expression that can be written as

$$\begin{aligned} D_M(\psi) = \frac{1}{4\pi^2 q'^2}\Bigg[& \left(\oint \frac{dl}{f_0}\right)\left(\oint g_1 dl\right) \\ & + \left(\oint \frac{dl}{f_0}\right)\left(\oint g_0^2 \frac{dl}{f_0}\right) - \left(\oint g_0 \frac{dl}{f_0}\right)^2 \\ & + \left(\oint \frac{\partial Q}{\partial \psi} dl\right)\left(\oint g_0 \frac{dl}{f_0}\right) - \left(\oint \frac{dl}{f_0}\right)\left(\oint g_0 \frac{\partial Q}{\partial \psi} dl\right)\Bigg] \end{aligned} \tag{12.81}$$

The roots of the indicial equation are

$$v = -\frac{1}{2} \pm \frac{1}{2}(1 - 4D_M)^{1/2} \tag{12.82}$$

In analogy with the Suydam criterion one sees that the transition from oscillatory to non-oscillatory behavior occurs for $D_M = 1/4$. Consequently, the Mercier criterion for interchange stability, which coincides with the criterion for validity of the ballooning mode differential equation, is given by

$$D_M < \frac{1}{4} \tag{12.83}$$

The derivation is completed by rewriting D_M in terms of physical variables as follows:

$$\begin{aligned} D_M &= \frac{\mu_0 p'}{q'^2}\left[2I(B^2)I(RB_p\kappa_n) + I(B^2)I(\Gamma/B^2) - I(1)I(\Gamma)\right] \\ \Gamma &= F\left(\mu_0 F p' - R^2 B_p^3 \frac{\partial Q}{\partial \psi}\right) \\ I(U) &= \frac{1}{2\pi}\oint \frac{dl}{R^2 B_p^3} U \end{aligned} \tag{12.84}$$

Here, prime denotes $d/d\psi$. Although the Mercier criterion involves a complicated expression, it is nonetheless a function only of the equilibrium quantities and can be tested one flux surface at a time. It must be satisfied on each surface to guarantee

interchange stability. In general, numerical calculations are required to test the Mercier criterion. However, there are some simple analytic limits that shed more insight into the physics and these are discussed next.

12.5.4 Analytic limits of the Mercier criterion

If one first takes the limit $\varepsilon \ll 1$, $\mu_0 p/B_\phi^2 \sim B_p^2/B_\phi^2 \sim 1$ then as expected the result is the cylindrical Suydam criterion,

$$\left(\frac{rq'}{q}\right)^2 + \frac{8\mu_0}{B_\phi^2} rp' > 0 \qquad \text{for stability} \tag{12.85}$$

Here, prime now denotes d/dr.

In contrast, if one assumes the tokamak ordering $\varepsilon \ll 1$, $\mu_0 p/B_\phi^2 \sim B_p^2/B_\phi^2 \sim \varepsilon^2$, and carries out the expansion carefully, then Eq. (12.85) is modified in an important way, leading to the large aspect ratio toroidal limit of the Mercier criterion. The result for a circular cross section plasma with $\beta_p \sim 1$ has been calculated by Ware and Haas (1966) and Shafranov and Yurchenko (1968). The modified stability criterion is given by

$$\left(\frac{rq'}{q}\right)^2 + \frac{8\mu_0}{B_\phi^2} rp'(1 - q^2) > 0 \qquad \text{for stability} \tag{12.86}$$

The expression is similar to Suydam's criterion except for the factor $(1 - q^2)$. The modification shows that for typical configurations with a negative pressure gradient, including the region near the axis, stability can be achieved if $q_0 > 1$. As previously shown in Chapter 11, Suydam's criterion always predicts a small region of instability near the axis.

The additional stability found in the torus is associated with the curvature of the toroidal magnetic field. On the inside of the torus ($\theta = \pi$) the toroidal field bends away from the plasma producing favorable curvature. The opposite is true on the outside ($\theta = 0$). The oscillation in curvature tends to average to zero with an interchange perturbation because such perturbations are nearly constant along a field line; in other words, there is essentially a uniform sampling of the curvature with an interchange perturbation.

However, to second order in ε there is a net favorable contribution to the average toroidal curvature that enters competitively with the poloidal field curvature. This can be seen qualitatively by noting that in the large aspect ratio limit

$$\boldsymbol{\kappa} \approx -\frac{B_\theta^2}{rB_0^2}\mathbf{e}_r - \frac{\mathbf{e}_R}{R} \tag{12.87}$$

Now, the normal component of $\boldsymbol{\kappa}$ is approximately given by $\kappa_n \approx \mathbf{e}_r \cdot \boldsymbol{\kappa}$ which can be written as

$$\begin{aligned}\kappa_n &\approx -\frac{B_\theta^2}{rB_0^2} - \frac{\cos\theta}{R_0}\left(1 - \frac{r}{R_0}\cos\theta + \cdots\right) \\ &\approx -\frac{B_\theta^2}{rB_0^2}\left(1 - \frac{q^2}{2}\right) - \frac{\cos\theta}{R_0} + \frac{r\cos 2\theta}{2R_0^2} + \cdots\end{aligned} \tag{12.88}$$

Observe that the toroidal curvature ($\sim 1/R_0$) is actually $1/\varepsilon$ larger than the poloidal curvature ($\sim B_\theta^2/R_0B_0^2$) under the usual assumption that $B_\theta/B_0 \sim \varepsilon$. Equation (12.88) implies that the last two terms tend to average to zero around one poloidal circuit. The remaining term has an additional stabilizing contribution equal to $(q^2/2)(B_\theta^2/rB_0^2)$.

The correct result, as given by Eq.(12.86), contains an extra factor of $q^2/2$ and requires a surprisingly lengthy calculation. All of the terms in the Mercier criterion must be maintained as well as the small toroidal shift of the flux surfaces. The more careful averaging with the correct weight factors indicates that the net average curvature is favorable when $q > 1$.

For tokamaks, which are usually characterized by low β and finite shear, the rq'/q in Mercier's criterion dominates over most of the profile. However, near the origin the shear is small and it is in this region that the criterion is most easily violated. The conclusion then is that the Mercier criterion basically sets a limit on the minimum q_0.

The value of the minimum q_0 depends on geometry. For circular flux surfaces, as stated above, $q_0 > 1$. The case of non-circular flux surfaces near the axis has been investigated by a number of authors: Solov'ev *et al.* (1969), Laval *et al.* (1971), Lortz and Nuhrenberg (1973), Mikhailovskii and Shafranov (1974), and Mikhailovskii (1974). Their results can be summarized as follows. For non-circular cross sections, the on-axis stability criterion $1 < q_0^2$ is replaced by

$$1 < q_0^2\left\{1 - \frac{4}{1+3\kappa^2}\left[\frac{3}{4}\frac{\kappa^2-1}{\kappa^2+1}\left(\kappa^2 - \frac{2\delta}{\varepsilon}\right) + \frac{(\kappa-1)^2\beta_{p0}}{\kappa(\kappa+1)}\right]\right\} \tag{12.89}$$

where κ is the elongation, $\beta_{p0} = -\mu_0 p''(0)/B_\theta'^2(0)$ is the poloidal beta on axis, δ is the triangularity, $\varepsilon = r_0/R_0$ is the inverse aspect ratio of the flux surface of interest, and the axis corresponds to the limit $r_0 \to 0$. Note that in this limit δ/ε remains finite. The geometric interpretation of κ, δ, ε is illustrated in Fig. 12.2.

Observe the following points. For cross sections with zero elongation ($\kappa = 1$), triangularity and finite β_{p0} have no effect on the stability boundary. Elongation by itself ($\kappa > 1$, $\delta = \beta_{p0} = 0$) is destabilizing. However, a combination of elongation

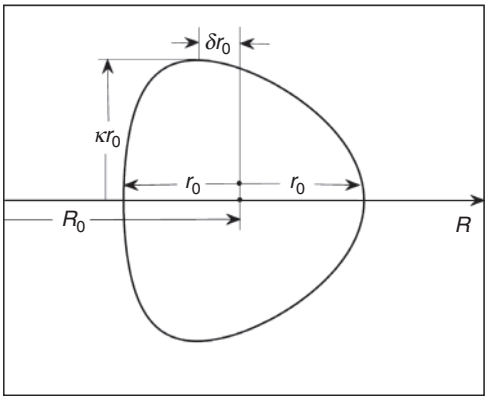

Figure 12.2 Geometry defining κ, δ, and r_0/R_0 in a non-circular tokamak. Note that $\delta > 0$ corresponds to an outward pointing triangle.

and sufficient outward pointing triangularity ($\kappa > 1$, $\delta/\varepsilon > \kappa^2/2$, $\beta_{p0} = 0$) is stabilizing. For any elongation the effect of β_{p0} is destabilizing. Here stabilizing corresponds to a lower value of the minimum q_0.

The improved stability associated with elongated "D" shapes is related to the fact that for such cross sections a magnetic line has a relatively large fraction of its trajectory located in the favorable curvature region on the inside of the torus.

12.5.5 Summary

In summary the Mercier criterion represents one limit on the maximum allowable value of $J_{\phi 0} \propto 1/q_0$ on axis in a toroidal tokamak. For sufficiently high q_0 the average curvature of a field line becomes favorable. Thus, a negative pressure gradient on axis, which is always unstable in the straight cylinder, is stabilized in a torus. As with the Suydam criterion, a Mercier interchange perturbation by itself is unlikely to be important in an actual experiment. However, because of the oscillation theorem, the presence of localized interchange instabilities implies that more dangerous large-scale instabilities are also very likely to exist. Lastly, if a plasma is stable with respect to the Mercier criterion, then the ballooning mode differential equation is valid and can be used to test ballooning mode stability.

12.6 Stability of tokamaks – ballooning modes

12.6.1 Introduction

In this subsection it is assumed that the Mercier criterion is satisfied. The task then is to solve the ballooning mode differential equation with the goal of determining the critical β for stability against ballooning modes. As a general feature, note that ballooning modes can occur almost anywhere in the profile, wherever the pressure

gradient is sufficiently steep. Even so, ballooning modes most often do not set the most severe limits on β – these are set by external ballooning-kink modes.

Nevertheless, one area where ballooning modes may be particularly important is near the plasma boundary where there are sharp edge gradients, most often arising in H-mode operation. As described in Chapter 11, MHD instabilities, usually called peeling–ballooning modes, are believed to play an important role in the excitation of edge localized modes (ELMs) (Snyder *et al.*, 2005). The peeling contribution is due to the gradient in the current density and has been qualitatively described by the straight tokamak model. The ballooning contribution, on the other hand, requires a toroidal calculation, namely the solution to the ballooning mode differential equation.

A simple, well-known model is introduced that provides good physical insight into the behavior of ballooning modes near the plasma edge. The quasi-analytic investigation of this model yields a relation between the critical β and the shear. More accurately, the relation involves a limit, not on β, but on $\beta q^2/\varepsilon \sim p/I^2$. In principle, one could then achieve stability against ballooning modes at high pressures by operating at high current (i.e., low q). Ballooning mode stability does not require high q operation since the kink term vanishes in the large n expansion. In addition to the simple analytic model a description is presented of more extensive numerical studies which gives rise to a general ballooning mode stability boundary known as the "Sykes limit."

Mathematically, the marginal stability boundaries can be obtained by Newcomb's analysis. One integrates the ballooning mode differential equation from $-\infty < l < \infty$ assuming that $X(l = -\infty)$ starts off with the small, square integrable branch of the solution. If any zero crossings in X occur before $l = +\infty$, the plasma is unstable. An alternate approach is to introduce a convenient normalization and then compute the corresponding eigenvalue (basically proportional to ω^2). Stability is determined by the sign of the eigenvalue. In both methods, stability must be tested separately for all ψ and l_0.

12.6.2 The s–α model for ballooning modes

Reduction of the general ballooning mode equation

A relatively simple model that provides insight into the behavior of ballooning modes is the large aspect ratio, circular cross section tokamak with a special choice of equilibrium profiles as illustrated in Fig. 12.3 (Connor *et al.*, 1979). The critical feature of the profile is that the average value of the global β is assumed to be small ($\beta \sim \varepsilon^2$) although the local β' in a narrow layer near the plasma edge is larger by $1/\varepsilon$: $r_0\beta' \sim \varepsilon$ near $r \approx r_0$.

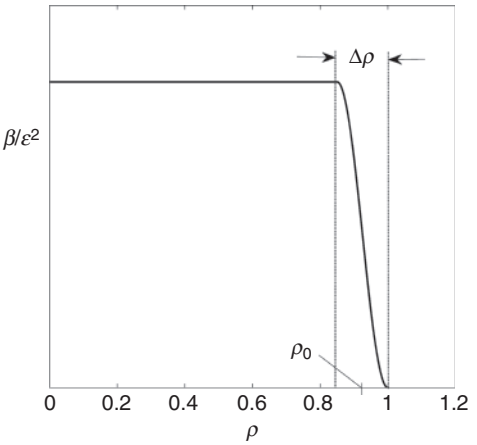

Figure 12.3 Simple $\beta(r)$ profile used in the analytic study of the ballooning mode. Here, $\rho = r/a$.

This equilibrium leads to a great simplification in the analysis. When $\beta \sim \varepsilon^2$ the flux surface shifts are small and most quantities assume their cylindrical values. Even so, there remains a small edge region where $r_0\beta'$ is sufficiently large to drive ballooning mode instabilities. From a practical point of view this is a pessimistic profile in that the global β is small while high $r_0\beta'$ ballooning modes can still be excited. On the positive side the model is quite reliable for developing qualitative insight because of its analytic simplicity.

The analysis begins with the reduction of the general tokamak ballooning mode equation given by Eq. (12.71) which is exact. The coefficients f_0, f_1, g_0, g_1 as well as $\hat{l}$ must all be evaluated using the large aspect ratio expansion. As implied by Eq. (12.71) several of these quantities are easily evaluated using simple cylindrical limits:

$$\begin{aligned} f_0 &= \frac{R_0^2 B_\theta^3}{B_0^2} \\ f_1 &= \frac{1}{R_0^2 B_\theta} \\ g_1 &= -\frac{2\mu_0}{R_0^3 B_\theta^3}\frac{dp}{dr}\cos\theta \end{aligned} \tag{12.90}$$

Here, $l = r\theta$ and $r \approx r_0 =$ constant describes the flux surface of interest. Also, in g_1 use has been made of the approximation $\kappa_n \approx -(1/R_0)\cos\theta$. The only curvature that enters is due to the toroidal field.

Slightly more care is required to evaluate g_0 and $\hat{l}$. The coefficient g_0 must be calculated to first order since the leading order contribution is only a function of r

while the quantity actually required is $\partial g_0/\partial l = (1/r)(\partial g_0/\partial\theta)$. This evaluation is carried out by noting that, correct to first order in ε, $B \approx B_\phi = F/R$. Thus, from Eq. (12.71) one finds

$$g_0 \approx \left(\frac{\mu_0}{F}\frac{dp}{d\psi}\right)R^2 \approx \left(\frac{\mu_0}{F}\frac{dp}{d\psi}\right)(R_0^2 + 2R_0 r\cos\theta) \tag{12.91}$$

Since $p(\psi)$ and $F(\psi)$ are constant on a flux surface it follows that

$$\frac{\partial g_0}{\partial l} \approx -\left(\frac{2\mu_0}{R_0 B_0 B_\theta}\frac{dp}{dr}\right)\sin\theta \tag{12.92}$$

Consider now $\hat{l}$ which involves a poloidal integral of $Q(\psi,l) = F(\psi)/R^2 B_p$. There is a zeroth-order contribution plus a first order contribution arising from the ε expansion. One of the nominally first-order contributions actually produces a zeroth-order effect when the local pressure gradient is large and it is only this contribution that must be maintained. To identify the contribution examine the expansion of the terms that appear in $\hat{l}$:

$$\hat{l}(\psi,l) = \int_{l_0}^{l}\frac{\partial Q}{\partial\psi}\,dl \approx \frac{\partial}{\partial\psi}\left[F(\psi)\int_{\theta_0}^{\theta}\frac{(r_0 + r_1\cos\theta)d\theta}{(R_0^2 + 2R_0 r_0\cos\theta)(B_{\theta 0} + B_{\theta 1}\cos\theta)}\right] \tag{12.93}$$

The expansion takes place around the flux surface $r \approx r_0 + r_1\cos\theta$. Most of the correction terms in Eq. (12.93) are small by ε and can be neglected. However, the term with $B_{\theta 1}$ contains a first (radial) derivative of the perturbed flux function: $B_{\theta 1} \propto \psi'_1(r_0)$. While this term by itself is small its derivative with respect to r_0 in the edge layer is large since it results in a contribution to $\hat{l}$ proportional to dp/dr_0. Specifically, the term is larger by $1/\varepsilon$ than the other correction terms because of the large edge gradient assumption. It thus becomes competitive with the zeroth-order term.

The total zeroth-order contribution to $\hat{l}$ reduces to

$$\hat{l}(\psi,l) \approx \frac{\partial}{\partial\psi}\left[\frac{F r_0}{R_0^2 B_{\theta 0}(r_0)}\int_{\theta_0}^{\theta}\left(1 - \frac{B_{\theta 1}}{B_{\theta 0}}\cos\theta\right)d\theta\right] \tag{12.94}$$

If one now recalls that $B_\theta = (1/R)(\partial\psi/\partial r)$ then a short calculation shows that Eq. (12.94) simplifies to

$$\hat{l}(\psi,l) \approx \frac{1}{R_0 B_{\theta 0}}\frac{d}{dr_0}\left[q(r_0)(\theta - \theta_0) - \frac{q(r_0)}{R_0 B_{\theta 0}}\frac{d\psi_1}{dr_0}(\sin\theta - \sin\theta_0)\right] \tag{12.95}$$

The final form is obtained by substituting for ψ''_1 from Eq. (6.65): $\psi''_1 \approx -2\mu_0 r_0 p'/B_{\theta 0}$ plus smaller corrections which are neglected. For the case

$\theta_0 = 0$, which, although not proven, turns out to be the most unstable case, the expression for $\hat{l}$ reduces to

$$\hat{l}(r,\theta) \approx \frac{1}{R_0 B_\theta}\left(\frac{dq}{dr}\theta + \frac{2\mu_0 q\, r}{R_0 B_\theta^2}\frac{dp}{dr}\sin\theta\right) \tag{12.96}$$

where the subscript zero has been suppressed from r_0

The above results are substituted into Eq. (12.71) leading to the desired form of the simplified ballooning mode equation (Connor *et al.*, 1979):

$$\begin{aligned} &\frac{\partial}{\partial\theta}\left[(1+\Lambda^2)\frac{\partial X}{\partial\theta}\right] + \alpha(\Lambda\sin\theta + \cos\theta)X = 0 \\ &\Lambda = s\theta - \alpha\sin\theta \\ &s = \frac{r}{q}\frac{dq}{dr} \\ &\alpha = -\frac{2\mu_0 r^2}{R_0 B_\theta^2}\frac{dp}{dr} = -q^2 R_0\frac{d\beta}{dr} \end{aligned} \tag{12.97}$$

with $\beta(r) = 2\mu_0 p(r)/B_0^2$. Note that $s(r)$ is the magnetic shear while $\alpha(r)$ is a parameter that measures the pressure gradient and scales as $\beta_t q^2/\varepsilon$. The terms with the θ derivatives represent the effects of line bending. The $\alpha\cos\theta$ term represents the effect of the normal curvature, favorable on the inside ($\theta = \pi$) and unfavorable on the outside ($\theta = 0$). The remaining $\alpha\sin\theta$ term represents the effect of the geodesic curvature. The range of θ is $-\infty < \theta < \infty$ and $X(\theta)$ is required to vanish at both $\theta \to \pm\infty$. Although Eq. (12.97) cannot be solved purely analytically it has the advantage of depending only upon two parameters, s and α. As stated previously, there is no separate dependence on the safety factor that would prevent low q operation since the kink term vanishes in the ballooning mode expansion.

Solution

The solution to Eq.(12.97) is easily obtained numerically. A typical marginally stable quasi-mode perturbation (for $-\infty < \theta < \infty$) and the corresponding full mode perturbation (for $0 < \theta < 2\pi$) are illustrated in Fig. 12.4 as well as a sketch of a perturbed plasma flux surface exhibiting a ballooning mode instability. As previously stated the quasi mode has small oscillations superimposed on a decaying envelope. The full eigenfunction, obtained by summing up shifted quasi-modes, is indeed periodic as required.

The main quantitative result of the numerical solutions is a curve of marginal stability in s, α space and is illustrated in Fig. 12.5. Observe that there are two branches in the diagram. The left branch separates the first region of stability from

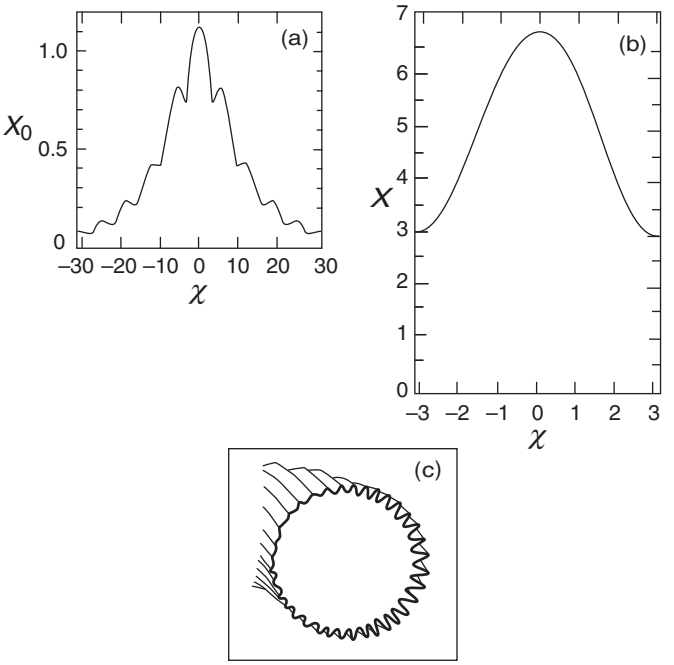

Figure 12.4 Ballooning mode perturbation: (a) quasi-mode, (b) full eigenfunction, and (c) ballooning mode perturbation in physical space.

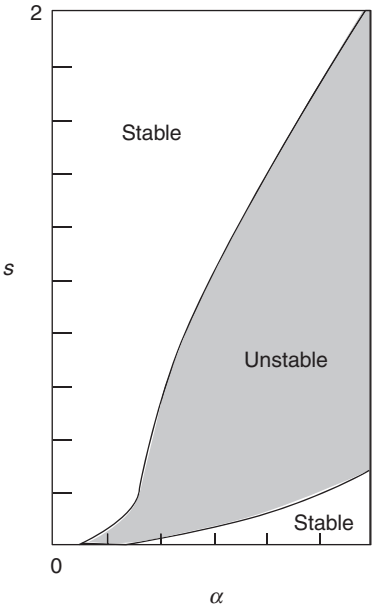

Figure 12.5 The s vs. α marginal stability diagram for the analytic ballooning mode model. From Lortz, 1973. Reproduced with permission from Elsevier.

the unstable region and is consistent with the intuition that has been developed for the behavior of ballooning modes. Specifically, at a fixed value of shear the plasma is stable for sufficiently small pressure gradients. As the pressure gradient (i.e., α) increases the perturbation develops a progressively larger ballooning component. Eventually, at sufficiently large α the destabilizing contribution from the unfavorable curvature region overcomes the shear and the system becomes unstable. As expected, when the shear increases the maximum allowable pressure gradient also increases.

A surprising feature of the s, α diagram is the second curve on the right which separates the unstable region from the so-called second region of stability (Coppi, 1977; Connor *et al.*, 1979; Greene and Chance, 1981). In this region stability is achieved when the pressure gradient becomes sufficiently large! Interestingly, this region is most easily accessed at low values of shear. This behavior is counter-intuitive but can be explained as follows. From Eq. (12.97) it follows that a local (in θ) shear $\hat{s}(r,\theta)$ can defined by

$$\Lambda(r,\theta) \equiv \int_0^\theta \hat{s}\, d\theta \tag{12.98}$$

where

$$\hat{s}(r,\theta) = s(r) - \alpha(r)\cos\theta \tag{12.99}$$

Here $s(r)$ represents the average shear and $\alpha(r)\cos\theta$ is the local pressure driven modulation. Now, as the pressure gradient increases from zero the local shear in the unfavorable curvature region ($\theta = 0$) initially decreases, thereby increasing instability. However, as the pressure gradient further increases so that $\alpha > s$ the shear becomes large and negative in the region of unfavorable curvature. Since shear stabilization is proportional to $\hat{s}^2$ this produces a stabilizing effect in the unfavorable curvature region. Although the local shear becomes zero somewhere near the inside of the torus ($\pi/2 < \theta < \pi$) this is not critical since the curvature is favorable in this region.

For a number of years considerable effort has been devoted to creating plasmas that operate at very high β in the second region of stability. The results have not been completely convincing in that they have mainly been achieved during transient operation. This is because access to the second stability region is sensitive to profile and shape. Equally importantly, other external resistive wall ballooning-kink instabilities are excited at lower values of β and would require successful feedback control before second stability operation could become accessible. Still, second stability is an interesting physical phenomenon that may still play some operational role, particularly near the plasma edge in connection with ELMs.

12.6.3 β limits due to ballooning modes

Predictions from the s–α *diagram*

It is worth noting that because of its simplicity the s, α diagram is sometimes used as a local criterion valid at all plasma radii and not just the edge. This clearly violates the original assumptions used in its derivation but, perhaps fortuitously, still gives reasonable scaling predictions for the global critical β for stability. Below a simple calculation based on the analytic model is presented that predicts the global critical β. The results are then compared to a much more comprehensive numerical study that includes finite aspect ratio and plasma shape.

The admittedly poorly justified local application of the s, α diagram can be used to predict global stability as follows. It is assumed that the plasma relaxes to a state that is marginally stable to the first stability boundary in the s, α diagram over the entire pressure profile. For simplicity this boundary can be reasonably well approximated by the simple relation $\alpha = Ks$ where $K \approx 0.6$. The approximation is valid over most of the plasma except near the origin. Therefore, at every radius in the plasma the pressure gradient satisfies

$$-R_0 \frac{d\beta}{dr} = K \frac{r}{q^3} \frac{dq}{dr} \tag{12.100}$$

One now multiplies Eq. (12.100) by r^2 and integrates over the plasma volume. A short calculation yields

$$\beta_t = \frac{K\varepsilon}{2} \left(-\frac{1}{q_a^2} + 3 \int_0^1 \frac{\rho^2}{q^2} d\rho \right) \tag{12.101}$$

where $\rho = r/a$ and

$$\beta_t \equiv 2 \int_0^1 \beta \rho d\rho \tag{12.102}$$

is the global average beta.

The critical value of β_t can be calculated by choosing a profile for $q(\rho)$ and carrying out the integration. A convenient choice that makes the integration simple is

$$q(\rho) = q_0(1 + \sigma\rho^3) \tag{12.103}$$

Here, the parameter σ is related to q_a/q_0 by $q_a/q_0 = 1 + \sigma$. The $q(\rho)$ profile is flat near the axis (i.e., a broad current profile) and increases monotonically towards the outside of the plasma. The resulting β_t limit is easily evaluated and can be written as

$$\beta_t = 0.3\frac{\varepsilon}{q_0^2}\left[\frac{q_0}{q_a}\left(1-\frac{q_0}{q_a}\right)\right] = 0.3\varepsilon\left[\frac{1}{q_a}\left(1-\frac{1}{q_a}\right)\right] \tag{12.104}$$

The second expression corresponds to the interesting case $q_0 = 1$. Observe that the critical β_t increases linearly with the current for large q_a: $\beta_t \approx 0.3\varepsilon/q_a \propto I$. For much larger current the critical β_t starts to decrease. The optimum for arbitrary q_0 occurs at $q_a/q_0 = 2$ and gives $\beta_t = 0.075\varepsilon/q_0^2$.

For typical tokamak parameters, $\varepsilon = 1/3$, $q_0 = 1$, $q_a = 3$, Eq. (12.104) predicts $\beta_t = 2.2\%$. As is shown shortly this value is perhaps fortuitously similar to realistic diffuse profile numerical calculations.

A final point worth noting is that if one substitutes the simple analytic profiles into the double adiabatic model the result is a stabilizing correction whose magnitude can be easily estimated in terms of the potential energies as follows:

$$\delta\overline{W}_{CGL} = \delta\overline{W}_{MHD}\left[1 + O\left(\varepsilon\frac{\Delta r}{a}\right)\right] \tag{12.105}$$

The conclusion is that the corrections are small implying that ideal MHD provides a good estimate of ballooning mode stability.

Numerical studies of ballooning mode stability

Many numerical codes have been developed to study ideal MHD equilibrium and stability. These codes contain an equilibrium Grad–Shafranov solver valid for arbitrary β, ε, and cross section. They can treat either fixed or free boundary configurations. General profiles are allowed and usually $p(\psi)$ and one of $F(\psi)$, $q(\psi)$, or $\langle J_\phi(\psi)\rangle$ are specified. Once an equilibrium is calculated the following stability tests can be made: (1) Mercier criterion; (2) high n ballooning modes; (3) low-n internal modes; and (4) external ballooning-kink modes.

Such studies, while time consuming, provide a complete and detailed picture of tokamak stability. They are very helpful in the design of new experiments and in the interpretation and analysis of existing experimental data. These studies also play a major role in the determination of optimized configurations and are ultimately able to make quantitative predictions for the maximum β_t and q_* that can be stably maintained in MHD equilibrium.

Many of the stability studies have been analyzed and merged, the end result being a surprisingly simple picture of overall tokamak stability. One such study involves ballooning modes. The main results have been assembled, unified, and expanded in the well-known calculations of Sykes and Wesson (1974) and Sykes *et al*. (1983). The problem addressed here is to determine the optimum tokamak profiles that achieve the maximum stable β_t against ballooning modes.

In these studies the safety factor is always set to $q_0 = 1.05$ to ensure stability against low-n internal kinks. Different q profiles are examined by varying the plasma current $I \propto 1/q_*$ For a given q profile the amplitude and shape of the pressure profile is varied iteratively until the maximum β_t is found. In the optimized state the profiles are essentially marginally stable to ballooning modes on every surface and satisfy the Mercier criterion on axis. This optimization procedure is carried out for different shaped cross sections.

The end result has a simple form. The maximized β_t for all cases studied is accurately represented by the Sykes limit,

$$\begin{aligned} \beta_t &= \beta_N \frac{I}{aB_0} \\ \beta_N &= 0.044 = 4.4\% \end{aligned} \tag{12.106}$$

where the units are I (MA), a (m), and B_0 (T), and β_N is the standard notation for the numerical coefficient multiplying I/aB_0. When β_N is given as a % then β_t also converts from a decimal to a percentage. An alternate form of Eq. (12.106) can be written as

$$\beta_t = 0.22\left(\frac{1+\kappa^2}{2}\right)\frac{\varepsilon}{q_*} \tag{12.107}$$

There are several points to observe. Equation (12.107) implies that high β_t is achieved by operating at high I/B_0. Clearly though, from a physical point of view one would not expect this relation to hold as $I \to \infty$, $B_0 \to 0$. In practice two additional non-ballooning factors limit the maximum ratio of I/B_0. First, as I/B_0 increases the flux surfaces near the axis become highly elongated causing violation of the Mercier criterion. As previously discussed, outward triangularity helps alleviate this problem although not indefinitely. Second, for sufficiently large I/B_0 external kink modes are excited, even at low β_t. Even so, the linear relation between β_t and I is valid over a reasonably wide practical parameter range.

Putting aside the question of external kink stability and assuming Mercier stable profiles, Sykes *et al.* (1983) discovered that the scaling given in Eq. (12.107) persists at moderate triangularity ($\delta = 0.24$) down to the low value of $q_* \approx 1.4$ for $\kappa = 2$. As an example, for $\kappa = 2$, $q_* = 1.5$, and $\varepsilon = 1/3$, one finds $\beta_t \approx 12\%$, a very encouraging value if achievable.

One final slightly puzzling feature of the Sykes limit is the fact that the relation between β_t and $1/q_* \sim I$ is linear and not quadratic as one would expect from the basic scaling relations for the high β tokamak ordering. In fact there is an implied quadratic scaling in the Sykes limit that has been masked since q_0 has been held fixed at a value near unity. Indeed, a comparison of Eq. (12.107) with Eq. (12.104)

suggests that the Sykes limit may actually scale as $\beta_t \propto \varepsilon/q_0 q_*$ (after noting that $q_a = q_*$ for the simple model profiles).

12.6.4 Summary

Ballooning modes are high n MHD instabilities that tend to localize near the outside of the torus in the region of unfavorable curvature. They may be particularly important in driving ELMs in H-mode operation because of the high edge pressure and current gradients. In the first region of stability the maximum β_t is limited by a maximum κ to avoid violating the Mercier criterion and by a minimum q_* to avoid external kink modes.

12.7 Stability of tokamaks – low n internal modes

12.7.1 Introduction

Localized high n internal MHD modes set a limit on β due to ballooning instabilities and a limit on q_0 due to interchange instabilities. The q_0 limit is approximately consistent with the current density limit on axis which, if violated, leads to the development of sawtooth oscillations. Still, because of their highly localized structure coupled with the corresponding high m and n mode numbers, interchange instabilities are not believed to be the main drive for sawtooth oscillations.

Instead, there is a large amount of experimental evidence that indicates that sawtooth oscillations have a macroscopic mode structure characterized by a low $m = 1$, $n = 1$ mode structure. These observations motivate an analysis of low n internal modes in a tokamak including the effect of toroidicity. In this connection recall that the corresponding analysis in the straight tokamak shows that $q_0 > 1$ is required for stability.

It is shown below that toroidal effects play an important role in the ideal MHD stability of low n internal modes. There are two qualitatively different regimes of interest which are distinguished by the amount of magnetic shear near the axis. The first corresponds to finite shear while the second corresponds to very small shear. Although a complete picture of the ideal MHD stability of low n is now well in hand, actual theoretical predictions of sawtooth behavior require the inclusion of resistivity, two-fluid effects, and non-linear simulations. Even with these more sophisticated models there is still not an entirely self-consistent explanation of all aspects of sawtooth behavior. This remains an area of active research with more work to be done.

In spite of these uncertainties, if one takes a step back it still remains true that the stability of low n internal ideal MHD modes play an important role in determining the approximate onset condition for sawtooth oscillations. These conditions are described below.

12.7.2 Low n internal modes with finite shear

Since low n internal modes have a large-scale radial structure the stability boundaries can often only be determined by numerical calculations. However, an interesting analytic calculation has been carried out by Bussac *et al*. (1975) that sheds considerable light on the problem. Their calculation considers the limit of a large aspect ratio, circular cross section tokamak. By applying the low β tokamak expansion, $\beta \sim \varepsilon^2$, $\beta_p \sim 1$, $q \sim 1$ they are able to calculate an expression for δW_F for the toroidal case which shows how toroidicity modifies the stability criterion for low n modes.

To put their analysis into perspective it is useful to briefly review the results of the straight tokamak. The analysis of the $m = 1$ mode in Chapter 11 has shown that δW_F for a straight tokamak, which uses the same low β expansion as Bussac *et al*., can be written as (see Eqs. (11.176) and (11.178))

$$\begin{aligned}
\frac{\delta W_F}{W_0} &= \varepsilon^2 \delta\hat{W}_2 + \varepsilon^4 \delta\hat{W}_4 + \cdots \\
W_0 &= \frac{2\pi^2 R_0 B_0^2}{\mu_0 a^2} \\
\delta\hat{W}_2 &= \int_0^a \left(\frac{n}{m} - \frac{1}{q}\right)^2 r^2 \xi'^2 \, r dr \\
\delta\hat{W}_4 &= \int_0^{r_1} \left[r\beta' + \frac{n^2 r^2}{R_0^2}\left(1 - \frac{1}{nq}\right)\left(3 + \frac{1}{nq}\right)\right] r dr
\end{aligned} \tag{12.108}$$

where the resonant surface r_1 is defined by $nq(r_1) = 1$ and without loss in generality the unimportant amplitude scale factor ξ_0 has been set to $\xi_0 = 1$. The reason why the fourth-order correction, $\delta\hat{W}_4$, is required is that $\delta\hat{W}_2$ vanishes for the "top hat" trial function illustrated in Fig. 11.27. Therefore, $\delta\hat{W}_4$ is the first non-vanishing contribution, which is always negative (unstable) if $nq_0 < 1$.

Now, observe that toroidal effects, which could be neglected if $\delta\hat{W}_2 \neq 0$ but not when $\delta\hat{W}_2 = 0$, also enter the analysis in the ε^4 order and are competitive with the cylindrical corrections. Using the same "top hat" trial function Bussac *et al*. again find that $\delta\hat{W}_2 = 0$ but that $\delta\hat{W}_4$ is modified by toroidal effects. After a rather involved calculation too complicated to reproduce here, Bussac *et al*. derive a modified expression for $\delta\hat{W}_4$ that can be schematically written as

$$\frac{\delta W_F}{W_0} = \varepsilon^4 \left[\left(1 - \frac{1}{n^2}\right)\delta\hat{W}_{4C} + \frac{1}{n^2}\delta\hat{W}_{4T} \right] \tag{12.109}$$

Here, $\delta\hat{W}_{4C}$ is the cylindrical contribution shown in Eq. (12.108) and $\delta\hat{W}_{4T}$ is the toroidal modification. This modification is quite complicated for general profiles.

However, in the sawtooth relevant limit $|q_0 - 1| \ll 1$, $q_0 < 1$, with a parabolic current density profile, a simple expression is obtained, given by

$$\delta\hat{W}_{4T} \approx \frac{3n^2 r_1^4}{R_0^2}(1 - q_0)\left(\frac{13}{144} - \beta_p^2\right)$$
$$\beta_p = -\frac{R_0^2}{n^2 r_1^2}\int_0^{r_1} r^2 \beta' \, dr \tag{12.110}$$

Note that for $n \gg 1$, $\delta W_F / W_0 \approx \varepsilon^4 \delta\hat{W}_{4C}$ and the stability condition is identical to that in the straight tokamak: $nq_0 > 1$. In the more interesting and restrictive case corresponding to $n = 1$, the cylindrical contribution vanishes and all that remains is the toroidal modification: $\delta W_F / W_0 \approx \varepsilon^4 \delta\hat{W}_{4T}$. Here, in contrast to the cylindrical result, the internal kink mode is stabilized by toroidal effects in the limit $\beta_p \to 0$, $q_0 < 1$. For both the cylindrical and toroidal contributions, increasing β_p is destabilizing. For the $n = 1$ mode the toroidal calculation predicts instability for $\beta_p > (13)^{1/2}/12 \approx 0.3$. Lastly, be aware that one cannot achieve stability at high β_p by setting for $q_0 > 1$ since $q_0 < 1$ is a requirement for the top hat trial function that makes $\delta\hat{W}_2 = 0$.

The physical phenomena at play in Eq. (12.110) involve a competition between the average curvature, which is unfavorable near the axis if $q_0 < 1$, and the toroidal correction to line bending which is a stabilizing effect.

12.7.3 *Low* n *internal modes with small shear*

Wesson and Sykes (1974) have pointed out that the low β_p stabilization of the $m = 1$, $n = 1$ mode is a strong function of the shear near the axis. Quantitatively, in deriving the stability criterion in Eq. (12.110) it has been assumed that near the $q(r_1) = 1$ resonant surface the quantity $1 - q_0$ can be approximated by

$$1 - q(r) \approx -q'(r_1)(r - r_1) \tag{12.111}$$

Critically, for a system with finite shear it is further assumed that at the radius r_1, the following ordering applies:

$$r_1 \, q'(r_1) \sim 1 \tag{12.112}$$

This is the definition of "finite" shear.

Wesson and Sykes observed that many tokamaks actually have a very flat $q(r)$ profile within the $q(r_1) = 1$ resonant surface. For sufficient flatness it would then be a better approximation to assume that

$$r \, q'(r_1) \sim \varepsilon \tag{12.113}$$

This is the definition of "low" shear.

Under this assumption the previous analysis, which allowed one to write $\delta W_F/W_0 = \varepsilon^2\delta W_2 + \varepsilon^4\delta\hat{W}_4$, breaks down. The reason is that $\varepsilon^2\delta\hat{W}_2$ actually becomes an ε^4 contribution and must be treated competitively with the other cylindrical and toroidal terms. The uniform shift, top hat trial function is no longer the most unstable perturbation. Instead, analysis shows that the most unstable trial function has a much smoother profile having the approximate form of an interchange perturbation. In fact the mode is often referred to as a quasi-interchange instability.

As might be expected, in the regime of low shear, line bending is substantially reduced as compared to the finite shear case. The end result is that one again requires

$$q_0 > 1 \tag{12.114}$$

for stability.

12.7.4 Summary

To summarize, low n internal modes can be excited in a tokamak when $q_0 < 1$. This conclusion, based on the simple model described above, is confirmed in more accurate numerical simulations. Since the instability requires the existence of a $q = 1$ resonant surface in the plasma one does not expect non-circularity to significantly alter the $q_0 = 1$ stability condition, particularly in low-shear systems. The $m = 1$, $n = 1$ internal mode is quite possibly the initial drive for sawtooth oscillations although the actual phenomenon requires more sophisticated physical models plus non-linear simulations for a quantitative explanation of experimental results. Sawtooth oscillations, which limit the current density on axis, are usually not very harmful to tokamak operation. The main concern involves the situation where the q profile is very flat and the $q = 1$ surface occurs a considerable distance out from the axis. Then the non-linear rearrangement of pressure and magnetic flux might have the opportunity to interact with the first wall, an undesirable situation.

12.8 Stability of tokamaks – low n external ballooning-kink modes

12.8.1 Introduction

Low n external ballooning-kink modes are the most dangerous instabilities in a tokamak. If exited, these modes invariably lead to major disruptions. Thus, it is critical to learn how to avoid such modes. As the name implies, the corresponding eigenfunctions are composed of contributions from both the pressure gradient (i.e., ballooning) and parallel current (i.e., kinking) terms in δW_F. For comparison recall that pure high n ballooning modes are driven solely by the pressure gradient term. The kink term vanishes.

The practical consequences of this difference in driving terms are as follows. Ballooning modes actually produce a limit on the ratio $p/I^2 \sim \varepsilon\beta_p$. In principle, to achieve high pressures one could operate at very high currents, equivalent to very low q values, and still be stable against pure ballooning modes. In contrast, low n ballooning-kink modes produce a limit on both p/I^2 and $I/B_0 \sim 1/q_*$, the latter limit arising from the presence of the kink term. In general, there is an optimum I/B_0 at which to operate if the goal is to maximize p/B_0^2.

Another important feature of ballooning-kink modes is the need to distinguish between q_a and q_*. In a low $\beta \sim \varepsilon^2$ circular cross section plasma $q_a \approx q_*$ so there is no need to make this distinction. However, in the high $\beta \sim \varepsilon$ regime the values of q_a and q_* diverge and one must learn which parameter is most relevant for determining ballooning-kink stability. The analysis presented here shows that q_* is the more important parameter.

Lastly, it is worth pointing out that one important advantage of the tokamak configuration is that stability at finite pressures and finite currents is possible without the presence of a perfectly conducting wall. For comparison, recall that an RFP always requires a conducting wall to stabilize external kink modes even when the pressure is zero.

To summarize, the study of low n external ballooning-kink modes shows that there is a maximum stable value of $\beta_t q_*^2/\varepsilon$ which occurs at a specific optimized value of q_*. These limits are finite and reactor relevant even with the conducting wall at infinity.

To help demonstrate the behavior of external ballooning-kink modes described above, three calculations are presented. The first shows how the general expression for δW_F, which is a function of the two components of $\boldsymbol{\xi}_\perp$, can be reduced to a form involving only a single scalar unknown $U(r,\theta)$ by applying the large aspect ratio, high β tokamak expansion. Not surprisingly, the reduced form is simpler than the original δW_F. More importantly it shows that in contrast to the high n pure ballooning analysis, the kink term survives in the expansion. It is this term that sets a separate limit on q_* in addition to the $\beta_t q_*^2/\varepsilon$ limit set by the pressure gradient term.

Even the reduced form of δW_F is still too complicated to obtain a quantitative analytic estimate of the stability limits using smooth simple profiles. This motivates the second calculation which makes use of the ultra-simple surface current model. In most of the analysis thus far presented realistic smooth current and pressure profiles have been assumed without the need for surface currents. Thus, when evaluating the total potential energy for these realistic cases, $\delta W_S = 0$. However, for the problem of interest the surface current model is perhaps the only one that is sufficiently simple to predict an explicit analytic stability boundary in the form of a β_t/ε vs. q_* curve. In addition, the surface current analysis shows in a clear way the presence of both the pressure gradient and kink driving terms. The final results give the correct scaling relations but are slightly

optimistic with respect to numerical values obtained from more complete computational studies.

In fact it is these computational studies that represent the third contribution to the study of ballooning-kink modes. Exhaustive numerical studies have been carried out to determine the pressure and current limits in toroidal tokamaks with no assumptions made about the size of β_t, ε, or the shape of the plasma cross section. These studies lead to another remarkably simple stability result known as the "Troyon limit" (Troyon *et al.*, 1984). This and follow-on numerical results are discussed at the end of this subsection.

12.8.2 Simplification of δW_F by the high β tokamak expansion

In general, the evaluation of the potential energy for external modes requires the evaluation of three contributions: $\delta W = \delta W_F + \delta W_S + \delta W_V$. The surface and vacuum terms depend only on the value of the normal component of displacement on the plasma surface: $\mathbf{n} \cdot \boldsymbol{\xi}_\perp(S)$. The fluid contribution is more complicated. Even after setting $\nabla \cdot \boldsymbol{\xi} = 0$ to minimize plasma compressibility, the remaining integrand in δW_F is still a function of the two vector components of $\boldsymbol{\xi}_\perp$. The goal now is to show how the integrand in δW_F can be written in terms of a single scalar $U(r,\theta)$ by introducing the high β tokamak expansion. The starting point is the intuitive form of δW_F for incompressible displacements given by Eq. (8.100) and repeated here for convenience:

$$\delta W_F(\boldsymbol{\xi}^*, \boldsymbol{\xi}) = \frac{1}{2\mu_0} \int_P \Big[|\mathbf{Q}_\perp|^2 + B^2 |\nabla \cdot \boldsymbol{\xi}_\perp + 2\boldsymbol{\xi}_\perp \cdot \boldsymbol{\kappa}|^2 - 2\mu_0 (\boldsymbol{\xi}_\perp \cdot \nabla p)(\boldsymbol{\xi}_\perp^* \cdot \kappa) - \mu_0 J_\parallel \boldsymbol{\xi}_\perp^* \times \mathbf{b} \cdot \mathbf{Q}_\perp \Big] d\mathbf{r} \tag{12.115}$$

Recall now that the basic ordering assumptions defining the high β tokamak expansion are given by $\beta \sim \varepsilon$, $q \sim 1$, $B_p/B_\phi \sim \varepsilon$, and $\delta B_\phi / B_\phi \sim \varepsilon$. With respect to the terms appearing in the integrand, this ordering implies that

$$\begin{aligned} \boldsymbol{\xi}_\perp &\sim 1 \\ \mathbf{Q}_\perp &\sim \varepsilon \\ p &\sim \varepsilon \\ \boldsymbol{\kappa} &\sim \varepsilon \\ J_\parallel &\sim \varepsilon \end{aligned} \tag{12.116}$$

The crucial difference compared to the ballooning mode analysis is that the toroidal mode number is ordered as

$$n \sim 1 \tag{12.117}$$

rather than $n \gg 1$ and having $1/n$ serve as a small expansion parameter.

However, as with the ballooning mode analysis, the dominant term is still due to magnetic compressibility and is of order unity whereas all other terms are of order ε^2. Since magnetic compressibility is always stabilizing the most unstable perturbations must be chosen to make this term as close to zero as possible. This can be accomplished by expanding the various terms appearing in the integrand as follows:

$$\begin{aligned}
\boldsymbol{\xi}_\perp &= (\boldsymbol{\xi}_{p0} + \boldsymbol{\xi}_{p1} + \cdots) + (\xi_{\phi 1} + \cdots)\,\mathbf{e}_\phi \\
\mathbf{B} &= (B_0 + B_{\phi 1} + \cdots)\,\mathbf{e}_\phi + (\mathbf{B}_{p1} + \cdots) \\
\boldsymbol{\kappa} &= -\frac{\mathbf{e}_R}{R_0} + \cdots \\
\nabla &= \nabla_p + \frac{\mathbf{e}_\phi}{R_0}\frac{\partial}{\partial \phi} + \cdots
\end{aligned} \tag{12.118}$$

Here, the subscript p refers to the poloidal (r, θ) plane and the numerical subscripts define the order in ε. Also, the condition that $\boldsymbol{\xi}_\perp$ be perpendicular to $\mathbf{B}$ requires that $\xi_{\phi 1} = -(\mathbf{B}_{p1} \cdot \boldsymbol{\xi}_{p0})/B_0$.

This ordering leads to a simplification of the magnetic compressibility term. Specifically, one can write

$$\nabla \cdot \boldsymbol{\xi}_\perp + 2\boldsymbol{\xi}_\perp \cdot \boldsymbol{\kappa} = \nabla_p \cdot \boldsymbol{\xi}_{p0} + \left(\nabla_p \cdot \boldsymbol{\xi}_{p1} - \frac{2}{R_0}\boldsymbol{\xi}_{p0} \cdot \mathbf{e}_R\right) + \cdots \tag{12.119}$$

The leading-order contribution to magnetic compressibility can be made to vanish by choosing

$$\boldsymbol{\xi}_{p0} = \mathbf{e}_\phi \times \nabla_p U \tag{12.120}$$

which implies that

$$\nabla_p \cdot \boldsymbol{\xi}_{p0} = \frac{1}{R_0}\nabla_p U \cdot \mathbf{e}_Z \sim \varepsilon \tag{12.121}$$

Here, $U = U(r,\theta)\exp(-in\phi)$ and except where obviously required the factor $\exp(-in\phi)$ is suppressed. The scalar quantity $U(r,\theta)$ is the basic unknown in the problem and defines the two components of $\boldsymbol{\xi}_{p0}$. All the remaining terms in δW_F can be written as functions of $U(r,\theta)$ to the required order in ε^2.

Note that $\boldsymbol{\xi}_{p1}$ appears only in the residual magnetic compressibility term which is also of order ε^2. This stabilizing contribution can also be made to vanish by choosing $\boldsymbol{\xi}_{p1}$ to satisfy

$$\nabla_p \cdot \boldsymbol{\xi}_{p1} = \frac{2}{R_0}\boldsymbol{\xi}_{p0} \cdot \mathbf{e}_R - \frac{1}{R_0}\nabla_p U \cdot \mathbf{e}_Z = \frac{1}{R_0}\nabla_p U \cdot \mathbf{e}_Z \tag{12.122}$$

The end result is that magnetic compressibility effects play no role in external ballooning-kink instabilities in a high β tokamak.

The desired form of δW_F for the high β tokamak is obtained by substituting Eq. (12.120) into the remaining terms in Eq. (12.115). A simple calculation yields

$$\delta W_F(U^*,U) = \frac{1}{2\mu_0}\int_P \left[|\mathbf{Q}_p|^2 + 2\mu_0 \frac{dp}{d\psi}(\mathbf{B}_p\cdot\nabla_p U)\frac{\partial U^*}{\partial Z} - \mu_0 J_\parallel \nabla_p U^*\cdot\mathbf{Q}_p\right] d\mathbf{r} \tag{12.123}$$

where, for convenience, the subscript "1" has been suppressed from $\mathbf{B}_p$. The poloidal component of $\mathbf{Q}_\perp$ requires a short calculation which leads to

$$\begin{aligned} \mathbf{Q}_p &= \mathbf{e}_\phi \times \left[\mathbf{B}\cdot\nabla(\nabla_p U)\right] - \left[(\mathbf{e}_\phi\times\nabla_p U)\cdot\nabla_p\right]\mathbf{B}_p \\ \mathbf{B}\cdot\nabla &= -in\frac{B_0}{R_0} + \mathbf{B}_p\cdot\nabla_p \end{aligned} \tag{12.124}$$

Observe that the reduced δW_F is considerably simpler than its original form. There are fewer terms and only a single unknown perturbation quantity $U(r,\theta)$. The three contributions to ballooning-kink stability are due to line bending, the pressure gradient, and the parallel current. Even though δW_F is simplified it is still too complicated to analyze for diffuse profiles because the system is essentially two dimensional (r,θ) with no further obvious small parameters about which to expand. In general, 2-D numerical solutions are required for both equilibrium and stability. There is, however, one special equilibrium that can be treated analytically and that is the surface current model which is the next topic of interest.

12.8.3 High β stability of the surface current model

The surface current model describes a particularly simple MHD equilibrium that still contains sufficient physics to describe the stability of external ballooning-kink modes in a high β tokamak (Freidberg and Haas, 1973). The goal of the analysis presented below is to derive the maximum stable value of β/ε as a function of q_*. Five steps are required. First, the surface current equilibrium is calculated including the equilibrium β limit. Second, the surface energy δW_S is evaluated for a ballooning-kink perturbation, demonstrating the effects of both the curvature and kink driving terms. Third, the fluid energy is calculated using the simplified high β tokamak form of δW_F. Fourth, the vacuum energy δW_V is evaluated which, perhaps surprisingly, requires the most amount of work. The total potential energy $\delta W = \delta W_F + \delta W_S + \delta W_V$ is then minimized with respect to the ratio of the ballooning to kink driving terms. This is an easy calculation from which it is then straightforward to calculate the maximum stable β. The analysis proceeds as follows.

Surface current equilibrium

To keep the algebra to a minimum the high β tokamak of interest is assumed to have a circular cross section. In terms of profiles, all the plasma current, as its name implies, flows on the plasma surface. Therefore, in the plasma the poloidal magnetic field is zero, the toroidal magnetic field has a vacuum dependence proportional to $1/R$, and the pressure is a constant. Mathematically this is equivalent to

$$\begin{aligned} \mathbf{B} &= B_i \frac{R_0}{R} \mathbf{e}_\phi \\ p &= \text{constant} \end{aligned} \tag{12.125}$$

where $B_i =$ constant represents the amplitude of the internal toroidal magnetic field on the axis $R = R_0$. Equation (12.125) trivially satisfies the MHD equilibrium equations.

In the vacuum region there is both a poloidal and toroidal magnetic field and zero pressure. The toroidal field also has a vacuum $1/R$ dependence. The poloidal magnetic field has a more complicated behavior arising from the non-uniform distribution of surface currents plus external sources, for example vertical field coils. Therefore, in the vacuum the equilibrium quantities can be written as

$$\begin{aligned} \hat{\mathbf{B}} &= B_0 \frac{R_0}{R} \mathbf{e}_\phi + \mathbf{B}_p(r,\theta) \\ p &= 0 \end{aligned} \tag{12.126}$$

where B_0 is the applied toroidal field at $R = R_0$.

The complete poloidal field requires a complicated calculation. Fortunately, for the surface current stability analysis only the poloidal field on the surface is required. This quantity can be easily determined from the pressure balance jump condition across the surface: $2\mu_0 p + B^2 = \hat{B}^2$. Specifically, for a circular plasma the poloidal field on the surface has the form $\mathbf{B}_p(a, \theta) = B_\theta(\theta)\mathbf{e}_\theta$ and satisfies

$$2\mu_0 p + B_i^2 \frac{R_0^2}{R^2} = B_0^2 \frac{R_0^2}{R^2} + B_\theta^2 \tag{12.127}$$

Here, $R(\theta) = R_0(1 + \varepsilon \cos\theta)$ and as usual $\varepsilon = a/R_0$.

In its present form Eq. (12.127) is exact – no aspect ratio expansion has been assumed. The next step is to assume that $\varepsilon \ll 1$ and to introduce the high β tokamak ordering. The appropriate expansion is given by

$$\begin{aligned} \frac{2\mu_0 p}{B_0^2} &\equiv \beta \sim \varepsilon \\ \frac{B_\theta^2}{B_0^2} &\sim \varepsilon^2 \\ \frac{B_i^2}{B_0^2} &\equiv 1 - \beta + b_2, \quad b_2 \sim \varepsilon^2 \end{aligned} \tag{12.128}$$

The quantity b_2 is a new constant replacing B_i and must be chosen as second order in ε to be consistent with the expansion. The first non-trivial contribution to the pressure balance relation occurs in second order and yields a simplified expression for $B_\theta^2(\theta)$,

$$\left(\frac{B_\theta}{\varepsilon B_0}\right)^2 = \frac{b_2}{\varepsilon^2} + 2\frac{\beta}{\varepsilon}\cos\theta = \frac{4\beta}{\varepsilon k^2}\left(1 - k^2\sin^2\frac{\theta}{2}\right) \tag{12.129}$$

where $k^2 = 4\varepsilon\beta/(b_2 + 2\varepsilon\beta)$ is yet another new constant replacing b_2 and ordered as $k^2 \sim 1$. In physical terms the value of k^2 can be related to the plasma current and pressure by means of the familiar definition

$$q_* = \frac{2\pi a^2 B_0}{\mu_0 R_0 I} = \varepsilon B_0\left(\frac{1}{2\pi}\int_0^{2\pi} B_\theta\, d\theta\right)^{-1} \tag{12.130}$$

The integral can be evaluated in terms of elliptic integrals yielding a transcendental relation for k given by

$$\left[\frac{k}{E(k)}\right]^2 = \frac{16}{\pi^2}\frac{\beta q_*^2}{\varepsilon} \tag{12.131}$$

Observe that similar to the diffuse profile case there is an equilibrium β limit which, from Eq. (12.129), corresponds to $k^2 = 1$. A higher value of k^2 leads to negative B_θ^2, which is unphysical. Since $E(1) = 1$ one sees from Eq. (12.131) that the equilibrium limit, which corresponds to the separatrix moving onto the plasma surface at $\theta = \pi$, can be written as

$$\frac{\beta q_*^2}{\varepsilon} \le \frac{\pi^2}{16} \approx 0.62 \tag{12.132}$$

The required equilibrium information has now been derived, enabling the stability analysis to proceed.

Evaluation of δW_S

The stability analysis begins with the evaluation of the surface energy δW_S whose exact form is given by Eq. (8.101)

$$\delta W_S = \frac{1}{2\mu_0}\int_S |\mathbf{n}\cdot\boldsymbol{\xi}_\perp|^2\mathbf{n}\cdot\left[\!\left[\nabla\left(\mu_0 p + \frac{B^2}{2}\right)\right]\!\right] dS \tag{12.133}$$

The integrand can be cast in a more convenient form for evaluation by using the general equilibrium relation

$$\nabla\left(\mu_0 p + \frac{B^2}{2}\right) = \mathbf{B}\cdot\nabla\mathbf{B} = B^2\boldsymbol{\kappa} + \mathbf{b}(\mathbf{B}\cdot\nabla B) \tag{12.134}$$

Then, a short calculation that makes use of the surface current pressure balance relation, allows one to rewrite the surface energy in terms of the plasma and vacuum curvature vectors, $\boldsymbol{\kappa}$ and $\hat{\boldsymbol{\kappa}}$ respectively,

$$\delta W_S = \frac{1}{2\mu_0}\int_S |\mathbf{n}\cdot\boldsymbol{\xi}_\perp|^2\left[2\mu_0 p\left(\frac{\hat{\kappa}_n+\kappa_n}{2}\right)+\left(\frac{\hat{B}^2+B^2}{2}\right)(\hat{\kappa}_n-\kappa_n)\right]dS \quad (12.135)$$

where $\kappa_n = \mathbf{n}\cdot\boldsymbol{\kappa}$ is the normal component of the curvature.

At present this form of δW_S is exact. Note that there are two contributions. The first involves the plasma pressure multiplied by the average curvature across the surface. This is ballooning mode drive for instabilities. The second contribution involves the average magnetic pressure multiplied by the jump in curvature across the surface. The jump in curvature is proportional to the parallel current flowing on the surface. Hence, this is the kink mode drive for instabilities. Both drives are clearly and explicitly exhibited in the surface current model, one of its advantages.

The expression for δW_S can be further simplified by introducing the high β tokamak expansion into the curvature coefficients. The curvatures need to be evaluated to first and second order. A straightforward calculation yields

$$\begin{aligned}\kappa_n &= -\frac{\cos\theta}{R_0}(1-\varepsilon\cos\theta)\\ \hat{\kappa}_n &= -\frac{\cos\theta}{R_0}(1-\varepsilon\cos\theta)-\frac{B_\theta^2}{aB_0^2}\end{aligned} \quad (12.136)$$

The surface energy reduces to

$$\delta W_S = -\frac{\pi a^2 B_0^2}{\mu_0 R_0}\int_0^{2\pi}|\mathbf{n}\cdot\boldsymbol{\xi}_\perp|^2\left[\frac{\beta}{\varepsilon}\cos\theta+\left(\frac{B_\theta}{\varepsilon B_0}\right)^2\right]d\theta \quad (12.137)$$

As expected the pressure gradient term is destabilizing on the outside of the cross section ($\theta = 0$) and stabilizing on the inside ($\theta = \pi$). The kink term is destabilizing around the entire cross section.

To complete the evaluation of δW_S one must specify $\mathbf{n}\cdot\boldsymbol{\xi}_\perp = \xi(\theta)$ on the plasma surface. A general form can be written in terms of a Fourier series as follows:

$$\xi(\theta) = \sum_{-\infty}^{\infty}\xi_m e^{im\theta} \quad (12.138)$$

With the advantage of hindsight from numerical calculations it is possible to choose a reduced form of Eq. (12.138) that contains only three harmonics, $m = 1,2,3$, but provides an accurate approximation to the infinite harmonic

solution. The $m = 1$ harmonic ξ_1 is shown to be dominant at low β/ε with the ξ_2, ξ_3 harmonics playing a negligible role. At finite β/ε the $m = 2$ harmonic ξ_2 is shown to be dominant although the ξ_1, ξ_3 sideband harmonics are also finite and are critical to allow the perturbation to balloon in the unfavorable curvature region. The reduced form of ξ is given by

$$\xi(\theta) = \xi_1 e^{i\theta} + \xi_2 e^{2i\theta} + \xi_3 e^{3i\theta} \tag{12.139}$$

where the relative sizes of the ξ_j are determined at the end of the analysis by minimizing δW.

Equation (12.139) is substituted into Eq. (12.137) leading to the desired expression for δW_S in terms of the ξ_j,

$$\begin{aligned}\frac{\delta W_S}{W_0} \equiv \delta\hat{W}_S &= -\frac{2\beta}{\varepsilon k^2}\left[2(2-k^2)(\xi_1^2+\xi_2^2+\xi_3^2) + 3k^2\xi_2(\xi_1+\xi_3)\right] \\ &= -\frac{2}{q_*^2}\left[\frac{\pi}{4E(k)}\right]^2\left[2(2-k^2)(\xi_1^2+\xi_2^2+\xi_3^2) + 3k^2\xi_2(\xi_1+\xi_3)\right]\end{aligned} \tag{12.140}$$

with $W_0 = \pi^2 a^2 B_0^2/\mu_0 R_0$. The second form is obtained by expressing β/ε in terms of k from Eq. (12.131). Note that the uncoupled quadratic terms correspond to the kink drive while the cross terms represent the ballooning drive.

Evaluation of δW_F

The evaluation of δW_F is obtained from the high β tokamak form given by Eq. (12.123). For the surface current model where $p =$ constant and $J_\parallel = 0$ this form reduces to

$$\delta W_F(U^*,U) = \frac{1}{2\mu_0}\int_P |\mathbf{Q}_p|^2 d\mathbf{r} \tag{12.141}$$

The expression for $\mathbf{Q}_p$ in Eq. (12.124) is also greatly simplified,

$$\mathbf{Q}_p = -\frac{inB_0}{R_0}\mathbf{e}_\phi \times \nabla U \tag{12.142}$$

Substituting $\mathbf{Q}_p$ into δW_F yields

$$\delta W_F = \frac{\pi B_0^2 n^2}{\mu_0 R_0}\int_P \left[\left|\frac{\partial U}{\partial r}\right|^2 + \left|\frac{1}{r}\frac{\partial U}{\partial \theta}\right|^2\right] r dr d\theta \tag{12.143}$$

Now, the function $U(r,\theta)$ that is regular at the origin and which minimizes the integral can be written as a general Fourier series

$$U(r,\theta) = \sum_{-\infty}^{\infty} U_m r^{|m|} e^{im\theta} \tag{12.144}$$

The coefficients U_m are chosen to match the trial function on the surface; that is, one chooses the U_m so that

$$\frac{1}{a}\frac{\partial U(a,\theta)}{\partial \theta} = \xi(\theta) = \xi_1 e^{i\theta} + \xi_2 e^{2i\theta} + \xi_3 e^{3i\theta} \tag{12.145}$$

Only three terms are needed for the matching, U_1, U_2, U_3. A short calculation shows that

$$U(r,\theta) = -ia\left(\xi_1 \rho\, e^{i\theta} + \frac{\xi_2}{2}\rho^2 e^{2i\theta} + \frac{\xi_3}{3}\rho^3 e^{3i\theta}\right) \tag{12.146}$$

where $\rho = r/a$.

Equation (12.146) is substituted into Eq. (12.143) yielding an expression for δW_F,

$$\frac{\delta W_F}{W_0} \equiv \delta \hat{W}_F = \frac{n^2}{3}\left(6\xi_1^2 + 3\xi_2^2 + 2\xi_3^2\right) \tag{12.147}$$

The simplicity of evaluating δW_F is the primary motivation for using the surface current model.

Evaluation of δW_V

The final term to evaluate is the vacuum energy given by

$$\delta W_V = \frac{1}{2\mu_0}\int_V |\ \hat{\mathbf{B}}_1| d\mathbf{r} \tag{12.148}$$

This is the most complicated term for the following reason. Even though only three harmonics (ξ_1, ξ_2, ξ_3) are needed to define the surface perturbation, each of these couples to an infinite number of magnetic field harmonics in the vacuum because of the non-trivial θ dependence of $B_\theta(\theta)$. Still, with a little bit of work, δW_V can be analytically evaluated for the two most interesting limits, β/ε approaching zero and the equilibrium limit.

The analysis starts by noting that in the vacuum region $\hat{\mathbf{B}}_1 = \nabla V$ with V satisfying $\nabla^2 V \approx \nabla_p^2 V = 0$. The general solution for V corresponding to a wall at infinity can be written as

$$V = V(\rho,\theta)e^{-in\phi} = e^{-in\phi}\sum_m V_m \rho^{-|m|} e^{im\theta} \tag{12.149}$$

where $\rho = r/a$ and it should be understood that the summation includes all m in the range $-\infty < m < \infty$ except $m = 0$. If one now notes that $|\hat{\mathbf{B}}_1|^2 = |\nabla V|^2 = \nabla\cdot(V^*\nabla V)$ then a simple application of the divergence theorem leads to an expression for δW_V that has the form of a surface integral,

$$\delta W_V = -\frac{1}{2\mu_0}\int_S V^*\frac{\partial V}{\partial r}\,dS = \frac{2\pi^2 R_0}{\mu_0}\sum |m||V_m|^2 \tag{12.150}$$

The next task is to relate the V_m to the ξ_m, which is accomplished by applying the boundary condition on the plasma surface $\mathbf{n}\cdot\hat{\mathbf{B}}_1(S) = \mathbf{n}\cdot\nabla\times(\boldsymbol{\xi}_\perp\times\hat{\mathbf{B}})$. A short calculation shows that this condition reduces to

$$\left.\frac{\partial V}{\partial\rho}\right|_{\rho=1} = -in\varepsilon B_0\xi + \frac{\partial}{\partial\theta}(B_\theta\xi) \tag{12.151}$$

Straightforward Fourier analysis then leads to an expression for the V_m,

$$\begin{aligned} V_m &= \frac{i\varepsilon B_0}{|m|}\sum_l G_{ml}\xi_l \\ G_{ml} &= \frac{1}{2\pi}\int_0^{2\pi}\left(-n + \frac{mB_\theta}{\varepsilon B_0}\right)\cos\left[(l-m)\theta\right]d\theta \end{aligned} \tag{12.152}$$

For the displacement under consideration l has the values 1,2,3. Even so, because of the θ dependence of $B_\theta(\theta)$ the V_m will be non-zero over the infinite range of m. This represents the coupling of each harmonic of ξ to an infinite number of harmonics in V that was previously mentioned.

The vacuum energy is now evaluated by substituting Eq. (12.152) into Eq. (12.150),

$$\frac{\delta W_V}{W_0} \equiv \delta\hat{W}_V = 2\sum_{m,l,p}\frac{G_{ml}G_{mp}}{|m|}\xi_l\xi_p \tag{12.153}$$

The coefficients G_{ml} can be evaluated analytically but lead to complicated combinations of elliptic integrals. A simpler approach is to consider the two limiting cases of low and high β/ε corresponding to $k^2 = 0$ and $k^2 = 1$. For these cases simpler analytic expressions can be found resulting in explicit stability boundaries on q_* and β/ε. These calculations are described below.

Stability analysis

The goal of the stability analysis is to determine the marginal stability boundaries resulting from external ballooning-kink modes in the form of a β/ε vs. $1/q_*$ diagram. This important goal is accomplished by evaluating $\delta W = \delta W_F + \delta W_S + \delta W_V$

by summing the three separate contributions just evaluated. As stated above, relatively simple analytic answers are obtained for the two limiting cases $k^2 = 0$ and $k^2 = 1$. Intermediate cases require a minor numerical calculation and these results are discussed as well.

To begin, consider the case of $\beta/\varepsilon \to 0$ corresponding to $k^2 = 0$. This case is easy to analyze because the magnetic field matrix becomes diagonal. Specifically, for $k^2 = 0$ one finds that $B_\theta/\varepsilon B_0 = 1/q_*$ implying that

$$G_{ml} = \left(-n + \frac{m}{q_*}\right)\delta_{l-m} \tag{12.154}$$

where δ_{l-m} is the Kronecker delta function. Using this relation it follows that the vacuum energy reduces to

$$\delta\hat{W}_V = 2\left[\left(1 - \frac{1}{q_*}\right)^2 \xi_1^2 + \left(1 - \frac{2}{q_*}\right)^2 \frac{\xi_2^2}{2} + \left(1 - \frac{3}{q_*}\right)^2 \frac{\xi_3^2}{3}\right] \tag{12.155}$$

Here, the toroidal mode number has been set to $n = 1$ which is the most unstable case. The complete δW can now be evaluated by summing the separate contributions. A short calculation yields

$$\delta\hat{W} = \frac{4}{q_*}(q_* - 1)\xi_1^2 + \frac{2}{q_*^2}(q_* - 2)^2\xi_2^2 + \frac{1}{3q_*^2}\left[(2q_* - 3)^2 + 3\right]\xi_3^2 \tag{12.156}$$

Observe that there are no cross terms; that is, at low β/ε there is no toroidal coupling and each mode is independent. Stated differently, in the limit of low β/ε the stability result reduces to that of the straight cylinder. Next, Eq. (12.156) shows that the coefficients of the $m = 2$ and $m = 3$ are both positive. Therefore, the most unstable perturbation corresponds to $\xi_2 = \xi_3 = 0$. The only mode that can become unstable is $m = 1$. Stabilization of this mode requires

$$q_* > 1 \tag{12.157}$$

which is just the Kruskal–Shafranov condition. This is the only purely current-driven kink mode that can be unstable in the surface current model.

The second limit of interest corresponds to $k^2 = 1$. This value corresponds to the β/ε equilibrium limit at which $\beta/\varepsilon = (\pi^2/16)(1/q_*^2)$. To calculate the maximum stable β/ε one must determine the smallest value of q_* that keeps δW positive. The procedure to do this is to write $\delta W = \delta W(q_*, \xi_1, \xi_2, \xi_3)$ and then minimize over the relative amplitudes of the harmonics. The resulting δW is then only a function of q_*: $\delta W = \delta W(q_*)$. A simple plot of this function yields the lowest stable q_* and the corresponding maximum stable value of β/ε.

The main mathematical advantage of focusing on $k^2 = 1$ is that it leads to a simple expression for the coefficient G_{ml}, a consequence of the fact that $B_\theta/\varepsilon B_0$ reduces to

$$\frac{B_\theta}{\varepsilon B_0} = \frac{\pi}{2q_*}\left|\cos\frac{\theta}{2}\right| \tag{12.158}$$

From this relation it follows that

$$G_{ml} = -n\delta_{m-l} + \frac{(-1)^{m-l+1}}{q_*}\frac{m}{4(m-l)^2 - 1} \tag{12.159}$$

The next step is to evaluate δW at $k^2 = 1$. The result is an expression of the form

$$\delta\hat{W} = W_{11}\xi_1^2 + W_{22}\xi_2^2 + W_{33}\xi_3^2 + 2W_{12}\xi_1\xi_2 + 2W_{13}\xi_1\xi_3 + 2W_{23}\xi_2\xi_3 \tag{12.160}$$

where use has been made of the symmetry relations $W_{lp} = W_{pl}$. Also each matrix element depends only on q_*: $W_{lp} = W_{lp}(q_*)$. The matrix elements are given shortly.

For the moment focus on the form of δW. Choose one of the amplitudes, for instance ξ_2, as the primary harmonic. The amplitudes ξ_1 and ξ_3 can be expressed in terms of ξ_2 by minimizing δW with respect to ξ_1, ξ_3. A simple calculation leads to two simultaneous equations for ξ_1 and ξ_3,

$$\begin{aligned} W_{11}\xi_1 + W_{13}\xi_3 &= -W_{12}\xi_2 \\ W_{13}\xi_1 + W_{33}\xi_3 &= -W_{23}\xi_2 \end{aligned} \tag{12.161}$$

whose solution is given by

$$\begin{aligned} \xi_1 &= \frac{W_{23}W_{13} - W_{12}W_{33}}{W_{11}W_{33} - W_{13}^2}\xi_2 \\ \xi_3 &= \frac{W_{12}W_{13} - W_{23}W_{11}}{W_{11}W_{33} - W_{13}^2}\xi_2 \end{aligned} \tag{12.162}$$

These expressions are substituted in δW. After a short calculation one obtains

$$\delta\hat{W} = W(q_*)\xi_2^2 = \left(W_{22} - \frac{W_{11}W_{23}^2 + W_{33}W_{12}^2 - 2W_{12}W_{13}W_{23}}{W_{11}W_{33} - W_{13}^2}\right)\xi_2^2 \tag{12.163}$$

To test for stability one just has to substitute the expressions for the $W_{lp}(q_*)$ into Eq. (12.163) and plot the resulting function $W(q_*)$ to see when it is positive or negative. The explicit expressions for the $W_{lp}(q_*)$ are obtained by combining the separate contributions to $\delta\hat{W}$. The results, again for $n = 1$, are given by

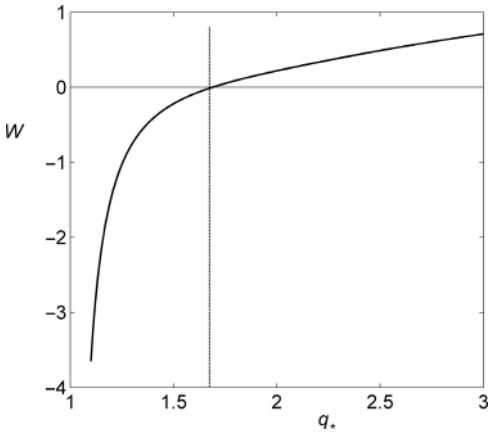

Figure 12.6 Curve of W vs. q_* at the equilibrium β limit.

$$
\begin{aligned}
W_{11} &= 4 - \frac{4}{q_*} - \left(\frac{\pi^2}{4} - 2M_{11}\right)\frac{1}{q_*^2} = 4 - \frac{4}{q_*} + \frac{0.033}{q_*^2} \\
W_{22} &= 2 - \frac{4}{q_*} - \left(\frac{\pi^2}{4} - 2M_{22}\right)\frac{1}{q_*^2} = 2 - \frac{4}{q_*} + \frac{2.48}{q_*^2} \\
W_{33} &= \frac{4}{3} - \frac{4}{q_*} - \left(\frac{\pi^2}{4} - 2M_{33}\right)\frac{1}{q_*^2} = \frac{4}{3} - \frac{4}{q_*} + \frac{4.94}{q_*^2} \\
W_{12} &= -\frac{4}{3q_*} - \left(\frac{3\pi^2}{16} + 2M_{12}\right)\frac{1}{q_*^2} = -\frac{4}{3q_*} - \frac{0.017}{q_*^2} \\
W_{23} &= -\frac{4}{3q_*} - \left(\frac{3\pi^2}{16} + 2M_{23}\right)\frac{1}{q_*^2} = -\frac{4}{3q_*} + \frac{1.23}{q_*^2} \\
W_{13} &= \frac{4}{15q_*} + \frac{2M_{13}}{q_*^2} = \frac{4}{15q_*} + \frac{0.011}{q_*^2}
\end{aligned}
\tag{12.164}
$$

where the M_{lp} are pure numerical coefficients defined by

$$
M_{lp} = \sum_{m=-\infty}^{\infty} \frac{|m|}{[4(m-l)^2 - 1][4(m-p)^2 - 1]} \tag{12.165}
$$

The coefficients can be evaluated either numerically or, with some effort, analytically. Their values are $M_{11} = 5/4$, $M_{22} = 89/36$, $M_{33} = 1111/300$, $M_{12} = -11/12$, $M_{23} = -277/180$, and $M_{13} = 1/180$. These values have been substituted into Eq. (12.164) to give the simpler numerical forms on the far right.

The resulting expression for $W(q_*)$ is plotted vs. q_* in Fig. 12.6. As expected the plasma is unstable [$W(q_*) < 0$] for low q_* and stable [$W(q_*) > 0$] for high q_*. The

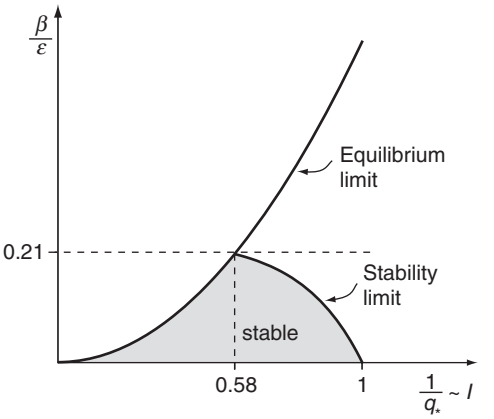

Figure 12.7 Stability diagram for external modes in a high β tokamak described by the surface current model.

transition occurs for $q_* = 1.69$. A more accurate numerical calculation keeping 20 harmonics yields $q_* = 1.71$ and this more accurate value is used hereafter.

The basic conclusion is that the optimum q_* and corresponding highest β/ε that are stable against ballooning-kink modes in a high β tokamak with a circular cross section are given by

$$q_* = q_{crit} = 1.71$$
$$\frac{\beta}{\varepsilon} = \frac{\beta_{crit}}{\varepsilon} = \left(\frac{\pi}{4q_{crit}}\right)^2 = 0.21 \tag{12.166}$$

There are several additional points worth noting. The scaling $\beta_{crit} \sim a/R_0$ suggests that a tight aspect ratio is desirable for favorable MHD stability. Even so one must keep in mind that fusion really requires high p rather than high $\beta \sim p/B_0^2$ although the two are related. For tight aspect ratio tokamaks the strong $1/R$ dependence of the toroidal field reduces B_0 at $R = R_0$ as compared to larger aspect ratio devices assuming the same maximum field on the toroidal field coil. Therefore, while β may be higher in a tight aspect ratio tokamak, the actual pressure may be smaller.

A second point is that the optimized value of stable q_* has been raised from $q_* = 1$ at $\beta/\varepsilon = 0$ to $q_* = 1.71$ at $\beta/\varepsilon = 0.21$. The maximum allowable plasma current has decreased by nearly a factor of 2. Lastly, by comparing with detailed numerical studies using realistic profiles, one finds that the surface current model predicts the correct scaling of $\beta_{crit} \sim \varepsilon$, although the numerical coefficient 0.21 is optimistic. The numerical results are described in the next subsection.

The overall picture of surface current model stability can be summarized by plotting the marginally stable β/ε vs. $1/q_*$ (i.e., essentially p vs. I) as illustrated in Fig. 12.7. Shown here are the equilibrium limit and the marginal stability boundary

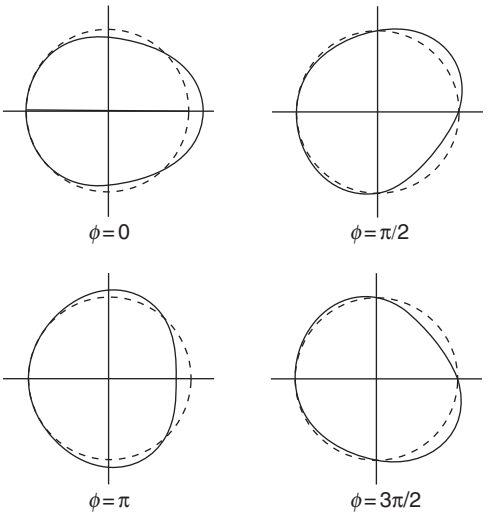

Figure 12.8 Marginally stable eigenfunction for the surface current model at four different ϕ locations. The major axis is to the left. The dashed and solid curves represent the unperturbed and perturbed surfaces respectively.

for arbitrary k^2 obtained using 20 harmonics and numerically evaluating the matrix coefficients. The analytic stability results correspond to the end points on the stability curve. Observe that there is a stable operating regime without a conducting wall for sufficiently low p and sufficiently low I.

The final point of interest concerns the shape of the eigenfunction. One wants to learn whether or not the most unstable mode has the form of a ballooning-kink perturbation of the plasma surface. This is easily demonstrated by substituting $q_* = 1.71$ into Eq. (12.162), yielding

$$\begin{aligned} \xi_1/\xi_2 &= 0.429 \\ \xi_3/\xi_2 &= 0.427 \end{aligned} \tag{12.167}$$

Equation (12.167) shows that at the high β/ε limit, the perturbation is dominated by $m = 2$ but that there are substantial $m = 1$, $m = 3$ sidebands. The ballooning-kink nature of the perturbation is shown graphically in Fig. 12.8, where the perturbed surface $r = a + \xi_1 \cos(\theta - \phi) + \xi_2 \cos(2\theta - \phi) + \xi_3 \cos(3\theta - \phi)$ overlays the unperturbed surface $r = a$. The figure shows the poloidal cross section at four different toroidal angles assuming $\xi_2/a = 0.09$. One sees that the surface distortion rotates with the toroidal angle, demonstrating the kink component of the mode. Equally importantly, the perturbation is always much larger on the outside of the torus than the inside: $r(\theta = 0) - a = 1.86\xi_2 \cos\phi$ while $r(\theta = \pi) - a = 0.14\xi_2 \cos\phi$. This clearly demonstrates that the perturbation balloons in the region of unfavorable curvature.

This completes the analysis of ballooning-kink instabilities in a high β tokamak as described by the surface current model. It is now of interest to discuss more realistic results using diffuse profiles as obtained from detailed numerical studies.

12.8.4 Numerical studies of ballooning-kink instabilities

Many sophisticated numerical codes have been written that examine the MHD stability of tokamaks against a variety of modes. These codes are "exact" in that they treat finite aspect ratio, finite β, finite shaping, as well as arbitrary diffuse profiles. Several excellent textbooks (e.g., Jardin, 2010; Goedbloed *et al.*, 2010) have been written that describe the numerical aspects of these codes as well as presenting results. The discussion below focuses primarily on the results described in these books as well as many related scientific papers.

In terms of an overview it is accurate to say that standard tokamaks with an increasing $q(\psi)$ profile are dominated by either $n = \infty$ ballooning modes or $n = 1$ ballooning-kink modes. Intermediate n modes lie between these two limiting cases. Invariably, if no conducting wall is present, then the $n = 1$ mode sets the most stringent limit on β. When the wall is very close, then the $n = 1$ mode is wall stabilized. In this case the $n = \infty$ mode, which is unaffected by the wall because of its highly localized eigenfunction, becomes the more important instability. It is also worth pointing out that with hollow $q(\psi)$ profiles the situation can change. Intermediate n modes, known as "infernal modes" may then set the strictest limits on β (Manickam *et al.*, 1987). Such hollow profiles can occur naturally in the "advanced tokamak" mode of operation which is discussed in the next subsection. For the present discussion, however, attention is focused on standard tokamaks with monotonically increasing $q(\psi)$ profiles.

To begin note that the numerical codes, in addition to treating all relevant parameters as finite, also are used to optimize over profile shape to determine the maximum stable β for a given geometry. Results for such an optimization against $n = \infty$ ballooning modes have already been discussed in Section 12.2.6, the conclusion being the Sykes limit given by

$$\beta_t = \beta_N \frac{I}{aB_0} \qquad \beta_N = 0.044 = 4.4\% \tag{12.168}$$

where the units are I (MA), B_0 (T), and a (m).

A similar but more comprehensive stability study has been carried out by Troyon and co-workers (Troyon *et al.*, 1984). These studies determine the optimized profiles for stability against the Mercier criterion, ballooning modes, internal modes, and external ballooning-kink modes in a tokamak without a conducting

wall over a variety of cross sectional shapes. As stated above, the external ballooning-kink mode is usually the most difficult to stabilize. Like the Sykes limit the result of these studies is remarkably simple. The critical β for stability is known as the "Troyon limit" and can be written as

$$\beta_t = \beta_N \frac{I}{aB_0} \qquad \beta_N = 0.028 = 2.8\% \tag{12.169}$$

Typically the most stable systems have elongated, outward pointing D-shapes. Also the optimized profiles tend to have peaked current distributions.

The numerical results also show that non-optimized profile effects can be incorporated into the stability criterion by considering β_N to be a function of a current peaking parameter. Specifically, for typical inverse aspect ratios on order of $\varepsilon \sim 1/3$ the numerical studies show that

$$\beta_N \approx 4\, l_i \tag{12.170}$$

where l_i is the internal inductance per unit length defined by Eq. (6.85). More peaked profiles have larger l_i than broad or hollow profiles.

The most striking feature of the (essentially ballooning-kink) Troyon β limit given by Eq. (12.169) is that it is identical in form to the Sykes limit, except that the numerical value of β_N is slightly reduced from 0.044 to 0.028. There are, however, two additional points to consider. First, the numerical studies are carried out assuming that $q_0 \approx 1$ to avoid internal sawtooth modes. Thus, the expected inverse quadratic scaling of $\beta \propto 1/q^2$ arising from the basic physics probably should be included by the replacement $I/aB_0 \rightarrow I/q_0 aB_0 \propto 1/q_0 q_*$.

More importantly, the pure ballooning mode yields a criterion on the ratio p/I for a fixed geometry which in principle allows high p by operating at high I. Ballooning modes by themselves do not directly limit the size of I. In contrast, the Troyon ballooning-kink stability criterion only applies for $q_a > 2$. This fact is known by most fusion researchers but is often hidden in applications of the Troyon limit. The requirement $q_a > 2$ is frequently introduced as a separate independent criterion but is actually directly coupled to the Troyon limit.

The issue with the current limit has been clarified and sharpened by more recent numerical studies by Menard *et al.* (2004). These authors basically extended the studies of Troyon *et al.* (1984) to include very tight aspect ratios because of their interest in spherical tokamaks. They found that by introducing an appropriately defined β the Troyon limit remains valid even for very tight aspect ratios. In the generalized definition the toroidal β is redefined as follows:

$$\beta_t = \frac{2\mu_0 \langle p \rangle}{B_0^2} \quad \rightarrow \quad \frac{2\mu_0 \langle p \rangle}{\langle B^2 \rangle} \tag{12.171}$$

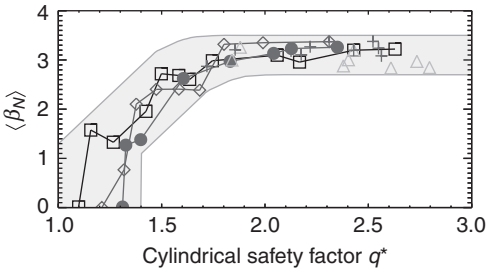

Figure 12.9 Approximately universal curve of $\beta_N = \beta_N(q_*)$ obtained by Menard *et al.* (2002). Reproduced with permission.

Here, $\langle B^2 \rangle$ is the volume average of the total magnetic energy. Interestingly, this definition was originally suggested by Troyon but the definition with B_0^2 has come into wide use because of its simplicity. The two definitions nearly coincide at large aspect ratio but are noticeably different at tight aspect ratio. An equally important contribution of Menard *et al.* is that they calculated the stability limit directly as a function of q_* after carefully defining this quantity in terms of the current. Their definition coincides with the one used in the text, namely

$$q_* = \frac{2\pi a^2 B_0}{\mu_0 R_0 I}\left(\frac{1+\kappa^2}{2}\right) \tag{12.172}$$

Using their generalized definitions one finds that the results of Menard *et al.* can be summarized in the form of an approximately universal β limit, valid for arbitrary aspect ratio. The limit has the form

$$\beta_t = 5\beta_N\left(\frac{1+\kappa^2}{2}\right)\frac{\varepsilon}{q_*} \tag{12.173}$$

where $\beta_N = \beta_N(q_*)$ is illustrated in Fig. 12.9.

Observe that for $q_* > 2$, $\beta_N \approx 0.03 = 3\% =$ constant. In this regime the β_t limit scales as $\beta_t \propto 1/q_* \propto I$ corresponding to the original Troyon result. In contrast, for $q_* \to 1.2$ then $\beta_t \to 0$, indicating the degradation due to too large a current. Now, the numerical data in Fig. 12.9 can be approximated by the following simple formula (in decimal units):

$$\beta_N \approx 0.03\left(\frac{q_*^v - 1.2^v}{q_*^v}\right)^{1/v} \tag{12.174}$$

with $v = 3$. Using this approximate relation one can see that β_t in Eq. (12.173) has a maximum as a function of q_*. The optimum can easily be calculated leading to a critical q_* and corresponding β_t given by

$$q_* = 1.51$$
$$\frac{\beta_t}{\varepsilon} = 0.079\left(\frac{1+\kappa^2}{2}\right) \tag{12.175}$$

Equation (12.175) with $\kappa = 1$ can be directly compared with the results of the surface current model. The critical q_* values are similar: $q_* = 1.51$ from the Menard results and $q_* = 1.71$ from the surface current model. The maximum β_t values show a wider discrepancy: $\beta_t/\varepsilon = 0.079$ from the Menard relation while $\beta_t/\varepsilon = 0.21$ for the surface current model. The surface current profiles, perhaps unsurprisingly, lead to more optimistic β_t limits than those obtained from realistic diffuse profiles by a factor of about 2.7. The reason is that in addition to external ballooning-kink modes, the diffuse model must also take into account low n internal modes and ballooning modes which are not present in the surface current model.

As a final numerical example consider a tokamak with $\kappa = 1.8$ and $\varepsilon = 0.4$. This yields a no-wall maximum $\beta_t = 0.067 = 6.7\%$. At a toroidal field $B_0 = 6\,\mathrm{T}$ this translates into a total plasma pressure $p = 9.6\,\mathrm{atm}$, which should be sufficient for a fusion reactor typically requiring $p \sim 5-8\,\mathrm{atm}$. However, the safety margin is not as large as one might like since there is no guarantee that the optimum profiles can be achieved experimentally. For example, one might need to operate closer to $q_* \approx 2$ to avoid disruptions. Also, the need for a large bootstrap fraction puts further constraints on the profiles. Still, do not lose sight of the forest for the trees.

A tokamak is capable of achieving complete stability against all $n \geq 1$ ideal MHD modes without the need of a conducting wall at values of β_t and pressure sufficient for a reactor.

Standard tokamak experiments have achieved β_t values in the range of 5%–10% although at lower toroidal fields than in a reactor (see for instance Lazarus *et al.*, 1991; Strait, 2005). Thus, the actual pressures are lower than ultimately needed. Spherical tokamaks have achieved much higher β_t values, on the order of 30% (see for instance Menard *et al.*, 2002). Here too this performance is achieved at a low toroidal field so the absolute pressures are still below what is needed in a reactor. However, from the point of view of understanding plasma science the MHD model has proven to be a reliable guide to the maximum achievable values of β_t thereby representing a good collaborative theory-experimental success story.

12.9 Stability of tokamaks – advanced tokamak (AT) operation

12.9.1 Introduction

The advanced tokamak (AT) actually refers to a mode of operation of standard tokamaks. It is accessible to some but not all experiments. The AT has the goal of solving one of the basic problems facing the tokamak concept in its quest to

become a fusion reactor – the need for steady state operation. To accomplish this a method is needed to non-inductively drive a steady state toroidal current. While RF methods have been known for many years and have demonstrated that they can indeed non-inductively drive current, they are not very efficient. Too many watts (typically 10–20 watts absorbed power) are required to drive one ampere of current. This inefficiency leads to poor reactor power balance. On the order of 300–500 MWe would be required to drive all the current in a 1 GWe tokamak reactor.

A possible resolution to this basic difficulty is to take advantage of the bootstrap current, a naturally driven neoclassical transport current that is automatically generated for "free" in a tokamak. No external drives are required. Reactor studies show that it is necessary for about 75–90% of the total toroidal current to consist of the bootstrap current. Only the remaining 10–25% must be produced by RF current drive, leading to greatly improved power balance.

The purpose of this subsection is to provide some understanding of the requirements and constraints involved in generating 75% bootstrap current. To do this one has to understand the profile shape and magnitude of the bootstrap current. This is accomplished by combining some toroidal and cylindrical tokamak physics.

The overall picture is as follows. Bootstrap current profiles are hollow, not monotonically decreasing as in a standard tokamak. The magnitude of the current is proportional to the pressure. Therefore, high bootstrap current requires high pressure and one must test whether the required pressure exceeds the Troyon limit. Invariably the no-wall Troyon limit is violated, suggesting that wall stabilization is required, which in practice translates into resistive wall mode stabilization. In addition, the profiles are sufficiently different that a new class of ideal MHD modes, known by the tongue-in-cheek name of "infernal modes," can be excited and these too must be stabilized.

Experimentally, the achievement of high bootstrap current requires heating a plasma to sufficiently high temperatures so that the low collisionality bootstrap current physics is applicable. In addition, this must be accomplished at high density so the magnitude of the bootstrap current is large. High bootstrap fractions have been obtained transiently by current programming and RF profile control, but maintaining these high fractions is still far from routine. Additionally, once the profiles can be maintained there will likely be the extra complication of resistive wall stabilization. High-performance AT operation currently remains an important area of tokamak research.

To demonstrate the physics of AT operation, two simple calculations are presented in this section. First, a simplified formula for the bootstrap current obtained from neoclassical transport theory is used to determine the current profiles and amplitude. After some simple analysis the amplitude can be expressed in terms

of β_N whose value is determined by requiring the bootstrap fraction f_B to equal 75%. The resulting β_N is shown to exceed the Troyon limit. This motivates the second calculation whose goal is to show how close to place a perfectly conducting wall in order to stabilize the higher value of β_N. This task is carried out using the surface current model.

12.9.2 Bootstrap current profile – the β_N limit

To begin, assume that a high-density plasma has been heated to a sufficient temperature to generate a substantial bootstrap current. Neoclassical transport theory shows that in a large aspect ratio, circular cross section tokamak, the bootstrap current generated has a profile and magnitude given by (see for instance Helander and Sigmar, 2002)

$$J_B(r) = -\frac{1}{B_\theta}\left(\frac{r}{R_0}\right)^{1/2}\left[2.44(T_e + T_i)\frac{dn}{dr} + 0.69\, n\frac{dT_e}{dr} - 0.42\, n\frac{dT_i}{dr}\right] \quad (12.176)$$

This expression can be simplified by assuming plausible profiles for the temperatures and density. A reasonable choice is $T_e = T_i \equiv T$ with a density profile that is flatter than the temperature, which is typical of H-mode tokamaks. The specific profiles chosen are given by

$$\begin{aligned} T(\rho) &= T_0(1-\rho^2)^{4/3} \\ n(\rho) &= n_0(1-\rho^2)^{2/3} \\ p(\rho) &= 2n_0T_0(1-\rho^2)^2 = 3\overline{p}(1-\rho^2)^2 \end{aligned} \quad (12.177)$$

where $\rho = r/a$ and $\overline{p}$ is the volume averaged pressure. When these profiles are substituted into Eq. (12.176) the expression for J_B reduces to

$$J_B(r) = 10.8\frac{\overline{p}}{a^{1/2}R_0^{1/2}}\frac{\rho^{1/2}}{B_\theta}\left[\rho(1-\rho^2)\right] \quad (12.178)$$

Now, the total toroidal current flowing in the plasma is $J = J_B + J_{CD}$ with J_{CD} representing the contribution from external current drive. A simple model for J_{CD} assumes that its main purpose is to fill in the current near the axis where $J_B = 0$ and in fact the neoclassical theory breaks down. The model chosen allows the total current to be written as

$$J(r) = 10.8\frac{\overline{p}}{a^{1/2}R_0^{1/2}}\frac{(\rho^{1/2}+\alpha)}{B_\theta}\left[\rho(1-\rho^2)\right] \quad (12.179)$$

Here, α is a free parameter representing the magnitude of J_{CD}. Its value is obtained by requiring the bootstrap fraction to be 75% of the total current.

To determine f_B one first needs to calculate the $B_\theta(r)$ profile and the corresponding total plasma current $\mu_0 I = 2\pi a B_\theta(a)$. The function $B_\theta(r)$ is determined by a straightforward application of Ampere's law leading to

$$\frac{B_\theta^2(r)}{B_\theta^2(a)} \equiv b_\theta^2(\rho) = 54\beta_N \frac{q_*}{\varepsilon^{1/2}}\left(\frac{2}{9}\rho^{5/2} - \frac{2}{13}\rho^{9/2} + \frac{\alpha}{4}\rho^2 - \frac{\alpha}{6}\rho^4\right) \tag{12.180}$$

In this expression $\overline{p}$ has been replaced by β_N by the transformation

$$\frac{2\mu_0\overline{p}}{B_\theta^2(a)} = \frac{\beta_t q_*^2}{\varepsilon^2} = \left(5\beta_N\frac{\varepsilon}{q_*}\right)\frac{q_*^2}{\varepsilon^2} = 5\frac{q_*}{\varepsilon}\beta_N \tag{12.181}$$

where β_t is maximized by operating at the MHD stability limit, which is assumed to have a Troyon scaling. However, β_N, at this point, is treated as a free parameter. It's value is directly related to the current drive parameter α and is determined by the requirement $f_B = 0.75$. The resulting β_N must then be compared to the actual Troyon value $\beta_N = 0.028$ to see whether or not the plasma is MHD stable. The explicit relationship between β_N and α is obtained by setting $\rho = 1$ in Eq. (12.180):

$$\beta_N = 0.271\frac{\varepsilon^{1/2}}{q_*}\left(\frac{1}{1+1.22\alpha}\right) \tag{12.182}$$

With the total $B_\theta(r)$ profile known from Eq. (12.180), one can next integrate Eq. (12.178) over the plasma cross section to determine the total bootstrap current. The bootstrap fraction is then simply the ratio of the bootstrap current to the total current. A short calculation yields

$$f_B = \frac{\mu_0 I_B}{2\pi a B_\theta(a)} = \frac{\mu_0 a}{B_\theta(a)}\int_0^1 J_B(\rho)\rho d\rho = 27\beta_N\frac{q_*}{\varepsilon^{1/2}}\int_0^1 \frac{\rho^{5/2}(1-\rho^2)}{b_\theta(\rho)}d\rho \tag{12.183}$$

Equation (12.183) is easily evaluated numerically leading to a relation of the form $f_B = f_B(\alpha)$, as is illustrated in Fig. 12.10. Observe that $f_B = 0.75$ corresponds to $\alpha = 0.24$. Using this value of α one can easily plot the total current and bootstrap current profiles as well as the total $q(r)$ profile. These are shown in Fig. 12.11. The total current profile is indeed hollow while the safety factor profile has an off-axis minimum. The off-axis minimum is often referred to as a "reversed shear" profile since the shear $S(r) \equiv rq'/q$ changes sign. Most AT tokamaks have reversed shear profiles.

Consider next the required value of β_N obtained from Eq. (12.182) with $\alpha = 0.24$. To keep the required β_N as low as possible one sees that small ε and large q_* are desirable. Even so, one cannot make ε too small or q_* too large since the corresponding $\beta_t \propto \beta_N\varepsilon/q_* \propto \varepsilon^{3/2}/q_*^2$ may be too small for reactor

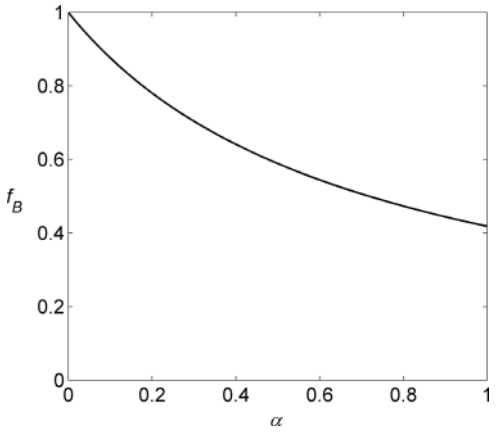

Figure 12.10 Bootstrap fraction f_B as a function of the current drive parameter α.

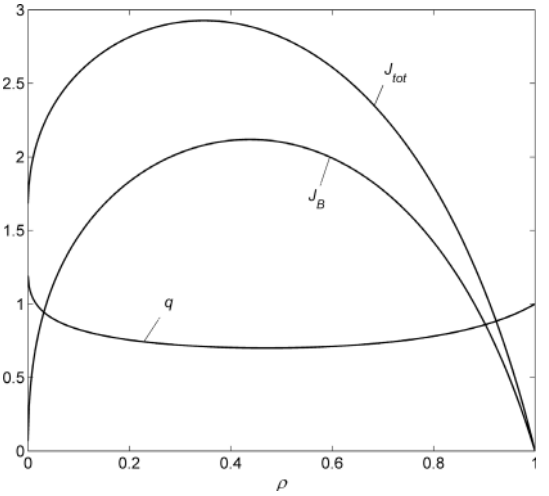

Figure 12.11 Profiles of the total current and the bootstrap current. Also shown is q/q_*. Here, $\rho = r/a$.

applications. For the case $\varepsilon = 1/3$ and $q_* = 3$, which is probably as favorable as possible for a high bootstrap fraction, the required value of β_N has the value

$$\beta_N = 0.04 \tag{12.184}$$

Even this optimistic case leads to a β_N that exceeds the actual Troyon limit $\beta_N = 0.028$. The implication is that a close fitting conducting wall is needed in conjunction with resistive wall stabilization. Also, keep in mind that the required β_N cannot exceed the Troyon value by too large a factor, even assuming wall stabilization is possible. The reason is that internal ballooning modes can be excited which are not affected by wall position.

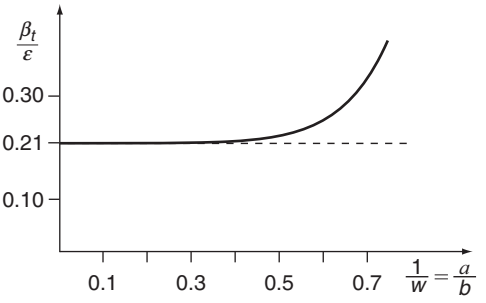

Figure 12.12 The maximum stable β_t/ε vs. normalized wall radius b/a.

12.9.3 Wall stabilization in an advanced tokamak

If a close fitting wall is required for an advanced tokamak then the question that naturally arises is how close must this wall actually be with respect to the plasma? A reasonable estimate can be obtained from the circular cross section sharp boundary model. The idea is to introduce the stabilizing effect of the wall into the evaluation of δW_V and then calculate the critical b/a to produce a gain in critical β equal to the amount necessary for 75% bootstrap operation. Specifically, from the calculation in the previous subsection it follows that the critical β_t for stability must increase by the ratio of $0.04/0.028 = 1.43$ because of the wall.

The calculation proceeds by noting that in the surface current model the vacuum energy in the presence of a wall can be expressed in terms of the no-wall result by a simple transformation of Eq. (12.153) given by

$$\delta\hat{W}_V = 2\sum_{m,l,p} \frac{G_{ml}G_{mp}}{|m|}\xi_l\xi_p \quad \rightarrow \quad 2\sum_{m,l,p} \frac{G_{ml}G_{mp}}{|m|}\left[\frac{1+(a/b)^{2|m|}}{1-(a/b)^{2|m|}}\right]\xi_l\xi_p \qquad (12.185)$$

The maximum stable β_t is found by again assuming that the plasma operates along the equilibrium curve $\beta_t q_*^2/\varepsilon = \pi^2/16$. Next, the full $\delta W = \delta W_P + \delta W_S + \delta W_V$ is evaluated and set to zero to determine the critical $q_* = q_*(a/b)$. For this case the sums involved in the vacuum energy are calculated numerically.

The resulting critical q_* is substituted into the equilibrium limit yielding the desired curve of β_t/ε vs. a/b. This curve is illustrated in Fig. 12.12. One sees that to increase the critical β_t/ε by a factor of 1.43 (i.e., from 0.21 to 0.3) requires the wall to be at a normalized radius $b/a \approx 1.5$. This is a reasonable estimate although it is somewhat optimistic when compared to diffuse profile numerical studies. Still, it is comparable to the wall location needed to stabilize vertical instabilities.

To summarize, AT operation using reversed shear profiles can produce high fractions of bootstrap current. However, to reach $f_B = 75\%$ requires a high value of

β_N that exceeds the Troyon limit. Hence, a conducting wall is required with $b/a < 1.5$. The ideal mode is then transformed into a resistive wall mode requiring feedback stabilization. The goal of simultaneously achieving high f_B and high β_t is a challenging problem and is a major area of current tokamak research.

12.9.4 "Infernal" modes

The last topic of interest related to AT operation concerns infernal modes. The problem arises as follows. Assume that a suitable set of AT profiles exist that are stable against $n = \infty$ ballooning modes and $n = 1$ wall stabilized ballooning-kink modes. For a standard tokamak with a monotonically increasing $q(r)$ profile these are the most dangerous modes. Once their stability is ascertained, the tokamak is stable against all other MHD modes.

The problem with the AT is the existence of a low-shear region around the minimum of $q(r)$. This low-shear region can dramatically alter the stability behavior of the plasma. Qualitatively, when the shear is small, resonant MHD modes localized in this region are only weakly stabilized by line bending. Specifically, in the vicinity of a resonant surface $r = r_s$ line bending stabilization is proportional to $(m - nq)^2 \approx [nq'(r_s)(r - r_s)]^2$. In a low-shear region $q'(r_S)$ is small by definition.

The difficulty that then arises can be understood in the context of the internal mode stability of a straight tokamak. Recall from Eq. (11.176) that the leading-order contribution to the potential energy is of order $\delta W \approx \varepsilon^2 \delta W_2$. Pressure and current profile effects enter as $\varepsilon^4 \delta W_4$ and are normally small for $m \geq 2$. However, when a low-shear region exists then δW_2 itself becomes small since it is proportional to $(m - nq)^2$. When this occurs the distinction between $\varepsilon^2 \delta W_2$ and $\varepsilon^4 \delta W_4$ becomes blurred and a more careful analysis is required.

Such an analysis has been carried out by Manickam *et al.* (1987). They discovered, primarily through numerical calculations, that plasmas that were stable to both $n = \infty$ and $n = 1$ modes could be unstable to intermediate n modes in AT configurations with reversed shear. The instabilities have the form of internal modes that are somewhat but not highly localized about the shear reversal point. The modes are more likely to be excited when there is a substantial pressure gradient in this region. One can almost imagine the authors saying to themselves "We thought we were done after looking at $n = \infty$ and $n = 1$. Now we have to examine these 'infernal' intermediate n modes as well in order to demonstrate AT stability."

The conclusion is that a wide range of n modes must be tested for stability in AT configurations. In addition to the usual requirements related to ballooning and ballooning-kink modes one must make sure that the pressure gradient is not too large in the vicinity of the shear reversal point in order to avoid infernal modes.

There is as yet no simple analytic criterion that defines this critical pressure gradient and so numerical calculations are required.

12.10 Stability of tokamaks – $n = 0$ Axisymmetric modes

12.10.1 Introduction

The final instabilities to consider are the axisymmetric modes. These instabilities correspond to $n = 0$ external perturbations. They have no ϕ dependence and hence at marginal stability can be viewed as neighboring equilibria of the Grad–Shafranov equation. The most unstable mode usually has the form of a nearly rigid vertical shift of the entire plasma. In other words the eigenfunction is predominantly an $n = 0$, $m = 1$ mode.

If excited, the vertical axisymmetric mode is very dangerous, potentially leading to actual physical damage of the first wall, analogous to a major disruption. The mode can be stabilized by feedback and it is an important success story of fusion research that such feedback stabilization is almost routine in modern tokamaks.

This section describes three types of axisymmetric modes. First, vertical stability is investigated for a circular cross section plasma. The resulting stability criterion puts constraints on the curvature of the vertical field holding the plasma in toroidal force balance. With proper curvature, no feedback is required. Second, stability is investigated for a purely horizontal displacement, again for a circular cross section plasma. This analysis leads to further constraints on the vertical field curvature which if satisfied also lead to stability without feedback. Third, the circular cross section assumption is relaxed and the stability of elongated cross sections is investigated. This is an important topic since most modern tokamaks have elongated cross sections. It is shown that even a small amount of elongation leads to a dangerous vertical instability and it is here that feedback is essential.

12.10.2 Vertical instabilities in a circular plasma

A simple model has been studied by several authors that demonstrates the basic nature of the $n = 0$ axisymmetric mode in a circular cross section plasma. In this model the plasma is treated as a thin ($a/R_0 \ll 1$) current carrying loop of wire with a circular cross section embedded in an externally applied vertical field. For simplicity the effects of plasma pressure and the profile of internal magnetic flux are neglected. They are not essential to the discussion.

The goal of the ensuing analysis is to determine the appropriate constraints on the curvature of the vertical field to provide stability against rigid vertical and horizontal displacements. For vertical displacements one can see intuitively that a

perfectly uniform vertical field, $\mathbf{B}_V = B_V \mathbf{e}_Z$, B_V = constant, would provide neutral stability against a vertical displacement. If the plasma is moved upward it sees no change in the vertical field force, nor any change in the flux linking the plasma. For positive stability the critical question is then whether the vertical field should curve towards the plasma or away from the plasma.

The analysis proceeds by introducing a potential $\Phi(R, Z)$ such that the equilibrium forces acting on the plasma are given by $\mathbf{F}(R, Z) = -\nabla\Phi$. Equilibrium occurs at the location R_0, Z_0 where $\mathbf{e}_R \cdot \mathbf{F} \equiv F_R(R_0, Z_0) = 0$ and $\mathbf{e}_Z \cdot \mathbf{F} \equiv F_Z(R_0, Z_0) = 0$. If the plasma now undergoes a rigid vertical displacement δZ, then the perturbed vertical force acting on the plasma is given by

$$\delta F_Z = \frac{\partial F_Z(R_0, Z_0)}{\partial Z_0} \delta Z \tag{12.186}$$

The condition that the plasma be stable to a rigid displacement is that

$$\frac{\partial F_Z(R_0, Z_0)}{\partial Z_0} < 0 \qquad \text{for vertical stability} \tag{12.187}$$

In other words, stability occurs when the restoring force is in the opposite direction of the displacement; that is, when δZ is positive then δF_Z is negative. A similar argument holds for a rigid horizontal displacement. In this case the stability condition reduces to

$$\frac{\partial F_R(R_0, Z_0)}{\partial R_0} < 0 \qquad \text{for horizontal stability} \tag{12.188}$$

A key point in the analysis is to recognize that the plasma is a perfect conductor. This implies that the perturbed force must be evaluated subject to the constraint

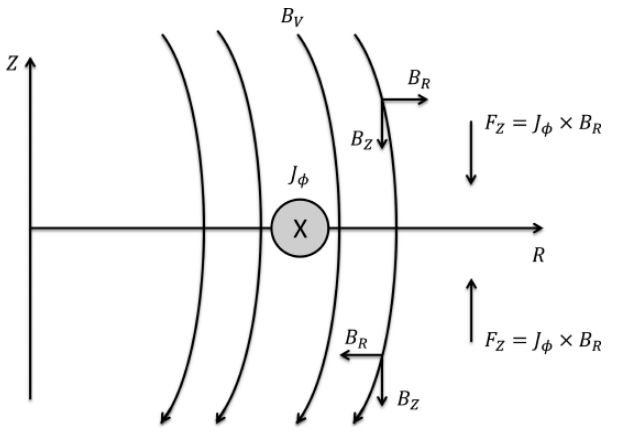

Figure 12.13 Geometry of the simple wire model showing vertical and horizontal stability in a circular cross section wire.

that the poloidal flux Ψ linking the current loop be conserved during the plasma displacement. For the simple model under consideration the appropriate expressions for the potential function and the linked poloidal flux can be written as (see Fig. 12.13 for the geometry)

$$\begin{aligned} \Phi(R,Z) &= \frac{1}{2}LI^2 \\ \Psi(R,Z) &= LI + 2\pi\int_0^R B_Z(R',Z)\,R'dR' \end{aligned} \tag{12.189}$$

Here, $L(R) = \mu_0 R[\ln(8R_0/a)-2]$ is the external inductance associated with the plasma current I and B_Z (and B_R) are the components of the externally applied vertical field $\mathbf{B}_V = B_R\mathbf{e}_R + B_Z\mathbf{e}_Z$. Note that with the geometry as illustrated in Fig. 12.13 it follows that $B_Z < 0$ for toroidal force balance. The constant flux constraint gives a relationship between $I(R, Z)$ and $L(R)$ as the plasma moves.

With these definitions the first step in the analysis is to calculate the equilibrium forces. Differentiating the potential function leads to

$$\begin{aligned} F_Z &= -LI\frac{\partial I}{\partial Z} \\ F_R &= -LI\frac{\partial I}{\partial R} - \frac{I^2}{2}\frac{dL}{dR} \end{aligned} \tag{12.190}$$

Constant flux requires setting $d\Psi = (\partial\Psi/\partial R)dR + (\partial\Psi/\partial Z)dZ = 0$. Each coefficient must independently vanish yielding two relations given by

$$\begin{aligned} &\frac{\partial\Psi}{\partial Z} = 0 \;\rightarrow\; L\frac{\partial I}{\partial Z} + 2\pi\int_0^R \frac{\partial B_Z}{\partial Z}\,R'dR' = L\frac{\partial I}{\partial Z} - 2\pi RB_R = 0 \\ &\frac{\partial\Psi}{\partial R} = 0 \;\rightarrow\; L\frac{\partial I}{\partial R} + I\frac{\partial L}{\partial R} + 2\pi RB_Z = 0 \end{aligned} \tag{12.191}$$

The first of these relations has made use of the $\nabla\cdot\mathbf{B}_V = 0$ relation. The equilibrium forces can thus be written as

$$\begin{aligned} &F_Z(R_0,Z_0) = 0 \;\rightarrow\; B_R(R_0,Z_0) = 0 \\ &F_R(R_0,Z_0) = 0 \;\rightarrow\; B_Z(R_0,Z_0) = -\frac{I}{4\pi R_0}\frac{dL}{dR_0} \end{aligned} \tag{12.192}$$

Observe that the second of these relations is identical to the term in the Shafranov shift (with a minus sign because of the different coordinate definitions) associated with the external poloidal flux (see Eq. (6.91)). Equation (12.192) describes the required properties for the applied vertical field to produce toroidal force balance.

Consider now stability against a rigid vertical shift. Using the fact that $\nabla \times \mathbf{B}_V = 0$ since $\mathbf{B}_V$ is the externally applied vacuum vertical field, one can easily calculate $\partial F_Z/\partial Z_0$. A short calculation yields

$$\frac{\partial F_Z}{\partial Z_0} = -\frac{I^2}{2R_0}\frac{dL}{dR_0}n \tag{12.193}$$

where, in standard notation,

$$n(R_0, Z_0) = -\left(\frac{R}{B_Z}\frac{\partial B_Z}{\partial R}\right)_{R_0, Z_0} \tag{12.194}$$

is known as the field index, (not to be confused with the mode number). The condition for vertical stability is therefore given by

$$n > 0 \tag{12.195}$$

This condition can be easily understood by examining Fig. 12.13. If the directions of the vertical field and toroidal plasma current are as shown then (1) the vertical field produces an inward force for toroidal force balance and (2) a small upward shift of the plasma gives rise to a downward $\mathbf{J} \times \mathbf{B}$ force of magnitude $2\pi RIB_R$ whose direction is to restore equilibrium. Thus, the curvature of the vertical field as shown in Fig. 12.13 is the correct one for stability and corresponds to the condition $n > 0$. If the vertical field were to bend away from the plasma then $n < 0$ and the plasma would be unstable.

12.10.3 Horizontal instabilities in a circular plasma

The next problem of interest is horizontal stability. Most of the analysis in the previous section applies here as well. The one main difference is that it is now required to calculate $\partial F_R/\partial R_0$. This is a slightly more complicated calculation but is still straightforward. A short calculation leads to

$$\frac{\partial F_R}{\partial R_0} = -\frac{I^2}{2R_0}\frac{dL}{dR_0}\left[-n + 1 + \frac{1}{2}\left(\frac{R_0 L'}{L} - 2\frac{R_0 L''}{L'}\right)\right] \tag{12.196}$$

where $L' = dL / dR_0$. Upon substituting the expressions for L, L' and L'' one finds that the term in the curved parenthesis is approximately equal to unity over the interesting range of aspect ratio $R_0/a > 3$. Within this approximation it then follows that the condition for horizontal stability is

$$n < \frac{3}{2} \tag{12.197}$$

The vertical field must curve inward for vertical stability but not too much or else the plasma becomes horizontally unstable.

There is a simple physical picture that helps provide insight to the horizontal stability criterion. Assume that the plasma is given a small outward shift. At constant flux, the outward hoop force per unit length acting on the plasma decreases because of the smaller current; that is, at $\Psi = LI =$ constant, L increases as R increases implying that I must decrease, thereby reducing the hoop force per unit length. Similarly, for an inward curving vertical field the magnitude of B_V decreases with increasing R because of the larger radius of curvature. Thus the toroidal restoring force also decreases as the plasma moves outward. The stability criterion given by Eq. (12.197) is an expression of the requirement that the curvature of the vertical field be sufficiently weak so that the toroidal restoring force decreases at a slower rate than the hoop force. When this occurs the restoring force dominates and the plasma is stable against horizontal displacements.

To summarize, the conditions on the field index for a circular cross section plasma to be stable against both vertical and horizontal displacements is given by

$$0 < n < \frac{3}{2} \tag{12.198}$$

In general, more accurate numerical calculations show that the axisymmetric stability of circular plasmas is relatively easy to achieve, requiring only a modest shaping of the vertical field.

12.10.4 Vertical instabilities in an elongated plasma

Vertical instabilities in an elongated tokamak are an important issue. Recall that high elongation is a desirable feature in that larger currents can flow with the same q_* as κ increases. This improves the ideal MHD β limit as well as the energy confinement time. Still, increasing elongation makes the plasma more susceptible to $n = 0$ vertical instabilities.

The goal in this subsection is to calculate the critical conducting wall radius required to stabilize more highly elongated plasmas. As in previous cases, since the actual wall is resistive, the instability is transformed into a resistive wall mode. The end result is that when engineering reality is taken into account most tokamak researchers would agree that elongations on the order of $\kappa \sim 1.6$–1.8 can be feedback stabilized. In fact elongations in this range are readily achieved in modern tokamaks, and even higher values are achieved in spherical tokamaks.

The analysis presented here has two components. The first is a simple wire model that shows physically why elongated plasmas are unstable. The second

calculates δW as a function of elongation and wall position using the Energy Principle. The calculation is greatly simplified by the use of hindsight, which has shown that the basic instability mechanism does not depend on either β or toroidicity. Thus, the calculation is carried out in a straight cylinder with an elliptic cross section plasma using the tokamak ordering. This calculation leads to an explicit relation between elongation and wall position. The results are then compared to more accurate numerical calculations.

The wire model

A simple physical picture that shows why elongated plasmas tend to be unstable can be obtained from a simple wire model as illustrated in Fig. 12.14. Assume the plasma wire is held in equilibrium by two equally spaced, rigidly mounted wires as shown in the diagram. By symmetry the global forces acting on the plasma wire, when it is centered, cancel and the plasma is in equilibrium. Now, to elongate the plasma vertically the currents in each wire must flow in the same direction as in the plasma wire. The resulting attractive force due to each equilibrium wire "pulls" on the top and bottom of the plasma causing it to become elongated while simultaneously holding the plasma in global force balance.

Assume next that the plasma wire undergoes a small vertical displacement ξ towards the upper wire. Recall that the force of the upper wire on the plasma wire is inversely proportional to the separation distance. Thus, the upward pulling force is increased since the wires are slightly closer together. Similarly, the pulling force of the lower wire is decreased since it is now slightly further away from the plasma wire. The conclusion is that there is a net global force, in addition to the elongation forces, acting on the plasma wire and pointing in the upward direction. The direction of this force causes the plasma to move even further away from its original equilibrium position. This clearly corresponds to an instability.

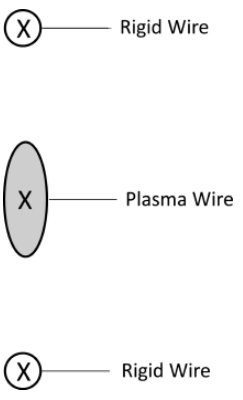

Figure 12.14 Wire model showing vertical instability in an elongated plasma.

The elliptic cylinder model

The properties of the instability, including the important effect of a conducting wall can be quantified by carrying out an Energy Principle analysis of $n = 0$ axisymmetric modes. The calculation is made tractable by neglecting β and toroidicity, neither of which is crucial for the basic excitation of the instability. The analysis is also simplified by using the tokamak expansion for the magnetic fields. The final simplification is to use a trial function, corresponding to a rigid vertical displacement, to evaluate δW. The analysis proceeds as follows.

The configuration of interest is a straight cylindrical plasma with an elliptic cross section of equivalent toroidal length $2\pi R_0$. The geometry is illustrated in Fig. 12.15. The strategy is to evaluate $\delta W = \delta W_F + \delta W_V$ using the $n = 0$ rigid shift trial function given by

$$\boldsymbol{\xi} = \xi_0 \mathbf{e}_y \tag{12.199}$$

where ξ_0 = constant. This is reasonably close to the actual eigenfunction as determined by detailed numerical calculations. As stated above the pressure is set to $p = 0$ and the equilibrium magnetic field is assumed to satisfy the tokamak ordering. Specifically it is assumed that

$$\mathbf{B} = B_0 \mathbf{e}_z + \mathbf{B}_p(x, y) \tag{12.200}$$

with B_0 = constant and $B_p/B_0 \sim \varepsilon$.

Consider first the evaluation of δW_F. If one starts with the intuitive form of δW_F given by Eq. (8.32) then a straightforward calculation leads to

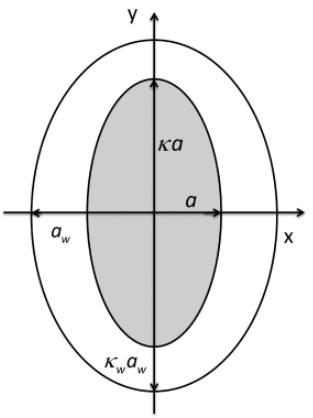

Figure 12.15 Geometry of the elliptic plasma model showing vertical instability in an elongated plasma.

$$\delta W_F = \frac{\pi R_0 \xi_0^2}{\mu_0} \int \left[\left(\frac{\partial B_y}{\partial y} \right)^2 + \frac{\partial B_y}{\partial x} \frac{\partial B_x}{\partial y} \right] dxdy \tag{12.201}$$

The terms that enter are the line bending and kink contributions. The plasma compressibility and curvature terms vanish because $p = 0$. The magnetic compressibility term is smaller by ε^2 than the other terms in Eq. (12.201) and is thus neglected.

To proceed further an equilibrium magnetic field is required. A convenient choice is the elliptical Solovev model given by Eq. (6.138) with $\beta = 0$. The equilibrium flux and corresponding magnetic fields are given by

$$\begin{aligned} \psi &= \frac{\psi_0}{2} \left(\frac{x^2}{a^2} + \frac{y^2}{\kappa^2 a^2} - 1 \right) \\ B_x &= -\frac{1}{R_0} \frac{\partial \psi}{\partial y} = -\frac{\psi_0}{R_0 a^2} \frac{y}{\kappa^2} \\ B_y &= \frac{1}{R_0} \frac{\partial \psi}{\partial x} = -\frac{\psi_0}{R_0 a^2} x \end{aligned} \tag{12.202}$$

Here, ψ_0 is a constant that will scale out of the problem. Equation (12.202) is substituted into Eq.(12.201). A short calculation that makes use of the fact that the elliptical plasma area is equal to $\pi\kappa\alpha^2$ yields the required expression for δW_F

$$\frac{\delta W_F}{W_0} = \delta \hat{W}_F = -\frac{1}{\kappa} \tag{12.203}$$

where $W_0 = \pi^2 \psi_0^2 \xi_0^2 / \mu_0 a^2 R_0$.

Clearly this term is destabilizing. However, destabilization is not directly due the edge current jump which led to $n \geq 1$ instabilities in a tokamak. It is in fact shown shortly that the circular tokamak ($\kappa = 1$) is stable to the $n = 0$ mode even in the presence of a current jump. In other words, if an instability arises it is due to elongation.

The next step in the analysis is to calculate the vacuum energy. This is accomplished by introducing elliptic coordinates u, v in the vacuum region,

$$\begin{aligned} x &= c \sin u \cos v \\ y &= c \cosh u \cos v \end{aligned} \tag{12.204}$$

Here, u is a radial-like variable while v is a poloidal angle-like variable. The parameter c is a constant. Its value is determined by the requirement that the plasma surface correspond to $u = u_p$. The implication is that c and u_p satisfy

$$\begin{aligned} c \sin u_p &= a \\ c \cosh u_p &= \kappa a \end{aligned} \tag{12.205}$$

which can easily be inverted

$$\begin{aligned} \coth u_p &= \kappa \\ c^2 &= a^2(\kappa^2 - 1) \end{aligned} \tag{12.206}$$

Similarly, the perfectly conducting wall is assumed to be located at $u = u_w$. Note that the wall is not concentric with the plasma. Instead it has the shape of a confocal ellipse which is slightly flattened with respect to the plasma. This wall shape assumption is primarily for mathematical simplicity. The wall radius a_w and elongation κ_w thus satisfy

$$\begin{aligned} c \sinh u_w &= a_w \qquad & \kappa_w &= \coth u_w \\ c \cosh u_w &= \kappa_w a_w \qquad & a_w^2 &= a^2(\kappa^2 - 1)\sinh^2 u_w \end{aligned} \tag{12.207}$$

The advantage of introducing elliptic coordinates is that Laplace's equations and the corresponding boundary conditions become quite simple. To see this observe that the perturbed vacuum magnetic field can be written as $\hat{\mathbf{B}}_1 = \nabla V$ with V satisfying $\nabla^2 V = 0$. After some algebra one can show that Laplace's equation in the laboratory coordinate system for $n = 0$ modes transforms to

$$\frac{\partial^2 V}{\partial x^2} + \frac{\partial^2 V}{\partial y^2} = c^2(\cosh^2 u - \sin^2 v)\left(\frac{\partial^2 V}{\partial u^2} + \frac{\partial^2 V}{\partial v^2}\right) = 0 \tag{12.208}$$

The boundary conditions, particularly the one on the plasma surface, also require some algebra. The key point is to recognize that the unit normal vector on any elliptic surface $S(x, y) = x^2 + y^2/\kappa^2 - a^2 = 0$ can be written as

$$\mathbf{n} = \frac{\nabla S}{|\nabla S|} = \frac{1}{(\kappa^4 x^2 + y^2)^{1/2}}(\kappa^2 x\, \mathbf{e}_x + y\, \mathbf{e}_y) \tag{12.209}$$

which can easily be converted into u, v coordinates. Using Eq. (12.209) one can then show that the boundary conditions on $V(u, v)$ are given by

$$\begin{aligned} \mathbf{n}\cdot\nabla V|_{wall} = 0 \qquad & \rightarrow \quad \left.\frac{\partial V}{\partial u}\right|_{u_w} = 0 \\ \mathbf{n}\cdot\nabla V|_{plasma} = \mathbf{n}\cdot\nabla \times (\xi_\perp \times \mathbf{B})|_{plasma} \qquad & \rightarrow \quad \left.\frac{\partial V}{\partial u}\right|_{u_p} = \frac{\psi_0 \xi_0}{aR_0\kappa}\cos v \end{aligned} \tag{12.210}$$

The solution for V satisfying Eqs. (12.208), subject to Eq. (12.210) has the form

$$V(u, v) = \frac{\psi_0 \xi_0}{aR_0\kappa}\frac{\cosh(u_w - u)}{\sinh(u_w - u_p)}\cos v \tag{12.211}$$

This solution is now substituted into the expression for δW_V,

$$\delta W_V = \frac{1}{2\mu_0}\int_{V_p} |\hat{\mathbf{B}}_1|^2\, d\mathbf{r} = -\frac{1}{2\mu_0}\int_{S_p} V\,\mathbf{n}\cdot\nabla V\, dS \tag{12.212}$$

After some standard manipulations one obtains

$$\frac{\delta W_V}{W_0} = \delta\hat{W}_V = \frac{1}{\kappa^2}\coth(u_w - u_p) \tag{12.213}$$

Equations (12.203) and (12.213) are combined yielding an expression for the total potential energy

$$\delta\hat{W} = \delta\hat{W}_F + \delta\hat{W}_V = -\frac{1}{\kappa} + \frac{1}{\kappa^2}\coth(u_w - u_p) \tag{12.214}$$

The final step is to eliminate u_p, u_w in terms of more recognizable geometric parameters. The quantity u_p has already been calculated in Eq. (12.206). The quantity u_w can be conveniently expressed in terms of a wall-closeness parameter A which measures the ratio of the area of the wall to the area of the plasma,

$$A \equiv \frac{\pi\kappa_w a_w^2}{\pi\kappa a^2} = \frac{c^2 \sinh u_w \cosh u_w}{\kappa a^2} = \frac{\kappa^2 - 1}{2\kappa}\sinh 2\, u_w \tag{12.215}$$

When the wall is at infinity then $A = \infty$. When it is on the plasma then $A = 1$. A short calculation leads to desired form of the potential energy

$$\delta\hat{W} = -\frac{1}{\kappa} + \frac{1}{\kappa^3}\frac{\kappa^2 + 1 + \left[(\kappa^2 - 1)^2 + 4\kappa^2 A^2\right]^{1/2}}{2(A - 1)} \tag{12.216}$$

Equation (12.216) describes the stability of an elongated plasma against vertical instabilities. There are some useful limits to this expression. First, for a circular plasma corresponding to $\kappa = 1, \delta\hat{W}$ simplifies to

$$\delta\hat{W} = \frac{2}{A - 1} > 0 \tag{12.217}$$

A circular plasma is stable to vertical displacements for any wall radius including placing the wall at infinity. Second, assume a finite ellipticity but move the wall to infinity, $A \to \infty$. The potential energy reduces to

$$\delta\hat{W} = -\frac{1}{\kappa} + \frac{1}{\kappa^2} < 0 \tag{12.218}$$

In this simple model the plasma is unstable for any elongation with the wall at infinity.

The most interesting relation results from setting $\delta\hat{W} = 0$. Doing this determines how close the wall has to be to stabilize a plasma with a given elongation. A short calculation yields the simple relation

$$A < 2\left(\frac{\kappa^2 + 1}{\kappa^2 - 1}\right) \qquad \text{for stability} \qquad (12.219)$$

Equation (12.219) implies that an area ratio of 2 or less would stabilize any elongation.

Numerical results

Compared to various numerical studies, the critical wall area given by Eq. (12.219) is somewhat optimistic. The reasons are as follows. First, a trial function is used rather than the actual eigenfunction. Second, the Solovev model has finite edge currents which are closer to the wall, thereby producing a stronger wall effect. Third, the choice of a confocal ellipse for the wall places the wall closer to the top of the plasma. This is exactly where the instability is driving the plasma, the result again being a stronger wall effect than, for instance, with a concentric wall.

On the other hand, numerical solutions indicate that toroidal effects are slightly stabilizing which would tend to make the elliptical cylinder model more pessimistic. When all the effects are included the numerical studies show that the net result is that realistic plasmas need a closer wall than indicated by Eq. (12.219). As stated earlier, even with such a closer wall, the vertical instability still persists but in the form of a resistive wall mode that must be feedback stabilized. When practical engineering constraints are taken into account the conclusion is that elongations in the range of 1.6–1.8 can be feedback stabilized. This range is representative of modern tokamak operation. Spherical tokamaks, because of their very tight aspect ratio, can achieve even higher elongations, on the order of 2–2.5.

The main conclusion to be drawn from this discussion is that axisymmetric instabilities lead to a serious operational limit on tokamak operation. Vertical instabilities in an elongated plasma limit κ to a value less than 2, even though for other MHD and transport reasons it would be desirable to have much larger elongations. Still, it has now become nearly routine to feedback stabilize elongated tokamaks and this in itself is a success story for fusion research.

12.11 Overview of the tokamak

By combining the results from the equilibrium and stability analysis presented in the text one can obtain an overview of the standard tokamak configuration with respect to ideal MHD behavior.

Consider first equilibrium. The tokamak is an axisymmetric toroidal configuration with a large toroidal and a smaller poloidal magnetic field. In the interesting auxiliary heated high β tokamak regime radial pressure balance is provided by poloidal currents which produce a diamagnetic dip in B_ϕ. Toroidal force balance is

produced by the interaction of the toroidal current with the applied vertical field, basically the $\mathbf{J}_\phi \times \mathbf{B}_V$ force. The high β tokamak regime is characterized by the following scaling relations: $\beta_t \sim \varepsilon$, $\beta_p \sim 1/\varepsilon$, and $q \sim 1$. A standard tokamak typically has $\varepsilon \approx 1/3$, $q(0) \approx 1$, and $q(a) \sim 2 - 3$. There are equilibrium pressure limits on tokamaks but these limits usually exceed reactor requirements by a substantial margin.

Most tokamaks have elongated cross sections with $\kappa \sim 1.5-2$ and have an outward pointing "D" shape. The maximum elongation is limited by $n = 0$ axisymmetric modes. Interesting variations on the standard tokamak are (1) the spherical tokamak which attempts to achieve high β_t by employing a very tight aspect ratio and (2) the advanced tokamak whose goal is to ease the achievement of steady state operation by means of a high bootstrap current which generates a reverse shear $q(r)$ profile.

The most important MHD limitations on tokamak performance involve both pressure and current limits as set by MHD instabilities. Successful operation of a tokamak requires that neither the pressure nor the current be too large. Current limits exist in both the straight and toroidal tokamak. They arise from the $n = 1$, $m = 1$ internal kink mode, the high n Mercier interchange instability, and the $n = 1$, $m \geq 1$ external kink modes.

The limitations due to these modes are as follows. The $n = 1$, $m = 1$ internal mode is closely connected to the excitation of sawtooth oscillations. This mode basically limits the current density on axis so that $q_0 \approx 1$. The Mercier criterion is most difficult to satisfy near the magnetic axis where the shear is small. To prevent such instabilities and the resulting turbulence, the tokamak must operate with $q_0 \gtrsim 1$. The exact threshold depends on the shape of the cross section. Elongated, outward pointing D-shapes are favorable for Mercier stability. The most dangerous current-driven modes are the $n = 1$ external kinks. The tokamak must operate with $q_a > 1$ to avoid the $m = 1$ Kruskal–Shafranov limit. The actual criterion is more stringent, requiring $q_a \sim 2-3$ to avoid $m \geq 2$ external kinks. If q_a becomes too small then a major disruption occurs. Much higher m instabilities can occur at the plasma surface if the edge current gradient does not vanish sufficiently rapidly. These high m instabilities represent the peeling component of the peeling–ballooning mode believed to be responsible for ELMs.

There are equally important pressure limits in a tokamak that arise from $n = \infty$ ballooning modes and $n = 1$ ballooning-kink modes. The ballooning modes are internal instabilities that set a maximum allowable value of p/I as given by the Sykes limit $\beta_t < 0.044(I/aB_0)$. These modes are the ballooning contribution to the peeling–ballooning modes that may be responsible for ELMs. The ballooning-kink mode also sets a limit on the maximum p/I in this case given by the Troyon limit, $\beta_t < 0.028(I/aB_0)$. However, this maximum is achieved at an optimum current defined by $q_* \approx 1.5$,

which when geometric and finite β_t/ε effects are correctly included corresponds to $q_a \approx 2$. Violation of the Troyon limit often leads to major disruptions.

The final word is that from the MHD point of view the standard tokamak is capable of achieving MHD stable profiles without a conducting wall at sufficiently high β_t to meet the requirements of a fusion reactor.

This is clearly a positive conclusion but still, two problems remain. First, a standard tokamak reactor is projected to be a large device implying a large capital cost. By utilizing a very tight aspect ratio the spherical tokamak can achieve much higher β_t in a more compact geometry. Compactness translates into reduced capital costs. One MHD difficulty with the spherical tokamak is that high β_t does not necessarily translate into high p because of the rapid $1/R$ decay of the toroidal field in a tight aspect ratio geometry.

The second problem faced by the standard tokamak is the need for steady state. Because RF current drive is expensive and inefficient, a large portion of the plasma current must be provided by the bootstrap current to achieve a favorable power balance. This has led to the idea of AT operation which is characterized by high bootstrap current and reverse shear profiles. The difficulty here is that the plasma pressure needed to achieve a high bootstrap fraction invariably violates the Troyon limit. The implication is that a close conducting wall is required accompanied by resistive wall feedback.

The standard tokamak, or one of its disciples, may be able to overcome the difficulties discussed above and achieve the fusion dream – a steady state, disruption-free, high-performance tokamak with sufficient pressure and current to meet the requirements of a fusion reactor.

12.12 Stellarator stability

As might be expected, determining the MHD stability of stellarators is one of the most challenging problems in MHD theory. The reasons are self-evident. The geometry is three dimensional. There are a wide variety of different stellarator configurations. Some have a circular magnetic axis and some a helical magnetic axis. There may be small expansion parameters that can serve as the basis for an asymptotic expansion, but often times no such parameters exist.

The result of this complexity is that most stellarator stability results are obtained numerically, a task now made possible by advances in computer modeling and in computers themselves. Carrying out such studies is a critical component in the design of new stellarator experiments as well as interpreting data from existing experiments. Even so, it would be useful if some simple analytic theory was available to shed insight into which geometric properties of stellarators are favorable for MHD stability. In this connection it is worth noting that there does exist

some analytic theory, although most of it was developed during the early years of the fusion program. This early work is the basis for much of the material presented below.

As an overview, note that, in general, stellarators are subject to many, but not all, of the same modes found in tokamaks. Specifically, localized interchanges and ballooning mode instabilities are important in stellarators. However, internal and external current-driven kinks are not very important since stellarators typically operate with only a small or zero net toroidal current. As a result, the low n external ballooning-kink mode in a tokamak is essentially transformed into an external ballooning mode which is important in setting β limits. Lastly, as has been stated previously, when an MHD stability limit is violated, stellarators do not disrupt, a consequence of the cage-like confinement resulting from the applied helical field. Instead, performance degrades because of MHD turbulence, which is not desirable but is still better than a major disruption.

The analysis described in this section is primarily focused on high n ballooning and interchange modes. A series of simple calculations is presented that provides some insight into the geometric features needed for favorable stability. It is shown that a straight stellarator always has unfavorable curvature. Shear can provide some stability but only at very low β. Stability at higher values of β requires a combination of toroidicity plus a vertical field. The stability against low n external modes is discussed by reviewing several numerical studies.

12.12.1 *High* n *modes in a stellarator*

Some initial insight into the high n stability of a stellarator can be obtained by examining the expression for the local shear associated with the s,α diagram of a tokamak. For the simple analytic model the local shear is given by Eq. (12.99), repeated here for convenience:

$$\hat{s}(r,\theta) = s(r) - \alpha(r)\cos\theta \tag{12.220}$$

where $s(r) = rq'(r)/q(r)$ is the average shear and $\alpha(r) = -q^2 R_0 d\beta(r)/dr$ is the normalized pressure gradient.

Now, in a tokamak both s and α are positive. Therefore, in the region of unfavorable toroidal curvature ($\theta = 0$), as the pressure gradient α increases from zero the local shear first decreases and then increases. The value of α for which the local shear vanishes corresponds to a region of vulnerability for ballooning modes. At sufficiently large $\alpha \gg s$ the local shear increases with further increases in pressure in the region of unfavorable curvature, leading to the second region of stability.

The situation is qualitatively different in a stellarator. The reason is that $q(r)$ is usually a decreasing function of r. A stellarator is characterized by a reversed shear

profile over the entire plasma: $s(r) < 0$. To the extent that a similar s,α diagram applies to a stellarator, one sees that as the pressure α is increased, the local shear in the unfavorable toroidal field curvature region ($\theta = 0$) also increases monotonically. At the inside of the plasma ($\theta = \pi$) the local shear first decreases and then increases as the pressure rises. However, the region where the local shear vanishes is not that important because it does so in a region of favorable toroidal field curvature.

The conclusion is that the situation with respect to local shear is more favorable in a stellarator than in a tokamak. The local shear in a stellarator increases monotonically in the region where it is needed most, the region of unfavorable curvature. This insight suggests that the balance between interchange and ballooning stability shifts towards interchanges which are usually easier to stabilize.

In order to approximately demonstrate the interchange/ballooning mode properties analytically the stellarator ballooning mode potential energy is evaluated for a simple trial function. This analysis leads naturally to the idea of "average favorable curvature" and the related concept of the "magnetic well." To obtain these results one first needs some subsidiary calculations, specifically a derivation of the parallel current constraint and the relation between average curvature and magnetic well. These and the follow-on stability results are discussed below.

12.12.2 The parallel current constraint

The parallel current constraint is a general relation obtained from the requirement that $\nabla \cdot \mathbf{J} = 0$. The relation is needed in order to simplify the potential energy of the stellarator ballooning mode equation for the trial function used in the analysis.

The derivation of the parallel current constraint proceeds as follows. The current density $\mathbf{J}$ is written as $\mathbf{J} = J_{\|}\mathbf{b} + \mathbf{J}_{\perp}$ and then substituted into the equation $\nabla \cdot \mathbf{J} = 0$, yielding

$$\mathbf{B} \cdot \nabla \frac{J_{\|}}{B} = -\nabla \cdot \mathbf{J}_{\perp} \tag{12.221}$$

Next, $\mathbf{J}_{\perp}$ is substituted from the momentum equation: $\mathbf{J}_{\perp} = \mathbf{B} \times \nabla p / B^2$. This gives

$$\mathbf{B} \cdot \nabla \frac{J_{\|}}{B} = -\nabla p \cdot \nabla \times \frac{\mathbf{B}}{B^2} \tag{12.222}$$

A simple calculation shows that

$$\left(\nabla \times \frac{\mathbf{B}}{B^2} \right)_{\perp} = -\frac{\nabla p \times \mathbf{B}}{B^4} - 2\frac{\boldsymbol{\kappa} \times \mathbf{B}}{B^2} \tag{12.223}$$

Substituting into Eq. (12.222) leads to the parallel current constraint

$$\mathbf{B}\cdot\nabla\frac{J_\parallel}{B}=\frac{2}{B}(\mathbf{b}\cdot\nabla p\times\boldsymbol{\kappa}) \tag{12.224}$$

The final desired form is obtained by introducing straight field line flux coordinates with arc length defining the Jacobian. From the analysis in Section 12.4 it then follows that

$$\frac{\partial}{\partial l}\frac{J_\parallel}{B}=\frac{2}{B}\frac{dp}{d\psi}\kappa_\alpha \tag{12.225}$$

where the curvature has been written as $\boldsymbol{\kappa}=\kappa_\psi\,\nabla\psi+\kappa_\alpha\,\nabla\alpha$.

The parallel current constraint requires that for a given pressure and flux surface shape, a specific amount of parallel current must flow in order to keep the total current density divergence free.

12.12.3 The relation between average curvature and magnetic well

A reasonable guideline for assessing the MHD stability of stellarators can be obtained by substituting a trial function into the ballooning mode potential energy and then making use of the parallel current constraint. The result of these steps is a natural definition of average favorable curvature, which after some additional analysis, leads to the concept of a magnetic well.

The starting point is the ballooning mode potential energy written in terms of arc length as given by Eq. (12.52) and repeated here for convenience

$$\overline{W}(\psi,\alpha,\alpha_0)=\int_{-\infty}^{\infty}\left[k_\perp^2\left|\frac{\partial X}{\partial l}\right|^2-2\mu_0\frac{dp}{d\psi}(k_\alpha^2\kappa_\psi-k_\alpha k_\psi\kappa_\alpha)|X|^2\right]\frac{dl}{B} \tag{12.226}$$

A simple trial function is now substituted into Eq. (12.226). The trial function chosen is given by

$$X(\psi,\alpha,l)=\lim_{\varepsilon\to 0}\left[e^{-\varepsilon^2 l^2}X(\psi,\alpha)\right] \tag{12.227}$$

In the resulting expression for $\overline{W}$ the stabilizing $|\partial X/\partial l|^2$ term is neglected for simplicity. The term tends to be small since X only depends weakly on l. On the other hand, it tends to be large since $k_\perp^2$ contains secular terms proportional to l^2. The net effect is a stabilizing contribution of the same order as the pressure gradient term. Still, by neglecting the term one obtains a lower bound on $\overline{W}$ that in the limit $\varepsilon\to 0$ can be written as

$$\overline{W}(\psi,\alpha,\alpha_0) \geq -2\mu_0 \frac{dp}{d\psi}|X|^2 \int_{-\infty}^{\infty} (k_\alpha^2 \kappa_\psi - k_\alpha k_\psi \kappa_\alpha) \frac{dl}{B} \tag{12.228}$$

Note, however, that since a trial function has been used rather than the true eigenfunction the resulting $\overline{W}$ also must lie above the true minimum value of the potential energy: $\overline{W}(\psi,\alpha,\alpha_0) \geq \overline{W}_{\min}(\psi,\alpha,\alpha_0)$. Since there are two lower bounds on $\overline{W}$ one cannot in general conclude that the expression in Eq. (12.228) is either necessary or sufficient for stability. It does, nonetheless, give a plausible estimate for $\overline{W}$ which can be used to gain some physical insight.

The next step in the analysis is a further simplification of Eq. (12.228) resulting from the application of the parallel current constraint. Focus for the moment on the κ_α term. Since $k_\alpha = \partial S(\psi,\alpha)/\partial\alpha$ and $k_\psi = \partial S(\psi,\alpha)/\partial\psi$ are both independent of l one sees that

$$\left[\overline{W}\right]_{\kappa_\alpha} = 2\mu_0 \frac{dp}{d\psi}|X|^2 \int_{-\infty}^{\infty} (k_\alpha k_\psi \kappa_\alpha) \frac{dl}{B} = 2\mu_0 \frac{dp}{d\psi} k_\alpha k_\psi |X|^2 \int_{-\infty}^{\infty} \kappa_\alpha \frac{dl}{B} \tag{12.229}$$

The quantity κ_α is eliminated by means of the parallel current constraint, leading to

$$\left[\overline{W}\right]_{\kappa_\alpha} = 2\mu_0 \frac{dp}{d\psi} k_\alpha k_\psi |X|^2 \int_{-\infty}^{\infty} \kappa_\alpha \frac{dl}{B} = \mu_0 k_\alpha k_\psi |X|^2 \int_{-\infty}^{\infty} \frac{\partial}{\partial l}\frac{J_\parallel}{B}\, dl = 0 \tag{12.230}$$

The integrand is a perfect differential implying that the κ_α term makes no contribution to the estimate for $\overline{W}$.

With this simplification, the expression for $\overline{W}$ reduces to

$$\overline{W}(\psi,\alpha,\alpha_0) \geq -2\mu_0 \frac{dp}{d\psi} k_\alpha^2 |X|^2 \int_{-\infty}^{\infty} \kappa_\psi \frac{dl}{B} \tag{12.231}$$

For a standard negative pressure gradient it thus follows that a good guideline for stability is

$$\langle \kappa_\psi \rangle > 0 \tag{12.232}$$

where, in normalized form,

$$\langle \kappa_\psi \rangle = \frac{\displaystyle\int_{-\infty}^{\infty} \kappa_\psi \frac{dl}{B}}{\displaystyle\int_{-\infty}^{\infty} \frac{dl}{B}} \tag{12.233}$$

is the average normal curvature. A positive average curvature is favorable for stability.

A slightly more convenient form of Eq. (12.199) for vacuum fields can be obtained by substituting κ_ψ from Eq. (12.48) after letting $p \to 0$. Specifically one substitutes

$$\kappa_\psi = \frac{1}{B}\frac{\partial B}{\partial \psi} \tag{12.234}$$

into Eq. (12.233), yielding

$$\langle \kappa_\psi \rangle = \frac{\int_{-\infty}^{\infty} \left(\frac{1}{B}\frac{\partial B}{\partial \psi}\right) \frac{dl}{B}}{\int_{-\infty}^{\infty} \frac{dl}{B}} = -\frac{\frac{\partial}{\partial \psi}\int_{-\infty}^{\infty} \frac{dl}{B}}{\int_{-\infty}^{\infty} \frac{dl}{B}} \tag{12.235}$$

Equation (12.235) shows that an equivalent definition of favorable average curvature for a vacuum magnetic field can be written as (Rosenbluth and Longmire, 1957; Lenard, 1964)

$$\frac{\partial}{\partial \psi}\int_{-\infty}^{\infty} \frac{dl}{B} < 0 \tag{12.236}$$

When a magnetic field satisfies this criterion it is said to possess a "vacuum magnetic well." Unfortunately, in terms of intuition, it is not at all obvious what actually lies at the bottom of the "well." One further mathematical transformation is needed to demonstrate in a more intuitive way what quantity the "well" actually describes.

The transformation makes use of the fact that a vacuum magnetic field can be written as a gradient: $\mathbf{B} = \nabla V(\psi,\alpha,l)$. Now, consider the current flowing through the closed loop illustrated in Fig. 12.16. The loop is assumed to lie in a fixed α surface. The upper and lower line segments represent the intersections with the surfaces $\psi = \psi_1$ and $\psi = \psi_2$ respectively. The vertical line segments are chosen to be parallel to the $\nabla\psi$ direction. There are no contributions on these segments since $\mathbf{B} \cdot \nabla\psi = 0$. The current enclosed must be zero since the field is a vacuum field.

This implies that

$$\mu_0 I = \oint \mathbf{B}\cdot d\mathbf{l} = \oint \nabla V \cdot d\mathbf{l} = V_1(\psi_1,\alpha,l)\Big|_{l_1}^{l_2} - V_2(\psi_2,\alpha,l)\Big|_{l_3}^{l_4} = 0 \tag{12.237}$$

The change in the potential function must be the same along each segment. Since this relation must be true for any two arbitrary flux surfaces, it follows that $\delta V = V(\psi,\alpha,l_2) - V(\psi,\alpha,l_1)$ must be independent of ψ: $\partial(\delta V)/\partial\psi = 0$.

The desired transformation is now obtained from the relation

$$\delta V = \int_{l_1}^{l_2} \mathbf{B}\cdot d\mathbf{l} = \int_{l_1}^{l_2} B dl \tag{12.238}$$

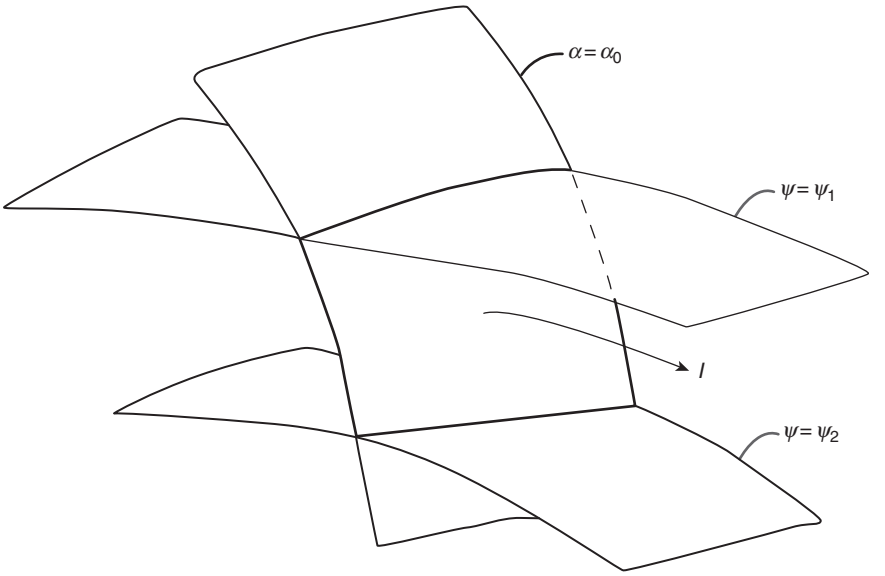

Figure 12.16 Geometry showing the current flowing through a closed loop used in the derivation of the magnetic well criterion.

where l_1 and l_2 are arbitrary points along the field line including $\pm\infty$. Specifically, the transformation makes use of the fact that

$$\frac{\partial}{\partial \psi}\int_{-\infty}^{\infty} B dl = 0 \tag{12.239}$$

The more intuitive form of the stability condition is finally obtained by a short calculation that makes use of Eqs. (12.236) and (12.238),

$$\begin{aligned} \frac{1}{\delta V}\frac{\partial U}{\partial \psi} &= \frac{\partial}{\partial \psi}\left(\frac{U}{\delta V}\right) = -\frac{U^2}{(\delta V)^2}\frac{\partial}{\partial \psi}\left(\frac{\delta V}{U}\right) < 0 \\ U &= \int \frac{dl}{B} \end{aligned} \tag{12.240}$$

The last term can be rewritten in a form that clearly shows why the stability condition corresponds to a "magnetic well,"

$$\frac{\partial}{\partial \psi}\langle B^2 \rangle > 0 \tag{12.241}$$

When $\langle B^2 \rangle$ lies at the bottom of a well and increases with flux away from the magnetic axis, the approximate stability criterion is satisfied.

The conclusion from the analysis is that there is a one-to-one relation between average curvature and magnetic well. A short calculation shows that this relationship is given by

$$\langle \kappa_\psi \rangle = \frac{1}{\langle B^2 \rangle} \frac{\partial}{\partial \psi} \langle B^2 \rangle \tag{12.242}$$

In practice one can use whichever form is more convenient to examine stability. Often the curvature expression requires less work to evaluate while the magnetic well expression is more intuitive to understand.

12.12.4 Average curvature of a straight helix

The simplest configuration to investigate is the straight, single helicity stellarator as described in Section 6.7. It is shown below that for a vacuum magnetic field, the configuration always has unfavorable average curvature. The analysis is relatively straightforward and makes extensive use of the results derived in Section 6.7. The calculation is most easily carried out assuming that the amplitude of the helical field δ is small and using the definition of average curvature rather than magnetic well.

The analysis begins by introducing the small δ approximation into the definition of average curvature. The expansion assumes that the magnetic field can be written as $\mathbf{B} = B_0 \mathbf{e}_z + \mathbf{B}_1(r, l\theta + hz)$ with $B_1/B_0 \sim \delta \ll 1$. The first non-vanishing contribution arises in order δ^2. The critical integral quantity required can thus be expanded as

$$\int \frac{dl}{B} = \int \frac{dz}{B_z} = \int \frac{dz}{B_0} \left[1 - \frac{B_{z1}}{B_0} - \frac{1}{B_0} \frac{\partial B_{z1}}{\partial r_0} r_1 - \frac{1}{B_0} \frac{\partial B_{z1}}{\partial \theta_0} \theta_1 + \frac{B_{z1}^2}{B_0^2} + \cdots \right] \tag{12.243}$$

Here, the field line of interest is labeled by r_0, θ_0 and, because of helical symmetry, the integration need only be carried out over one helical period $0 < z < L = 2\pi/h$. All quantities in the integrand are functions of r_0, θ_0, z.

The value of B_{z1} is obtained from Eq. (6.220) and can be written as

$$\begin{aligned} \frac{B_{z1}}{B_0} &= \Delta I_l(u_0) \cos(l\theta_0 + hz) \\ \Delta &= \frac{ha\delta}{(l^2 + h^2 a^2)^{1/2} I_l(ha)} \\ u_0 &= hr_0 \end{aligned} \tag{12.244}$$

where the specific definition of δ is given by

$$\delta \equiv \frac{B_h}{B_0} = \left[\frac{lB_{\theta 1} + hr_0 B_{z1}}{(l^2 + h^2 r_0^2)^{1/2} B_0}\right]_{r_0=a,\,\theta_0=0,\,z=0} \tag{12.245}$$

The remaining quantities in the integrand, r_1, θ_1, represent the helical oscillations of the field line trajectory. They are easily found from the field line trajectory equations

$$\begin{aligned} \frac{dr_1}{dz} &= \frac{B_{r1}}{B_0} = \Delta I_l'(u_0)\sin(l\theta_0 + hz) \\ \frac{d\theta_1}{dz} &= \frac{B_{\theta 1}}{r_0 B_0} = \Delta \frac{l\, I_l(u_0)}{u_0}\cos(l\theta_0 + hz) \end{aligned} \tag{12.246}$$

Integrating these equations yields

$$\begin{aligned} r_1 &= -\frac{\Delta}{h} I_l'(u_0)[\cos(l\theta_0 + hz) - 1] \\ \theta_1 &= l\Delta \frac{I_l(u_0)}{u_0^2}\sin(l\theta_0 + hz) \end{aligned} \tag{12.247}$$

All the quantities in the integrand have now been evaluated. A straightforward calculation now leads to an expression for the renormalized average curvature

$$\overline{\kappa} = u\frac{d\psi_0}{du}\langle \kappa_\psi \rangle = -\frac{u}{U}\frac{\partial U}{\partial u} \tag{12.248}$$

that can be written as

$$\begin{aligned} \overline{\kappa}(u) &= -\frac{\Delta^2}{2} u \frac{d}{du}\left[\left(\frac{dI_l}{du}\right)^2 + \left(\frac{l^2}{u^2} + 1\right) I_l^2\right] \\ &\approx -2(l-1)\delta^2 \left(\frac{r}{a}\right)^{2(l-1)} \qquad l \geq 2 \\ &\approx -h^2 a^2 \delta^2 \left(\frac{r}{a}\right)^2 \qquad l = 1 \\ &\approx -2h^2 a^2 \delta^2 \left(\frac{r}{a}\right)^2 \qquad l = 0 \end{aligned} \tag{12.249}$$

Here for simplicity the "0" subscript has been suppressed. The approximate expressions correspond to the loose helix limit $ha \ll 1$. Observe that for all l the average curvature $\overline{\kappa} < 0$. A straight stellarator always has unfavorable average curvature.

12.12.5 Shear stabilization of a straight helix

A natural question that now arises is whether or not shear can provide stability against the average unfavorable curvature. To answer this question one basically has to include the line bending $|\partial X/\partial l|^2$ term that was neglected in the evaluation of $\overline{W}$. Sinclair *et al.* (1965) have carried out such a calculation, the result being a generalized form of Suydam's criterion. Below, a heuristic derivation is presented of this result. The generalized Suydam's criterion is then applied to a loosely wound $l = 2$ stellarator where it is found that shear can indeed stabilize the unfavorable curvature but only for relatively small values of β_t.

The analysis begins by recalling Suydam's stability criterion (i.e., Eq. (11.109)),

$$rB_z^2\left(\frac{q'}{q}\right)^2 + 8\mu_0 p' > 0 \tag{12.250}$$

This equation, which is valid for a straight one-dimensional cylinder, can be easily cast in a form more suitable for generalization to a stellarator by replacing q by $2\pi/\iota \approx rB_0/R_0B_\theta$,

$$r^2\iota'^2 + 4r\beta'\iota^2 > 0 \tag{12.251}$$

where $\beta = 2\mu_0 p/B_0^2$. Next, the quantity ι^2 is expressed in terms of the actual curvature $\kappa \approx -B_\theta^2/rB_0^2$ which is then expressed in terms of κ_ψ as follows:

$$\frac{\iota^2}{4\pi^2} = \frac{R_0^2B_\theta^2}{r^2B_0^2} = -\frac{R_0^2}{r}\kappa = -\frac{R_0^2}{r}\psi'_0\kappa_\psi \tag{12.252}$$

Substituting Eq. (12.252) into Eq. (12.251) yields

$$r^2\left(\frac{\iota'}{2\pi}\right)^2 - 4R_0^2\beta'\psi'_0\kappa_\psi > 0 \tag{12.253}$$

The heuristic part of the derivation requires replacing κ_ψ with $\langle\kappa_\psi\rangle$ and then introducing the normalized curvature $\overline{\kappa} = r\psi'_0\langle\kappa_\psi\rangle$. One obtains

$$r^2\left(\frac{\iota'}{2\pi}\right)^2 - 4R_0^2\frac{\beta'}{r}\overline{\kappa} > 0 \tag{12.254}$$

Equation (12.254) shows how shear can potentially stabilize unfavorable curvature. To quantify the maximum β that can be shear stabilized assume that Eq. (12.254) is marginally stabilized at every value of radius. The maximum β satisfies

$$\beta' = \frac{1}{4R_0^2}\frac{r^3}{\overline{\kappa}}\left(\frac{\iota'}{2\pi}\right)^2 \tag{12.255}$$

Observe that $\beta' \propto r^3$ for a loosely wound $l = 2$ system implying a flat central pressure. The global β_t that can be stabilized is determined by multiplying Eq. (12.255) by r^2 and integrating over the plasma volume. A short calculation yields

$$\beta_t = -\frac{1}{a^2}\int_0^a \beta' r^2 dr = -\frac{1}{4R_0^2 a^2}\int_0^a r^5 \overline{\kappa}\left(\frac{\iota'}{2\pi}\right)^2 dr \tag{12.256}$$

The value of β_t can be easily evaluated for a loosely wound $l = 2$ stellarator for which

$$\begin{aligned} \overline{\kappa} &= -2\delta^2\left(\frac{r}{a}\right)^2 \\ \frac{\iota}{2\pi} &= \frac{R_0\delta^2}{ha^2}\left(1 + \frac{h^2 r^2}{2}\right) \\ \frac{\iota'}{2\pi} &= \frac{hR_0\delta^2}{a^2} r \end{aligned} \tag{12.257}$$

where $\overline{\kappa}$ and $\iota/2\pi$ have been obtained from Eqs. (12.249) and (6.243) respectively. The resulting maximum value of β_t is given by

$$\beta_t = \frac{1}{48} h^2 a^2 \delta^2 \tag{12.258}$$

Equation (12.258) can be rewritten in a more familiar form by noting that $\iota(r)/2\pi$ in a loosely wound $l = 2$ stellarator is approximately constant: $\iota/2\pi \approx \iota_H/2\pi \approx R_0\delta^2/ha^2$. Also, since $2\pi/h$ is the helical wavelength it follows that $ha = N\varepsilon$, where N is the number of helical periods. These substitutions lead to a more stellarator-like form for the β_t limit,

$$\beta_t = \frac{1}{48}(N\varepsilon)^3 \varepsilon\left(\frac{\iota_H}{2\pi}\right) \tag{12.259}$$

The β_t limit is quite small for LHD and W7-X. For instance, for LHD $N = 10$, $\varepsilon \approx 0.14$, and $\iota_H/2\pi \approx 0.4$ resulting in $\beta_t = 0.3\%$. The W7-X stellarator has an even lower limit. For this case, $N = 5$, $\varepsilon \approx 0.1$, and $\iota_H/2\pi \approx 1$ resulting in $\beta_t = 0.026\%$. The conclusion is that shear is not a very effective way to stabilize a predominantly straight, single helicity, $l = 2$ stellarator. To improve the situation toroidicity combined with a vertical field must be taken into account.

12.12.6 Stabilization of a toroidal stellarator

The average curvature in a stellarator can be made favorable by the addition of an externally applied vertical field with the proper sign and magnitude.

The addition of this field combined with toroidicity can produce a radially outward shift (along R) of the inner flux surfaces with respect to the outer flux surfaces. This relative shift, if large enough, is shown to produce average favorable curvature.

The derivation of the average curvature in a torus is similar to that for the straight stellarator. However, there is one subtlety that complicates the analysis. The issue is as follows. In a straight stellarator the θ trajectory of a field line along ϕ is composed of two contributions, a helical oscillation and a slow precession due to the rotational transform. Because of helical symmetry one need only calculate the transform over one helical period and then multiply by N, the total number of helical periods, to obtain the total transform. In contrast, in a torus as the field line slowly rotates with the transform it samples both the inside ($\theta = \pi$) and the outside ($\theta = 0$) of the torus. Since the toroidal field differs in each region by $(r/R_0)\cos\theta$, this modifies the field line trajectory and in turn, the average curvature. This is the new effect that must be taken into account.

The Greene–Johnson expansion

A convenient way to carry out the analysis is by means of the Greene–Johnson stellarator expansion (Greene and Johnson, 1961), which assumes that (for a vacuum field)

$$\begin{aligned} B_h^2/B_0^2 \sim \delta^2 \sim 1/hR_0 \sim 1/N \sim \varepsilon \ll 1 \\ ha \sim \iota/2\pi \sim 1 \end{aligned} \tag{12.260}$$

The expansion has the virtue of separating the rapid helical motion from the slow rotational transform motion since the number of helical periods N is assumed to be large. It is this separation of scales that simplifies the analysis. The end goal of the analysis is to determine $\overline{\kappa}$ whose derivation is given below.

The basic quantity of interest U needed to calculate $\overline{\kappa}$ is expanded as follows:

$$\begin{aligned} U &= \int \frac{dl}{B} = \operatorname*{Lim}_{M\to\infty} \int_{-2\pi M/N}^{2\pi M/N} \frac{R d\phi}{B_\phi} \\ &\approx \operatorname*{Lim}_{M\to\infty} \frac{R_0}{B_0} \int_{-2\pi M/N}^{2\pi M/N} \left[1 - \frac{B_{\phi 1}}{B_0} - \frac{B_{\phi 2}}{B_0} + \frac{B_{\phi 1}^2}{B_0^2} + \frac{r}{R_0}\cos\theta \right]_1 d\phi \end{aligned} \tag{12.261}$$

Note that the change in ϕ over one helical period is equal to $2\pi/N$ and that the integration is carried out over $2M$ helical periods with $M \to \infty$. This guarantees that the magnetic line will sample the entire flux surface, both inside and outside. Also, the quantity in the square bracket is to be evaluated along the magnetic line.

Now, to evaluate the integrand $I[r(\phi),\theta(\phi),\phi]$ one expands the field line trajectories as

$$\begin{aligned}\theta(\phi) &= \theta_0(\phi) + \theta_1(\theta_0 + N\phi)\\ r(\phi) &= r_0(\theta_0) + r_1(\theta_0 + N\phi)\end{aligned} \tag{12.262}$$

Here, θ_1, r_1 are the small amplitude (of order δ), rapidly oscillating helical contributions to the trajectory. The quantities r_0, θ_0 are slowly varying with ϕ as the field line moves from the outside to the inside of the torus with the rotational transform (of order δ^2 per helical period). During one helical period r_0, θ_0 can be assumed to be constant.

The helical field contribution

Using this representation one can separate U into helical and toroidal contributions given by

$$\begin{aligned}U &= U_h + U_t\\ U_h &= \operatorname*{Lim}_{M\to\infty}\frac{R_0}{B_0}\int_{-2\pi M/N}^{2\pi M/N}\left(1 - \frac{B_{\phi 1}}{B_0} - \frac{1}{B_0}\frac{\partial B_{\phi 1}}{\partial r_0}r_1 - \frac{1}{B_0}\frac{\partial B_{\phi 1}}{\partial \theta_0}\theta_1 + \frac{B_{\phi 1}^2}{B_0^2}\right)d\phi\\ U_t &= \operatorname*{Lim}_{M\to\infty}\frac{R_0}{B_0}\int_{-2\pi M/N}^{2\pi M/N}\left(-\frac{B_{\phi 2}}{B_0} + \frac{r_0}{R_0}\cos\theta_0\right)d\phi = \operatorname*{Lim}_{M\to\infty}\frac{2R_0}{B_0}\int_{-2\pi M/N}^{2\pi M/N}\left(\frac{r_0}{R_0}\cos\theta_0\right)d\phi\end{aligned} \tag{12.263}$$

All quantities in the integrand are evaluated at r_0, θ_0. Also, the contribution of $B_{\phi 2}$ to U_t is just the toroidal correction to B_ϕ: $B_{\phi 2}/B_0 = -(r_0/R_0)\cos\theta_0$.

The helical term U_h is identical to the straight stellarator contribution, discussed in the previous subsection as given by Eq. (12.243). Therefore, separating $\overline{\kappa}$ into helical and toroidal components

$$\overline{\kappa} = \overline{\kappa}_h + \overline{\kappa}_t \tag{12.264}$$

leads to

$$\overline{\kappa}_h = -2\delta^2\left(\frac{r}{a}\right)^2 = -\frac{2}{N}\left(\frac{\iota_H}{2\pi}\right)u^2 \tag{12.265}$$

for a loosely wound $l = 2$ stellarator. Also, from Eq. (12.257), $\iota_H/2\pi \approx R_0\delta^2/ha^2$ is the nearly constant $l = 2$ rotational transform.

The vertical field contribution

Next consider the toroidal contribution $\overline{\kappa}_t$ which requires the evaluation of U_t. This task can be carried out by switching from ϕ to θ_0 as the integration variable,

$$\begin{aligned} U_t &= \operatorname*{Lim}_{M\to\infty} \frac{2R_0}{B_0} \int_{-2\pi M/N}^{2\pi M/N} \left(\frac{r_0}{R_0}\cos\theta_0\right) d\phi \\ &= \operatorname*{Lim}_{M\to\infty} \frac{2R_0}{B_0} \int \left(\frac{r_0}{R_0}\cos\theta_0\right) \frac{d\phi}{d\theta_0} d\theta_0 \\ &= \operatorname*{Lim}_{M\to\infty} \frac{4\pi R_0}{B_0} \int \left[\frac{r_0}{\iota(r_0)R_0}\cos\theta_0\right] d\theta_0 \end{aligned} \tag{12.266}$$

Here, use has been made of the fact that as the magnetic line slowly moves around the flux surface due to the rotational transform, its helically averaged trajectory is given by $\theta_0(\phi) = \theta_i + [\iota(r_0)/2\pi]\phi$, where θ_i the starting angle. Therefore, $d\phi/d\theta_0 = 2\pi/\iota(r_0)$.

It is at this point that the vertical field enters the calculation. The vertical field causes the helically averaged flux surfaces to shift outward, along R, by an amount $\sigma(r_0)$. For mathematical self-consistency this shift should be finite corresponding to an ordering $\sigma/r_0 \sim 1$. However, to make the analysis simpler it is assumed that $\sigma/r_0 \ll 1$; the shift is assumed small for evaluation reasons and not because it scales with a small parameter. The small shift assumption implies that the field line trajectory can be approximated by

$$\begin{aligned} r_0(\theta_0) &\approx r_i + \sigma(r_i)\cos\theta_0 \\ \iota(r_0) &\approx \iota(r_i) + \iota'(r_i)\,\sigma(r_i)\cos\theta_0 \end{aligned} \tag{12.267}$$

where r_i is the initial radius and serves as the field line label.

Equation (12.267) is substituted into Eq. (12.266) yielding

$$\begin{aligned} U_t &= \operatorname*{Lim}_{M\to\infty} \frac{4\pi R_0}{B_0} \int \left[\frac{r_0}{\iota(r_0)R_0}\cos\theta_0\right] d\theta_0 \\ &= \operatorname*{Lim}_{M\to\infty} \frac{4\pi R_0}{B_0} \left[\frac{r_i}{R_0\iota(r_i)}\right] \int_{-2\pi M\iota/N}^{2\pi M\iota/N} \left[1 + \frac{\sigma(r_i)}{r_i}\cos\theta_0 - \frac{\iota'(r_i)}{\iota(r_i)}\sigma(r_i)\cos\theta_0\right] \cos\theta_0\, d\theta_0 \end{aligned} \tag{12.268}$$

This integral can be easily evaluated. All the oscillating terms average to essentially zero when integrating over many toroidal periods. Only the terms with a non-zero average value (the $\cos^2\theta_0$ terms) survive. The result is

$$U_t = \left(\frac{4\pi R_0 M}{B_0 N}\right)\left(1 - \frac{r}{\iota}\frac{d\iota}{dr}\right)\frac{\sigma}{R_0} \tag{12.269}$$

Note that the subscript i has been suppressed from r for simplicity.

The value of $\overline{\kappa}_t$ is calculated by noting (from Eq. (12.263)) that the large constant part of U has the value $U_0 \approx 4\pi R_0 M/B_0 N$. This, after setting $u = hr$, leads to

$$\overline{\kappa}_t \approx -\frac{u}{U_0}\frac{\partial U_t}{\partial u} = u\frac{\partial}{\partial u}\left[\frac{u^2\sigma}{\iota R_0}\frac{\partial}{\partial u}\left(\frac{\iota}{u}\right)\right] \tag{12.270}$$

Relation between σ and B_V

One further step is needed to complete the calculation and that is to find the relation between $\sigma(u)$ and the applied vertical field B_V. This relation is found as follows. In the context of the Greene–Johnson expansion, the total normalized flux function can be written as $\psi(r,\theta,\phi) = \overline{\psi}(r,\theta) + \psi_h(r, l\theta + N\phi)$ with $\psi_h/\overline{\psi} \sim \delta$. The toroidally averaged shift $\sigma(r)\cos\theta$ arises from the θ dependence of $\overline{\psi}$ which satisfies the Greene–Johnson equilibrium equation. This equation is given by Eq. (7.57) or (7.62). For a vacuum field both equations overlap and are given by

$$\nabla_\perp^2\left[\overline{\psi} - \left(\sum_1^\infty \frac{i}{n}\mathbf{e}_\phi\cdot\nabla_\perp A_n^* \times \nabla_\perp A_n\right)\right] = 0 \tag{12.271}$$

The solution, including an applied vertical field, which appears as a homogeneous contribution, can be written as

$$\overline{\psi} = \sum_1^\infty \frac{i}{n}\mathbf{e}_\phi\cdot\nabla_\perp A_n^* \times \nabla_\perp A_n + C_1 r\cos\theta \tag{12.272}$$

Here C_1 is known in terms of B_V, the amplitude of the vertical field, once the normalizations are disentangled. Also, the helical field harmonic A_n is known from Eq. (7.60). A short calculation then leads to the following expressions for $\overline{\psi}$ in terms of the normalizations used in this section

$$\begin{aligned}\overline{\psi}(u,\theta) &= \psi_0(u) + \psi_V(u)\cos\theta\\ \psi_0(u) &= -\left(\frac{l\Delta^2}{2N\varepsilon^2}\right)\frac{I_l I'_l}{u}\\ \psi_V(u) &= \left(\frac{1}{N\varepsilon^2}\frac{B_V}{B_0}\right)u\end{aligned} \tag{12.273}$$

The proper ordering requires $\psi_0 \sim \psi_V \sim 1$ but, as above, ψ_V is assumed to be small for evaluation reasons. This approximation leads to the standard formula for the shift $\sigma(u) = -\psi_V(u)/h\psi'_0(u)$. After another short calculation that makes use of the relation $\iota/2\pi \approx (lN\Delta^2/2u)(I_l I'_l/u)'$ one finds

$$\frac{\sigma(u)}{R_0} \approx \frac{B_V}{B_0}\frac{2\pi}{\iota(u)} \tag{12.274}$$

Equation (12.274) is substituted into Eq. (12.270) yielding

$$\overline{\kappa}_t(u) = -2\pi\frac{B_V}{B_0}u\frac{d^2}{du^2}\left(\frac{u}{\iota}\right) \tag{12.275}$$

Observe that for a uniform rotational transform, $\overline{\kappa}_t = 0$. Shear is required in order to generate favorable average curvature.

After an admittedly lengthy calculation one can combine Eqs. (12.265) and (12.275) to obtain the desired expression for the average curvature in a loosely wound $l = 2$ stellarator,

$$\overline{\kappa} = \left[-\frac{2}{N}\left(\frac{\iota_H}{2\pi}\right) + 3\frac{B_V}{B_0}\left(\frac{2\pi}{\iota_H}\right)\right]u^2 \tag{12.276}$$

Conclusions

Clearly, favorable average curvature is achieved for a sufficiently large vertical field satisfying

$$\frac{B_V}{B_0} > \frac{2}{3N}\left(\frac{\iota_H}{2\pi}\right)^2 \tag{12.277}$$

There are several further observations that can be made. First, from a practical point of view most stellarators have a set of external vertical field coils whose current can be adjusted to produce average favorable curvature. Second, the rotational transform appears in the numerator of $\overline{\kappa}_h$ and the denominator of $\overline{\kappa}_t$. Therefore, as one moves further out in r, one must maintain the corrections due to the full modified Bessel functions rather than just using the small argument approximations. Since the modified Bessel functions grow exponentially with r, the implication is that the destabilizing helical contribution grows faster than the stabilizing vertical field contribution; it is only possible to create average favorable curvature over a plasma whose outer radius is not too large.

Third, shear can help stabilize unfavorable curvature at the edge of the plasma where the local β is small but this is not a very large effect. Perhaps more importantly, high shear in conjunction with a vertical field increases $\overline{\kappa}_t$, thereby changing the average curvature in the stabilizing direction. The final point is that stellarators whose vacuum magnetic field possesses average favorable curvature should be stable against interchange instabilities. This stability should persist when finite pressure effects are included, up to the point where ballooning effects become important. Ballooning modes will then set the limit on β_t.

12.12.7 Numerical results

The analysis presented above provides some insight into the stability of stellarators. While this is helpful, when one is designing and interpreting actual experiments more accurate predictions are needed. These are obtained from three-dimensional stability codes (see Further reading). There are several features of such codes that are worth discussing.

To test stability it is necessary to begin with an equilibrium. At the time this book is being written most of the equilibria used in stability codes assume closed nested flux surfaces. Equilibria with islands are not considered. This is primarily for numerical convenience since closed surface equilibria are much easier to calculate than equilibria with islands. In essence these codes numerically average over any islands that may exist. Full stability analysis including islands should be forthcoming over the next several years.

Another point of interest concerns configurational optimization. For comparison recall that extensive optimization studies have been carried out for the tokamak that focus on maximizing the MHD stable β as a function of cross section and profile, giving rise to the Sykes and Troyon limits. Optimization in a stellarator is more complicated. Specifically, it is not aimed solely at maximizing MHD β limits but in addition includes neoclassical transport and realistic coil design constraints. In other words, the "best" stellarator is not in general the one with the highest MHD stable β, but the one that makes the best trade-offs between MHD, transport, and engineering constraints.

A further difference between stellarators and tokamaks is as follows. When the MHD β or q limit is violated in a tokamak, the end result is a catastrophic major disruption. Thus, MHD stability boundaries set rather rigid limits on tokamak operation. In contrast, when the maximum β limit in a stellarator is violated, the plasma does not disrupt. Instead, transport starts to gradually increase due to MHD turbulence, behavior often referred to as a "soft landing." This is the reason why MHD does not stand alone in stellarator optimization but can be combined with transport and engineering constraints to arrive at a best design.

Because of this multi-constrained optimization there is no relatively simple scaling relation, such as the Sykes or Troyon limit, that applies to all stellarators. Vastly different stellarator geometries, for example the large aspect ratio isodynamic W7-X, the continuously wound LHD heliotron, and the compact quasi-symmetric NCSX, all have numerically determined critical β values on the order of 5%. Stated differently, to a certain extent stellarator design takes stable $\beta \sim 5\%$ as a constraint and then proceeds to optimize with respect to neoclassical transport and coil design. Overall, $\beta \sim 5\%$ is probably sufficient for

energy applications and it is encouraging that a wide variety of stellarators can achieve this goal.

12.13 Summary

In Chapter 12 the Energy Principle has been used to investigate the stability of toroidal configurations, in particular the tokamak and the stellarator. A summary of the main results is given below.

General ballooning mode equation

There is a basic difference between cylindrical and toroidal systems with respect to MHD stability. Cylindrical symmetry implies that the curvature is unidirectional, unfavorable and only a function of r. In toroidal configurations there are usually alternating regions of favorable and unfavorable curvature. The $1/R$ dependence of the toroidal field produces favorable curvature on the inside of the torus ($\theta = \pi$) and unfavorable curvature on the outside ($\theta = 0$).

These alternating regions allow the possibility of ballooning modes. The corresponding eigenfunctions attempt to minimize δW by focusing in the unfavorable region while not causing too much line bending. The most dangerous ballooning modes correspond to $n = \infty$. They have long parallel wavelengths, short perpendicular wavelengths, and are localized about a rational flux surface. By exploiting the high-n limit plus the mode localization, one can reduce the general multidimensional Energy Principle to a one-dimensional differential equation along a field line on each flux surface. Stability can then be tested one field line at a time, representing a large savings in the effort required to test stability. The ballooning mode differential equation describes a competition between the stabilizing effects of line bending versus the destabilizing effects of local unfavorable curvature.

Tokamak stability

Toroidicity makes important modifications to the stability predictions of the straight tokamak. There are quantitative changes in the current-driven kink stability limits and qualitative differences when pressure is included.

In a low beta straight tokamak only current-driven modes are important. For internal modes, $m = 1$, $n = 1$ is usually the only instability and is the initial drive for sawtooth oscillations. The stability condition is $q_0 > 1$. In a torus the situation is more complicated with the results depending sensitively on the shape of the q profile near the axis. For a parabolic q profile the $n = 1$ mode is stable down to $q_0 = 1/2$ as $\beta_p \to 0$. Only when $\beta_p > 0.3$ does stability again require $q_0 > 1$. On the

other hand, for a very flat q profile the stability boundary is $q_0 > 1$ even as $\beta_p \to 0$. Experiments have observed sawtooth oscillations with $q_0 \sim 0.75$.

With respect to low beta external kink modes, the stability predictions are similar in both the straight and toroidal models. A value $q_a > 1$ is required to avoid the $m = 1$, $n = 1$ Kruskal–Shafranov limit. However, higher values are required to stabilize higher m number external kinks. Typically $q_a > 2.5$–3 to stabilize external kinks. When the stability criterion is violated, too much current is flowing in the plasma and the usual result is a major disruption.

Another source of major disruptions is due to the Greenwald density limit. Here, at high density a low current edge layer forms, effectively shrinking the size of the plasma. The same current in a smaller plasma is again sufficient to drive a major disruption.

Much higher m external kinks drive the peeling component of the peeling–ballooning mode thought to be responsible for ELMs. These modes are most easily excited when the edge current gradient is large.

Consider now pressure-driven effects. For a straight tokamak pressure-driven modes do not lead to any significant limits on β_t. In contrast, in a torus, interchanges, ballooning modes, and ballooning-kink modes all play an important role in setting stability limits. The toroidal interchange condition is given by the Mercier criterion, a two-dimensional generalization of the Suydam criterion. The $n \to \infty$ interchanges are most important near the magnetic axis where the shear is small. A circular cross section tokamak develops average favorable curvature when $q_0 > 1$. When this condition is satisfied the plasma is stable against localized interchanges across the entire profile. For non-circular tokamaks a combination of elongation and outward pointing triangularity improves stability, allowing operation slightly below $q_0 < 1$, although one must be careful to ensure that the sawtooth condition is also satisfied.

The $n \to \infty$ ballooning modes are more serious than interchanges in a tokamak. These modes set important limits on the maximum allowable pressure gradient, more accurately $\nabla p/I^2$. High shear and elongated outward pointing triangularity are again favorable for stability. Numerical studies by Sykes *et al*. (1983) show that for optimized profiles against ballooning modes the stability limit is given by $\beta_t = 0.11\ \varepsilon(1 + \kappa^2)/q_*$. For realistic experimental cases one finds $\beta_t \sim 0.1$. Ballooning effects play an important role in the peeling–ballooning modes thought to be responsible for ELMs.

Whereas ballooning modes set one limit on the maximum β_t in a tokamak, external ballooning-kink modes set an even stricter limit. As β_t is increased the current-driven kink mode develops a strong ballooning component, transforming to a ballooning-kink mode. A combination of elongation and outward triangularity also improves stability against these modes. The numerical studies of Troyon *et al*.

(1984) have shown that the maximum beta limit in a profile optimized tokamak is given by $\beta_t = 0.07\,\varepsilon(1+\kappa^2)/q_*$. For practical cases $\beta_t \sim 0.06$. Higher values can be stabilized with a conducting wall. However, for a finite conductivity wall the mode remains unstable but as a resistive wall mode which requires feedback stabilization. When the ballooning-kink mode does become unstable, it is a very dangerous mode, invariably leading to a major disruption.

A final class of modes that occur in tokamaks results from $n = 0$ axisymmetric perturbations. These are predominantly vertical instabilities which, with a conducting wall, have the form of resistive wall modes. Stability requires feedback control and practical engineering considerations usually limit the allowable elongations to about $\kappa < 1.8$. Excitation of an $n = 0$ axisymmetric mode usually leads to a major disruption.

With care, standard tokamaks can avoid, or limit the number of major disruptions. However, when the need for steady state operation is taken into account, advanced tokamak (AT) operation is required. This invariably results in a violation of the Troyon limit and the excitation of resistive wall modes.

The basic conclusion is that there are a variety of modes that can become unstable in a tokamak. Overall stability can be achieved by a combination of cross sectional shaping, tight aspect ratio, sufficiently low current and pressure, and feedback. The maximum stable values of β_t lie in the range $\beta_t \sim 0.05$–0.1, perhaps slightly low, but still within the regime of reactor interest. In AT operation, the β_t limit will likely be violated, leading to a resistive wall mode that requires feedback stabilization.

Stellarator stability

The stellarator is the most complicated of the configurations investigated. It is a truly three-dimensional system with a wide variety of strategies for optimizing performance. Because of the geometric complexity there are relatively few analytic guidelines to provide intuition. What does exist is largely due to studies carried out in the early days of the program. However, because of advances in computing and computers it has become possible to study the MHD stability of stellarators by means of large-scale codes.

As a general comment note that stability is dominated by pressure-driven modes since stellarators typically have small or zero net toroidal current. Also when the β_t limit is exceeded, stellarators do not suffer major disruptions. This is largely a consequence of the fact that the applied helical field has a fixed magnetic axis as opposed to a tokamak, where the axis can move with the plasma. Therefore, stellarators can sometimes operate above the ideal MHD limit, although once this occurs there is usually an increase in transport due to MHD turbulence. The MHD β_t limit thus sets a reasonable disruption-free limit on high-performance operation.

In terms of intuition, the analytic theory is largely focused on achieving average favorable curvature which is closely related to the existence of a magnetic well. A relatively simple expression is derived that is neither necessary nor sufficient for

stability but nonetheless provides some insight into the ways to achieve favorable average curvature.

One key feature of many stellarator configurations is that ballooning modes are often less unstable than in a tokamak. The reason is that the global shear is negative. This in turn implies that as β_t is increased, the local shear increases in the region of unfavorable curvature, exactly the opposite of a tokamak. This is desirable for stability and thereby decreases the relative importance of ballooning instabilities.

The average curvature criterion shows that a straight, single helicity stellarator always has unfavorable average curvature. Shear can provide stability but only at low values of β_t. To improve the situation toroidal effects must be taken into account, specifically the combination of toroidal curvature plus a vertical field. The vertical field affects the toroidally averaged shift of the magnetic axis which has a strong impact on stability.

In the end, there is no simple universal β_t limit for a stellarator because of the wide variety of possible configurations. Three-dimensional numerical studies show that stable β_t values on the order of $\beta_t \sim 0.05$ are possible in MHD-transport optimized stellarators. Higher values are possible but the need to optimize including neoclassical transport effects is a major limiting factor.

12.14 The final word

In the Introduction it is pointed out that a fusion reactor will require a pressure on the order of 5–10 atm for ignited operation. The goal of MHD studies is to discover magnetic geometries that can achieve such pressures with good equilibrium and stability properties. Well, what is the answer?

The tokamak and stellarator appear to be capable of stable operation with a maximum $\beta \sim 5\%$–10%, but without much safety margin. This translates into a pressure on the order of 5–10 atm assuming a reasonable aspect ratio and a maximum field on the (superconducting) coil of about 13 T. Most importantly, $n \geq 1$ stability should be achievable without the need of a conducting wall, a substantial saving in technological complexity. Still the situation is not completely resolved for the following reasons.

In addition to high β, disruption-free operation a tokamak reactor must operate as a steady state device for engineering reasons. This requires non-inductive current drive which because of its low efficiency must rely heavily on the bootstrap current. The resulting AT tokamak profiles that generate the nominal 75% bootstrap fraction required for economics invariably violate the MHD Troyon limit. The implication is that a conducting wall, accompanied by resistive wall stabilization is required. The need for a conducting wall erases some of the original advantages of the tokamak.

Much higher β values are possible in the spherical tokamak, on the order of 30%. However, these do not necessarily translate into high pressures because of

the lower maximum field ($\sim$ 7–8 T) on the central (copper) coil and the rapid decay of B_ϕ away from the TF coil because of the tight aspect ratio.

Stellarators, on the other hand, are inherently steady state and will likely be disruption free. Theoretical studies and experimental results indicate that stable β values on the order of 5% are possible. This is indeed a favorable result from the MHD point of view. However, because of the 3-D geometry neoclassical transport in a stellarator is in general substantially worse than in a tokamak. Clever magnetic geometries can produce omnigenous behavior which should reduce neoclassical transport to an acceptable level. This is one of the main goals of present stellarator research – achieve transport comparable to H-mode in a tokamak. Still, MHD has done its job. The problem now falls into the domain of the transport community.

Lastly, it is worth noting that the reversed field pinch should be capable of achieving a high stable β, on the order of 20–30%, against all internal ideal MHD modes with a relatively simple coil set, clearly a significant advantage technologically. On the other hand, the RFP is always unstable to a wide range of external MHD modes, which the naysayers believed could never all be simultaneously wall stabilized. Experiments in Europe have shown quite remarkably that a complex feedback system could be designed and built that indeed stabilizes the external modes. This promising result indicates that MHD stability is not a show-stopper for the RFP. Instead, the standard RFP must improve its transport properties, which are substantially poorer than for a tokamak, presumably because of resistive MHD turbulence. Edge profile control and the formation of single helicity states are two possible ideas that address the transport problem. There is also the need for a large amount of current drive since the bootstrap current is small in an RFP.

The final word? MHD has done a plausible job discovering configurations with reactor relevant values of pressure although there is not a lot of safety margin. The transport community still has to discover ways to further reduce cross-field heat conduction. The RF-neutral beam community still needs to develop more efficient ways to drive current in axisymmetric geometries.

References

Bussac, M. N., Pellat, R., Edery, D., and Soule, J. L. (1975). *Phys. Rev. Lett.* **35**, 1638.
Connor, J. W., Hastie, R. J., and Taylor, J. B. (1979). *Proc. R. Soc. London, Ser. A.* **365**, 1.
Coppi, B. (1977). *Phys. Rev. Lett.* **39**, 939.
Dewar, R. L. and Glasser, A. H. (1983). *Phys. Fluids* **26**, 3038.
Freidberg, J. P. and Haas, F. A. (1973). *Phys. Fluids* **16**, 1909.
Goedbloed, J. P., Keppens, R., and Poedts, S. (2010). *Advanced Magnetohydrodynamics*. Cambridge: Cambridge University Press.
Greene, J. M. and Johnson, J. L. (1961). *Phys. Fluids* **4**, 875.
Greene, J. M. and Chance, M. S. (1981). *Nucl. Fusion* **21**, 453.
Hegna, C. C. and Nakajima, N. (1998). *Phys. Plasmas* **5**, 1336.

Helander, P. and Sigmar, D. J. (2002). *Collisional Transport in Magnetized Plasmas*. Cambridge: Cambridge University Press.
Jardin, S. (2010). *Computational Methods in Plasma Physics*. Boca Raton, FL: Chapman and Hall/CRC Press.
Laval, G., Luc, H., Maschke, E. K., *et al*. (1971). In *Plasma Physics and Controlled Nuclear Fusion Research 1970*. Vienna: IAEA, Vol. II, p. 507.
Lazarus, E. A., Chu, M. S., Ferron, J. R. *et al*. (1991). *Phys. Fluids B* **3**, 2220.
Lenard, A. (1964). *Phys. Fluids* **7**, 1875.
Lortz, D. and Nuhrenberg, J. (1973). *Nucl. Fusion* **13**, 821.
Manickam, J., Pomphrey, N., and Todd, A. A. M. (1987). *Nucl. Fusion* **27**, 1461.
Menard, J. E., Bell, M. G., Bell, R. E. *et al*. (2002). *Proc. 19th International Atomic Energy Agency (IAEA) Fusion Energy Conference*, Lyon, France, paper EX/S1 5.
Menard, J. E., Bell, M. G. *et al*. (2004). *Phys. Plasmas* **11**, 639.
Mercier, C. (1960). *Nucl. Fusion* **1**, 47.
Mikhailovskii, A. B. (1974). *Nucl. Fusion* **14**, 483.
Mikhailovskii, A. B. and Shafranov, V. D. (1974). *Sov. Phys. – JETP* **39**, 88.
Rosenbluth, M. N. and Longmire, C. L. (1957). *Annal. Phys. NY* **1**, 120.
Shafranov, V. D. and Yurchenko, E. I. (1968). *Sov. Phys. – JETP* **26**, 682.
Sinclair, R. M., Yoshikawa, S., Harries, W. L., Young, K. M., Weimer, K. E., and Johnson, J. L. (1965). *Phys. Fluids* **8**, 118.
Snyder, P. B., Wilson, H. R., and Xu, X. Q. (2005). *Phys. Plasmas* **12**, 056115.
Solov'ev, L. S., Shafranov, V. D., and Yurchenko, E. I. (1969). In *Plasma Physics and Controlled Nuclear Fusion Research*. Vienna: IAEA, Vol. 1, p. 173.
Strait, E. J. (2005). *Fusion Sci. and Tech*. **48**, 864.
Sykes, A. and Wesson, J. A. (1974). *Nucl. Fusion* **14**, 645.
Sykes, A., Turner, M. F., and Patel, S. (1983). In *Controlled Fusion and Plasma Physics*, 11th European Conference, Aachen, West Germany, p. 363.
Troyon, F., Gruber, R., Saurenmann, H., Semenzato, S., and Succi, S. (1984). *Plasma Phys*. **26**, 209.
Ware, A. A. and Haas, F. A. (1966). *Phys. Fluids* **9**, 956.
Wesson, J. A. and Sykes, A. (1974). In *Plasma Physics and Controlled Nuclear Fusion Research 1974*. Vienna: IAEA, Vol. I, p. 449.

Further reading

Tokamak and stellarator analytic theory

Goedbloed, J. P., Keppens, R., and Poedts, S. (2010). *Advanced Magnetohydrodynamics*. Cambridge: Cambridge University Press.
Kikuchi, M., Lackner, K. and Tran, M. Q., eds. (2012). *Fusion Physics*. Vienna: International Atomic Energy Agency.
Wesson, J. A. (2011). *Tokamaks*, 4th edn. Oxford: Oxford University Press.

Stellarator numerical codes

Anderson, D. V., Cooper, W. A., Gruber, R. *et al*. (1990) *Scient. Comp. Supercomputer* II, 159.
Garabedian, P. (2002). *Proc. Nat. Acad. Sci*. **16**, 10257.
Hirshman, S. P. and Whitson, J. C. (1983). *Phy. Fluids* **26**, 3553.
Reiman, A. and Greenside, H. S. (1986). *Comput. Phys. Commun*. **43**, 157.

Problems

12.1 This problem demonstrates that any divergence-free vector field can be written in the form $\mathbf{B} = \nabla\alpha \times \nabla\beta$. Consider two functions $\hat{\alpha}(r)$, $\hat{\beta}(r)$ such that the magnetic lines lie in the contours $\hat{\alpha} =$ constant and $\hat{\beta} =$ constant. The intersection of two contours $\hat{\alpha} = \alpha_0$ and $\hat{\beta} = \beta_0$ defines a given magnetic line.

(a) Show that $\nabla\hat{\alpha} \times \nabla\hat{\beta}$ points in the direction of the magnetic field at every point in space.

(b) Assuming (a) to be true, one can write the magnetic field as $\mathbf{B} = A(\mathbf{r})\nabla\hat{\alpha} \times \nabla\hat{\beta}$. Here, $A(\mathbf{r})$ is a scalar function adjusted appropriately so that $\mathbf{B}$ has the correct magnitude. Show that the condition $\nabla \cdot \mathbf{B} = 0$ implies that $A(\mathbf{r}) = A\left(\hat{\alpha}, \hat{\beta}\right)$.

(c) Define new coordinates α and β as follows:

$$\alpha = \hat{\alpha}$$

$$\beta = \int_0^{\hat{\beta}} A(\hat{\alpha}, \beta')d\beta'$$

Show that

$$\mathbf{B} = \nabla\alpha \times \nabla\beta$$

12.2 Consider an ideal MHD plasma in the presence of a fixed external current density source $\mathbf{J}_e$. Show that δW_F can be written in the following intuitive form:

$$\delta W_F = \frac{1}{2\mu_0}\int d\mathbf{r}\Big[|\mathbf{Q}_\perp|^2 + B^2|\nabla\cdot\boldsymbol{\xi}_\perp + 2\boldsymbol{\xi}_\perp\cdot\boldsymbol{\kappa}_c|^2 + \gamma\mu_0 p_c|\nabla\cdot\boldsymbol{\xi}|^2$$

$$-\mu_0(\mathbf{b}\cdot\mathbf{J_c})\boldsymbol{\xi}_\perp^* \times \mathbf{b}\cdot\mathbf{Q}_\perp - 2\mu_0(\boldsymbol{\xi}_\perp\cdot\nabla p_c)\left(\boldsymbol{\xi}_\perp^*\cdot\boldsymbol{\kappa}_c\right)\Big]$$

where p_c is the plasma pressure, $\mathbf{J_c} = \mathbf{J} - \mathbf{J_e}$ is the plasma current, and

$$\boldsymbol{\kappa}_c = \boldsymbol{\kappa} + \frac{\mu_0}{2}\left(\frac{\mathbf{b}\times\mathbf{J}_e}{B}\right)$$

12.3 Consider the form of δW_F given in Problem 12.2. Introduce an eikonal representation for $\boldsymbol{\xi}_\perp$ and show that in the limit $k_\perp \to \infty$, δW_F can be written as

$$\delta W_F = \frac{1}{2\mu_0}\int d\mathbf{r}\left[k_\perp^2|\mathbf{b}\cdot\nabla X|^2 - \frac{2\mu_0}{B^2}(\mathbf{b}\times\mathbf{k}_\perp\cdot\nabla p_c)(\mathbf{b}\times\mathbf{k}_\perp\cdot\boldsymbol{\kappa}_c)|X|^2\right]$$

12.4 In this problem the effects of compressibility on the ballooning mode stability of closed line systems is investigated. For simplicity carry out the analysis in a straight 2-D "bumpy" θ-pinch geometry where the coordinates are the flux ψ, the

axial arc length l, and the poloidal angle θ (corresponding to the symmetry direction).

(a) Show that the terms giving rise to a zeroth-order contribution in δW proportional to $\mathbf{k}_\perp$ in the eikonal representation are given by

$$\delta W_0 = \frac{1}{2}\int \frac{d\theta d\psi dl}{B}\left[\frac{B^2}{\mu_0}|\nabla\cdot\boldsymbol{\xi}_\perp + 2\boldsymbol{\xi}_\perp\cdot\boldsymbol{\kappa}|^2 + \gamma p|\langle\nabla\cdot\boldsymbol{\xi}_\perp\rangle|^2\right]$$

where

$$\langle F\rangle = \oint \frac{F dl}{B}\Big/\oint\frac{dl}{B}$$

(b) Write $\boldsymbol{\xi}_\perp = \boldsymbol{\eta}_\perp \exp(iS)$, where $\mathbf{B}\cdot\nabla S = 0$ and $\mathbf{k}_\perp = \nabla S$. Expand $\boldsymbol{\eta}_\perp = \boldsymbol{\eta}_{\perp 0} + \boldsymbol{\eta}_{\perp 1}$. Minimize δW_0 and show that the first non-vanishing contribution is given by

$$\delta W_0 = \frac{1}{2}\int d\theta d\psi W_0$$

Here

$$W_0 = \oint \frac{dl}{B}\left[\frac{B^2}{\mu_0}(U + 2\boldsymbol{\eta}_{\perp 0}\cdot\boldsymbol{\kappa}_0)^2 + \gamma p\langle U\rangle^2\right]$$

with $U = i\mathbf{k}_\perp\cdot\boldsymbol{\eta}_{\perp 1} + \nabla\cdot\boldsymbol{\eta}_{\perp 0}$ and $\boldsymbol{\eta}_{\perp 0} = (X/B)(\mathbf{b}\times\mathbf{k}_\perp)$.

(c) Note that $\boldsymbol{\eta}_{\perp 1}$ appears only in W_0 and not in the remainder of δW. Minimize W_0 with respect to U. A convenient way to carry out the minimization is to introduce the variable

$$V(l) = \int_0^l U\frac{dl}{B}$$

It immediately follows that

$$U = B\frac{\partial V}{\partial l}$$

and

$$\langle U\rangle = V(L)/K_1$$

where

$$K_n = \oint \frac{dl}{B^n}$$

Show that the minimized W_0 can be written as

$$W_0 = \frac{4\gamma p K_1^2 \langle \boldsymbol{\eta}_{\perp 0} \cdot \boldsymbol{\kappa} \rangle^2}{\mu_0 \gamma p K_3 + K_1}$$

(d) Show that the full contribution to W (for ballooning modes) is given by

$$W = \frac{4\gamma p K_1^2}{\mu_0 \gamma p K_3 + K_1} \left\langle \frac{\kappa_n X}{rB} \right\rangle^2 + \oint dl \left[\frac{1}{\mu_0 r^2 B} \left(\frac{\partial X}{\partial l} \right)^2 - 2 \frac{dp}{d\psi} \frac{\kappa_n X^2}{rB^2} \right]$$

where $\kappa_n = \mathbf{n} \cdot \boldsymbol{\kappa}$ is the normal curvature.

(e) Consider the interchange perturbation $X = 1$. Show that the stability condition can be expressed

$$-2 \frac{dp}{d\psi} \left\langle \frac{\kappa_n}{rB} \right\rangle + \left[\frac{4\gamma p}{1 + \mu_0 \gamma p \langle 1/B^2 \rangle} \right] \left\langle \frac{\kappa_n}{rB} \right\rangle^2 > 0$$

12.5 This problem demonstrates a practical procedure for calculating the orthogonal flux coordinates used in the tokamak ballooning mode analysis. Assume that the flux function $\psi(R,Z)$ and its R and Z derivatives have been found either numerically or analytically by solving the Grad–Shafranov equation. The goal is to determine the coordinates $R = R(\psi,\chi)$, $Z = Z(\psi,\chi)$ where χ is an angle-like variable with period 2π orthogonal to ψ: $\nabla\psi \cdot \nabla\chi = 0$.

(a) Write the total differentials for $d\psi$ and $d\chi$. Show that for orthogonal coordinates, R and Z satisfy the equations

$$\frac{\partial R}{\partial \psi} = \frac{1}{(\nabla\psi)^2} \frac{\partial \psi}{\partial R}$$

$$\frac{\partial Z}{\partial \psi} = \frac{1}{(\nabla\psi)^2} \frac{\partial \psi}{\partial Z}$$

(b) The equations in part (a) represent a set of coupled, non-linear ordinary differential equations for R and Z with χ appearing as a parameter. R and Z can be obtained by a simple numerical integration once appropriate starting conditions in ψ and a value of χ are specified. The starting conditions are slightly subtle, but can be obtained as follows. Expand all quantities about the magnetic axis:

$$R = R_a + x, \quad Z = y, \quad \psi = \left(\psi_{RR} x^2 + \psi_{ZZ} y^2 \right)/2.$$

Here, ψ_{RR} and ψ_{ZZ} are constants, equal to the derivatives evaluated on the magnetic axis and the arbitrary constant in ψ has been chosen so that $\psi(R_a,0) = 0$. Show that the equations in the vicinity of the axis can be written as

$$\frac{\partial X}{\partial \psi} = 2\psi_{RR}\frac{X}{X+Y}$$

$$\frac{\partial Y}{\partial \psi} = 2\psi_{ZZ}\frac{Y}{X+Y}$$

where $X = \psi_{RR}^2 x^2$, $Y = \psi_{ZZ}^2 y^2$.

(c) Solve the equations in part (b) for X and Y. Show that

$$X = F(\chi)Y^{\alpha}$$

$$X + \alpha Y = 2\psi_{RR}\psi$$

where $F(\chi)$ is an arbitrary function and $\alpha = \psi_{RR}/\psi_{ZZ}$. For elongated flux surfaces $\alpha > 1$.

(d) The function $F(\chi)$ is not unique; that is, there are an infinite number of ways to label the orthogonal angle coordinate χ. A convenient choice, satisfying the 2π periodicity constraint and possessing the conventional properties that $\chi = 0$ when $y = 0$ and $\chi = \pi/2$ when $x = 0$ is given by

$$F(\chi) = K\cot^2\chi$$

The constant K is arbitrary and its value is of no great significance. Different K values correspond to different labels of the constant χ surfaces as χ varies from 0 to 2π. However, the shape of the constant χ surfaces remains unchanged. Choose $K = \psi_{RR}^2/\psi_{ZZ}^{2\alpha}$. Show that the proper starting conditions for small ψ can be written as a set of coupled transcendental algebraic equations given by

$$\frac{y^2}{\alpha^{1/2}} + y^{2\alpha}\alpha^{1/2}\cot^2\chi = \frac{2\psi}{(\psi_{RR}\psi_{ZZ})^{1/2}}$$

$$x^2 = y^{2\alpha}\cot^2\chi$$

(e) Sketch the $\psi =$ constant and $\chi =$ constant contours in the vicinity of the origin. To calculate the orthogonal coordinates $R(\psi,\chi)$, $Z(\psi,\chi)$ one specifies a value of χ and a small value of ψ (near the magnetic axis). The equations in part (d) are then solved simultaneously for y and x. These values are used as starting conditions for the basic equations in part (a). This process is then repeated for a sequence of χ values.

12.6 Consider the transformation of coordinates $(R,Z) \rightarrow (\psi,\chi)$ used in the discussion of axisymmetric tori. First carry out the transformation in the forward direction

$$RdRdZ = J\,d\psi d\chi$$

Next carry out the transformation in the reverse direction

$$d\psi d\chi = J' RdRdZ$$

By definition $J = 1/J'$. Show that

$$JB_p = \frac{1}{\mathbf{b}_p \cdot \nabla\chi} = \mathbf{b}_p \cdot \frac{\partial \mathbf{r}}{\partial \chi}$$

where $\mathbf{r} = R(\psi,\chi)\mathbf{e}_R + Z(\psi,\chi)\mathbf{e}_Z$ and $\mathbf{b}_p = \mathbf{B}_p/B_p$.

12.7 The maximum value of β_t allowed by ballooning instabilities has been investigated using a simple analytic model. This problem reexamines the analysis using a slightly more realistic model. Assume the entire profile is determined by operation on the marginal stability boundary of the ballooning mode. For simplicity assume the boundary is given by $\alpha = Ks$ where $K \approx 0.6$.

(a) Show that the critical β_t can be written as

$$\beta_t = \frac{\varepsilon K}{2}\left[-\frac{1}{q_a^2} + 3\int_0^1 \frac{x^2}{q^2}dx\right]$$

where $x = r/a$.

(b) Assume the q profile has the form

$$q(x) = q_0(1 + \lambda x^3)^v$$

Find the relationship between λ and v such that $J_\phi(a) = 0$.

(c) Calculate $\beta_t = (\varepsilon K/2)F(q_a,q_0)$. Set $q_0 = 1$ and plot $F(q_a)$ versus $1/q_a$. Compare the dependence of F on $1/q_a$ with the predictions of Sykes and Troyon: $F \propto 1/q_a$. Note that there is quite good scaling agreement over the experimentally interesting range $2 < q_a < 6$.

12.8

(a) Write down the general pressure-balance jump condition for the sharp boundary surface current model of an axisymmetric tokamak. Derive an analytic expression for $B_p = B_p(\theta)$ corresponding to an arbitrary plasma cross section $r = r_p(\theta)$. Do not make a large aspect ratio or low β expansion.

(b) Derive the $\beta_t q_*^2/\varepsilon$ equilibrium limit as a function of ε for a circular cross section plasma.

(c) Repeat step (b) for an elliptic cross section plasma with $\kappa = 2$.

12.9 Show that the surface term in δW for an arbitrary three-dimensional sharp boundary equilibrium can be written as

$$\delta W_S = \frac{1}{2}\int dS|\mathbf{n}\cdot\boldsymbol{\xi}_\perp|^2\left[2p\langle\kappa_n\rangle + \langle B^2/\mu_0\rangle(\hat{\kappa}_n - \kappa_n)\right]$$

where $\langle\kappa_n\rangle = (\hat{\kappa}_n + \kappa_n)/2$ is the average curvature across the surface and $\langle B^2\rangle = (\hat{B}^2 + B^2)/2$ is the average magnetic energy. Note that the first term is analogous to the pressure-driven contribution in δW proportional to the product of the pressure gradient and the curvature. The second term is analogous to the current-driven contribution in δW; the quantity $\hat{\kappa}_n - \kappa_n$ is non-zero only when there is a non-zero parallel current.

12.10 In this problem the high β tokamak expansion of δW_F is used to derive a ballooning mode equation. The goal is to see whether it makes any difference in the final equation whether one expands in ε and then takes the ballooning limit or vice versa. Starting with Eq. (12.123) introduce an eikonal representation for $U: U = \hat{U}(r,\theta)\exp[iS_\perp(r,\theta)]$, where $\mathbf{B}_p\cdot\nabla_\perp S_\perp - nB_0/R_0 = 0$ and $n\to\infty$. Derive the ballooning mode equation following the procedure given in Section 12.3. Does the resulting equation agree with the high β limit of the exact ballooning mode equation (i.e., Eq. (12.40)) in the limit of the high β expansion?

12.11 Evaluate the magnetic well for an ohmically heated tokamak as follows. Using the inverse aspect ratio expansion show that on a plasma flux surface $r = r_0 + \Delta(r_0\cos\theta)$,

$$B^2 \approx B_0^2\left[1 - 2\frac{r_0}{R_0}\cos\theta - \left(\frac{2\Delta}{R_0} - \frac{3r_0^2}{R_0^2}\right)\cos^2\theta + \frac{2B_{\phi 2}}{B_0} + \frac{B_{\theta 1}^2}{B_0^2}\right]$$

where $\Delta(r_0) = -\psi_1(r_0)/\psi_0'(r_0)$ is the flux surface shift. From this result show that the magnetic well $W(r_0)$ is given by

$$W = -\frac{B_{\theta 1}^2}{B_0^2} - \frac{r_0}{2R_0}\left[\frac{(r_0^2\Delta)'}{r_0}\right] + \frac{r^2}{2R_0^2}$$

12.12 Consider a large aspect ratio torsatron in which the magnetic fields are created by a surface current located at $r = a_c$, which is given by

$$\mathbf{K} = K_0[1 + \cos(l\theta - N\phi)]\left(\mathbf{e}_\theta\cos\alpha + \mathbf{e}_\phi\sin\alpha\right)$$

where $\tan\alpha = lR_0/Na_c$. Derive a formula for the rotational transform at $r = a$.

12.13 Show that the parallel current constraint given by Eq. (12.191) is automatically satisfied for an arbitrary one-dimensional screw pinch equilibrium. Repeat the calculation for an arbitrary axisymmetric torus as described by the Grad–Shafranov equation.